CrossMark

The Explored Asteroids: Science and Exploration in the Space Age

D.W.G. Sears[1]

Abstract Interest in asteroids is currently high in view of their scientific importance, the impact hazard, and the in situ resource opportunities they offer. They are also a case study of the intimate relationship between science and exploration. A detailed review of the twelve asteroids that have been visited by eight robotic spacecraft is presented here. While the twelve explored asteroids have many features in common, like their heavily cratered and regolith covered surfaces, they are a remarkably diverse group. Some have low-eccentricity orbits in the main belt, while some are potentially hazardous objects. They range from dwarf planets to primary planetesimals to fragments of larger precursor objects to tiny shards. One has a moon. Their surface compositions range from basaltic to various chondrite-like compositions. Here their properties are reviewed and what was confirmed and what was newly learned is discussed, and additionally the explored asteroids are compared with comets and meteorites. Several topics are developed. These topics are the internal structure of asteroids, water distribution in the inner solar system and its role in shaping surfaces, and the meteoritic links.

It is suggested, that asteroid-scale grooves, ridges, and catenas on several explored asteroids argue against these asteroids having rubble pile interiors, i.e. interiors made when impact fragments reaccumulate. The only body for which this is not true is the tiny Itokawa and it is argued that this asteroid is a regolith breccia. The discovery of water on Vesta, fluidization textures on comets and possibly Eros, and the relatively large number of active asteroids inside the purported snowline, suggests that significant subsurface water may be present on asteroids in the inner solar system and may partly account for their low densities. The explored asteroids have also confirmed the linkage of the HED meteorites with Vesta and Itokawa with the ordinary chondrite meteorites, Eros is somewhat problematical. So while diversity, and the range of sizes, histories, and surface compositions, is the hall mark of the explored asteroids, the number of explored asteroids is small compared with the diversity of material expected on the basis of asteroid astronomy and meteorite geochemistry. The exploration of the solar system's asteroids has only just begun.

✉ D.W.G. Sears
derek.sears@nasa.gov

[1] Space Science and Astrobiology Division (MS 245-3), Bay Area Environmental Institute/NASA Ames Research Center, Mountain View, CA 94035, USA

Springer

1 Introduction

Interest in asteroids has increased in recent years as solar system exploration has moved them into center-stage as they are viewed as a stepping stone from the Moon to Mars. At the same time, studies of meteorites and early solar system evolution have stressed the importance of the small bodies and several competitive mission proposals have been successful, for example NEAR-Shoemaker, Stardust, and OSIRIS-REx. Asteroid science has also advanced considerably through the availability of modern ground-based astronomical techniques (Stokes et al. 2002), the discovery that impact may have played a major role in biological evolution in the past and that the impact threat to life on Earth continues (Belton et al. 2004), and the realization that they could provide *in-situ* resources for space exploration (Lewis 1996). This paper is a review of what is known about asteroids seen mostly through the lens of spacecraft exploration.

1.1 Why a Review Focused on the Explored Asteroids

While our understanding of the solar system evolves like any other branch of Science, our exploration of the solar system proceeds in a number of discrete steps. There is a progression of techniques and there are significant differences in the information provided by each.

a. Telescopic observations locate an asteroid and enable orbits, spins, compositions (within limits), and shape to be determined, but usually provide no resolution of features.
b. Radar observations of many asteroids provide overlapping and complementary data to the other techniques.
c. Flyby missions provide images of part of the body with varying resolution.
d. Orbital missions provide high resolution stereo imagery over the whole object and the ability to measure properties that require long observing periods or close proximity.
e. Landings allow surface properties to be measured.
f. Finally, sample return provides geochemical analyses of great precision and enables comparison with meteorite data.

The present paper is largely concerned with steps (c) to (f), what has been learned from space missions. The exploration of space has analogs in many past explorations of the Earth that also yielded considerable scientific returns (Lewis and Clark 2004; Pallas 1776; Darwin 2006; Forster 2010; Von Humboldt 1996; Thomson 1880). The space program and the exploration of the solar system are no different, and the present paper discusses the science that has been learned through the exploration of asteroids.

1.2 100,000s of Asteroids and Only 8 Missions to 12 Asteroids

There are several hundreds of thousand asteroids, which are largely points of light. From this we can determine orbits and magnitudes. For a small proportion of them we can gain information on shape and rotation from ground based optical and radar data. Missions have the potential to provide a new kind of data on a few objects, at very large expense, which not only sheds light on the mission targets, but on the 100,000s of asteroids that we will never visit. The missions have become more sophisticated and more ambitious with time.

Eros, Vesta and Ceres, which were orbited by robotic spacecraft, form a complementary set in which detailed space-borne exploration has been possible. Itokawa is unique in that close exploration and sample return has been possible. Exploration of this asteroid can be considered as a complement to studies of the LL chondrites. The remaining asteroids have been the subject of flybys and therefore only partially explored. These mission targets might be considered the third category.

In an attempt to give context to the data obtained for the explored asteroids, I will make comparisons with other small bodies. There are two ways to do this. In some cases, comparison with other asteroids is possible, for example mass, size, rotation rate, pole, density and composition. Then there is data where no other asteroid comparisons are possible but data for the explored asteroids can be compared with data for other small bodies, for example cratering and regolith processes on the explored asteroids can be compared with these processes on the Moon and comets. The degassing of Ceres, and other asteroids, can be compared with degassing on comets.

To date the asteroids that have been visited by spacecraft consist of Gaspra, Ida and its moon Dactyl, Annefranck, Braille, Mathilde, Eros, Itokawa, Lutetia, Steins, Vesta, Toutatis, and Ceres (Table 1). As discussed above, while some missions have produced vast amounts of data others have produced relatively little data but their inclusion helps in the comparative planetology of asteroid science. A review of missions and their scientific accomplishments provides a number of perspectives of our knowledge of asteroids. To review their discovery is to take a walk through the history, from the search for the missing planet to the search for the asteroid that could destroy us, with all this entails for telling the story of new techniques and methods. This approach also means writing a history of asteroid exploration, or how robots and their instruments evolved, and how confidence and competence grew with time. Finally, to focus a review this way underscores the way science and exploration can productively go together.

This article begins with a summary of the discovery of the explored asteroids and missions that have been sent to explore them. The explored asteroids are then reviewed in terms of their physical properties,—their orbits, photometric properties, spin, mass, volume, density, magnetic fields, and interiors—their geological properties, discussing their maps and their surface features, and finally compositional properties. The article then concludes with a discussion of several themes in asteroid science as an example of what can be learned with data from the asteroid missions; continuity of the asteroid/cometary population, the distribution and role of water in the inner solar system, and the nature of asteroid interiors.

2 Discovery of the Explored Asteroids

As mentioned above, by recounting the discovery of the explored asteroids, we review the history of asteroid discovery in general since their discovery is spread rather uniformly over the last 200 years or so. Portraits of some of the discoverers of the present asteroids are shown in Fig. 1. Much of the following material was taken from the websites of the Minor Planet Center, the JPL Asteroid Database, and Wikipedia (whose asteroid entries are generally excellent although the primary source has been consulted wherever possible).

The story of how Bode's Law led to the discovery of the first asteroids is legend (Nieto 1972). When G. Piazzi (Fig. 1a) discovered Ceres in 1801, from the observatory at Palermo, it was by accident, he was working on a star catalog and not searching for the missing

Table 1 Asteroids visited by robotic spacecraft and representative sources of information

Asteroid	Spacecraft	Encounter dates	Mission type	Overview references[a]	
				Description of mission	Description of asteroid
5535 Annefrank (1942 EM)	Stardust	Nov 2, 2002	Flyby	1	2
9969 Braille (1992 KD)	Deep Space 1	July 29, 1999	Flyby	3	4
1 Ceres	Dawn	March 6th, 2015 to present	Orbit	5	6
433 Eros (1898 DQ)	Shoemaker-NEAR	Feb 14, 2000 to Feb 12, 2001	Orbit	7	8
951 Gaspra (1916 S45)	Galileo	Oct 29, 1991	Flyby	9	10
243 Ida (1988 DB1)	Galileo	Aug 28, 1993	Flyby	9	11
Dactyl	Galileo	Aug 28, 1993	Flyby	9	12
25143 Itokawa (1998 SF36)	Hayabusa	Sept 15, 2005 to April 25, 2006	Touch and go	13	14
21 Lutetia	Rosetta	July 10, 2010	Flyby	15	16
253 Mathilde (1949 OL1)	Shoemaker-NEAR	June 27, 1997	Flyby	17	18
2867 Steins (1969 VC)	Rosetta	Sept 5, 2008	Flyby	15	19
4179 Toutatis (1989 AC)	Chang'e 2	Sept 12, 2012	Flyby	20	21
4 Vesta	Dawn	July 16, 2011 to Sept 5, 2012	Orbit	5	22

[a] 1: Brownlee et al. (2003), 2: Duxbury (2004a, 2004b), 3: Rayman et al. (1999), 4: Buratti et al. (2004), 5: Rayman et al. (2006), 6: Nathues et al. (2015), 7: Cheng et al. (1997), 8: Robinson et al. (2002), 9: Veverka et al. (1994), 10: Carr et al. (1994), 11: Sullivan et al. (1996), 12: Chapman et al. (1995), 13: Yano et al. (2006), 14: Nakamura et al. (2011), 15: Glassmeier et al. (2007), 16: Sierks et al. (2011), 17: Cheng et al. (1997), 18: Thomas et al. (1999), 19: Jorda et al. (2012), 20: Huang et al. (2013), 21: Zou et al. (2014), 22: Russell et al. (2012).

Fig. 1 Some of the discoverers of the explored asteroids. (**a**) G. Piazzi discovered of Ceres in 1801. (**b**) H.W. Olbers discoverer of Vesta in 1807. (**c**) H. Goldschmidt who discovered Lutetia in 1885 shown here on a medal with J.R. Hinds to his *left* and R. Luther to high *right*. (**d**) J. Palisa who discovered Ida in 1884 and Mathilde in 1885. (**e**) G. Witt who discovered Eros (simultaneously with A. Charlois) in 1898. (**f**) G. Neujmin who discovered Gaspra in 1916. (**g**) Karl Wilhelm Reinmuth who discovered Annefrank in 1942. (**h**) E.F. Helin and (**i**) K.J. Lawrence who discovered Braille in 1992. Missing are C. Pollas who discovered Toutatis in 1989, A. Charlois who co-discovered Eros, and N. Chernykh who discovered Steins in 1969. Itokawa was discovered by the LINEAR team in 1998

planet. However, it was soon widely assumed that the missing planet between Mars and Jupiter, which was predicted by the law, had been discovered. However, three more were quickly found, Pallas by W.H. Olbers (Fig. 1b) in 1802, Juno by K.L. Harding in 1804, and Vesta by Olbers in 1807. For forty years these were the known asteroids, supposedly

the fragments of the exploded missing planet. Olbers, made his discoveries from his home observatory in Bremen. He announced his latest "planet" on the 29th March 1807 in a letter Schröter dated 31st March (Lynn 1907) and later that year published his finding in Annalen der Physik (Olbers 1807).

Starting in 1847 with the discovery of Iris by J.H. Hind, a well-known London astronomer, asteroids were discovered at a steady rate for the rest of the century. In 1852 the most successful mid-nineteenth century asteroid hunter, artist-turned-astronomer, Hermann Goldschmidt (Fig. 1c), discovered Lutetia (Goldschmidt 1852). In fact, it was to be the first of fourteen asteroids he would detect using two to four inch refractor telescopes from his home in Paris.

Goldschmidt held the admiration of the astronomical community for his success in asteroid discovery for some time, but Johann Palisa was to surpass him. Between 1874 and 1923, from the Naval Observatory at Pola and then the university observatory in Vienna, Palisa (Fig. 1d) was to discover 122 asteroids, including Ida and Mathilde, mostly using a six inch refractor (Raab 2002). Palisa frequently sold the naming rights to anyone willing to pay, and in this way supported his work.

The first near-Earth asteroid to be discovered, and second largest (after Ganymed), Eros, was an accidental discovery by Carl Gustav Witt (Fig. 1e) in Berlin on August 13, 1898. Earlier that night, August Charlois, who was to discover 99 asteroids between 1887 and 1904, often using the new method of astronomical photography. Within weeks Adolf J. Berberich realized that the perihelion distance of Eros was well inside the orbit of Mars and that the asteroid had come to within 0.15 AU of Earth on January 21, 1894. In 1901, E. Von Oppolzer obtained one of the first asteroid light curves and twelve years later a rotation period of about 5 hours was established (Yeomans, undated).

Gaspra was discovered on July 30, 1916, by Grigory Neujim (Fig. 1f), a Russian astronomer who was to discover 74 asteroids between 1913 and 1936 from the Simeis Observatory in the Crimea using a 12 cm double astrograph photographic telescope (Chernykh and Chernykh 2002). While Gaspra was discovered during the First World War, asteroid Annefrank was discovered in the Second World War, on March 23, 1942, by Karl Wilhelm Reinmuth (Fig. 1g) at the Königstuhl Observatory in Heidelberg. Reinmuth was the most successful discoverer of asteroids at the time, discovering over 395 permanently number asteroids.

The remaining asteroids that have been visited by spacecraft illustrate the transition from discoveries by individual astronomers to those made as a result of an institutionalized program of asteroid discovery. The second NEA in our group is Toutatis which was first detected in 1934 (and designated 1934 CT) but subsequently lost. It was recovered on the 4th January, 1989, by Christian Pollas at the CERGA Observatory, Caussols, now part of the Observatoire de la Côte d'Azur. Steins was discovered by N. Chernykh, of the Crimean Astrophysical Observatory in the Ukraine, who has discovered 537 asteroids, on the 10th November 1969. With the space program ramping up, and after a successful Apollo program, NASA became involved in asteroid discovery and it was Eleanor Helin (Fig. 1h) and Kenneth Lawrence (Fig. 1i) at the Palomar Observatory under a NASA program of detecting planet-crossing asteroids, who discovered our next asteroid target, Braille, on May 27th, 1992. The asteroid received its name as a result of a national contest organized by The Planetary Society. Also as part of the modern thrust to detect near-Earth asteroids, Itokawa was discovered September 26th, 1998, by the US Air Force-NAS-Massachusetts Institute of Technology joint LINEAR (Lincoln Near-Earth Asteroid Research) program operating at Lincoln Laboratory's site on the White Sands Missile Range near Socorro, New Mexico. The asteroid was named after Hideo Itokawa, the prominent Japanese rocket scientist, during the Hayabusa mission to the asteroid. As of 15 September 2011, LINEAR had detected

Fig. 2 Rate of discovery of near-Earth asteroids redrawn from a figure by Alan B. Chamberlin (JPL)
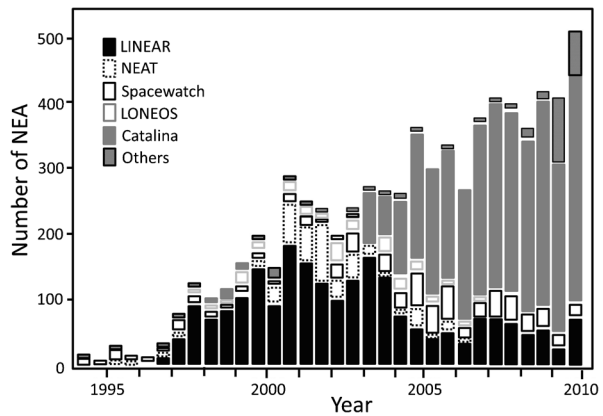
231,082 new objects, of which at least 2,423 were near-Earth asteroids and 279 were comets. LINEAR was responsible for the majority of near-Earth asteroid detections from 1998 until it was overtaken by the Catalina Sky Survey in 2005 (Fig. 2).

3 The Missions

Details of the space missions to asteroids are given in Table 1. There is a very wide range in the type and size of asteroids visited by robotic spacecraft (Table 2, Fig. 3). From the dwarf planets Vesta and Ceres to the relatively large asteroids Lutetia, Matthilde and Ida, Gaspra and Eros, and to the tiny Steins and Itokawa. Also noteworthy is the variety of shapes, which range from a distorted spheroid in the case of Vesta and Ceres, approximate spheroids for Lutetia and Mathilde, elongated shapes Ida, Gaspra and Eros, to the bifurcated shape of Itokawa. Similarly, surface compositions, as indicated by their reflectance spectra and taxonomy, vary widely.

The first asteroid to be visited by a robotic spacecraft was Gaspra (Fig. 4a), an olivine-rich S class asteroid, which orbits in the inner edge of the asteroid belt (Belton et al. 1992). Galileo was a high-cost mission to Jupiter that observed asteroids while passing through the main asteroid belt. On the 29th October 1991, the Galileo spacecraft obtained four images of Gaspra at wavelengths of 0.40, 0.56, 0.89, and 0.99 μm while at a distance of 6,065 km obtained. The spacecraft eventually passed within 1600 km of the asteroid. Information was thus obtained on size, shape, and crater density, while spatially resolved spectra provided data on composition and compositional variations across the asteroid.

Shoemaker-NEAR, the first of NASA's Discovery class of relatively cheap missions, was designed to explore the near-Earth asteroid Eros. On its way to Eros, on 27th June 1997, the spacecraft encountered Mathilde (Fig. 4b), a C class asteroid, and obtained over 330 images covering 60 % of the surface (Veverka et al. 1999a). Because of the large distance from the Sun at the time of encounter, 1.9 AU, and power limitations, only the imager was turned on.

On the 28th August 1993, while passing through the outer fringes of the asteroid belt, Galileo encountered the S asteroid Ida (Fig. 4c) and was able to take 96 images over 18 time intervals at distances of 240,429–2,494 km, the closest approach being 2,391 km (Belton et al. 1996a). Thus 95 % of the surface was imaged, mostly at four wavelengths, some at five. In February 15, 16th, 1994, while 10,760 km from the asteroid, a satellite, later named Dactyl (Fig. 4d), was observed in 47 images taken by two instruments (ISI and NIMS)

Table 2 Orbit, orbital period, and dimensions of asteroids that have been visited by spacecraft

| Asteroid	Orbit class	Orbit							Period (y)	Dimensions (km)
		e	a	q	i	Ω	ω			
5535 Annefrank (1942 EM)	Main	0.064	2.213	2.071	4.247	121	8.989		3.29	6.6 × 5.0 × 3.4
9969 Braille (1992 KD)	Mars crossing	0.433	2.341	1.328	29.00	241	356		3.58	2.1 × 1.0 × 1.0
1 Ceres (1943 XB)	Main	0.076	2.767	2.557	10.59	80	75		4.60	958 eqt × 906 pol
433 Eros (1898 DQ)	Amor	0.222	1.457	1.133	10.83	303	179		1.76	34.4 × 11.2 × 11.2
951 Gaspra (1916 S45)	Main	0.174	2.209	1.825	4.103	253	130		3.28	18.2 × 10.5 × 8.9
243 Ida (1988 DB1)	Main	0.0415	2.862	2.743	1.132	342	110		4.84	59.8 × 25.4 × 18.6
Dactyl	Satellite of Ida	0.0415	2.862	2.743	1.132	342	110			1.6 × 1.4 × 1.2
25143 Itokawa (1998 SF36)	Apollo (PHA)	0.28	1.324	0.953	1.622	69	163		1.52	0.535 × 0.294 × 0.209
21 Lutetia	Main	0.164	2.434	2.034	3.063	87	250		3.80	121 × 101 × 75
253 Mathilde (1949 OL1)	Main	0.266	2.647	1.943	6.74	180	157		4.31	66 × 48 × 46
2867 Steins (1969 VC)	Main	0.145	2.364	2.021	9.941	55	250		3.64	6.67 × 5.81 × 4.47
4179 Toutatis (1989 AC)	Apollo (PHA)	0.63	2.533	0.937	0.447	124	279		4.03	1.70 × 2.03 × 4.26
4 Vesta	Main	0.088	2.361	2.152	7.14	104	151		3.63	573 × 557 × 446
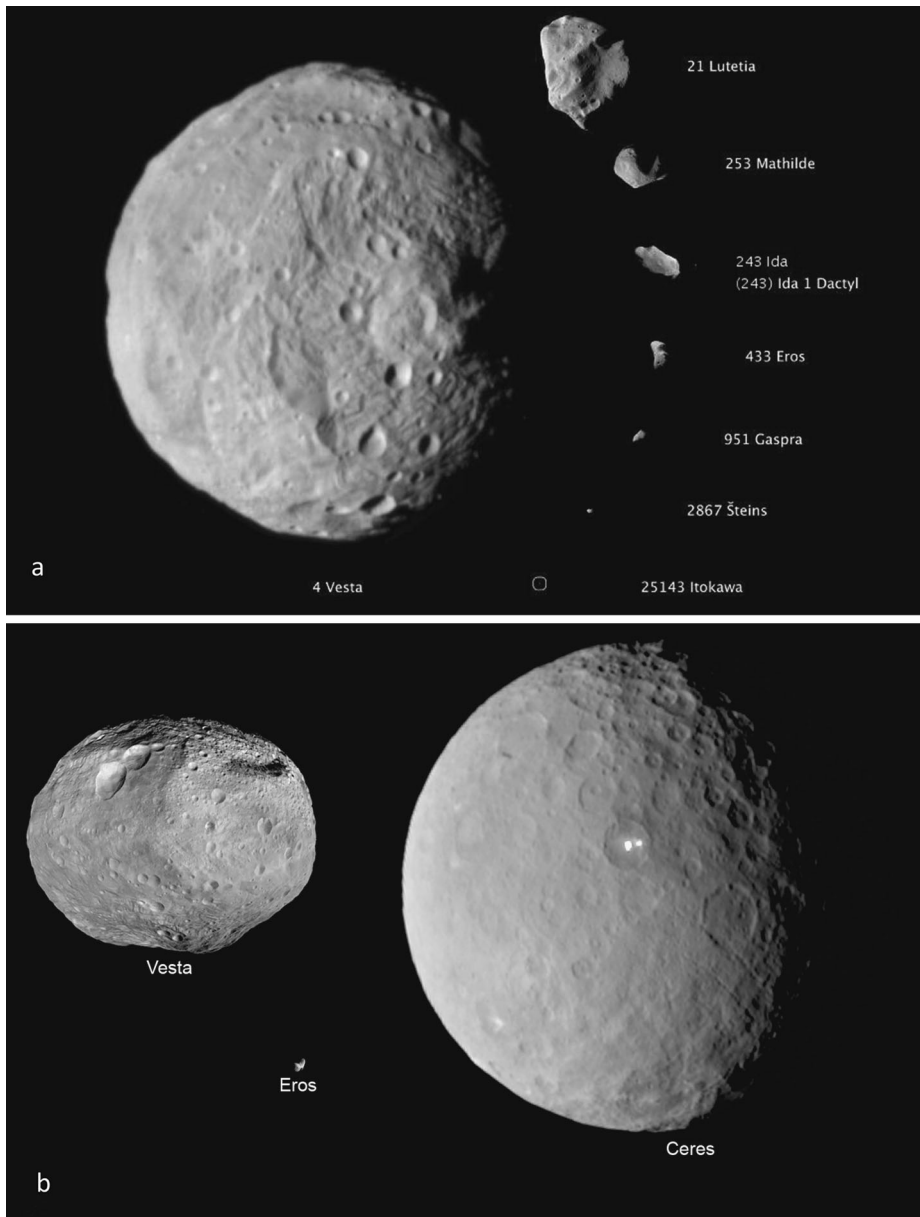
Fig. 3 (**a**) A compilation of asteroid images to illustrate their relative sizes (from Russell et al. 2012). Braille and Toutatis not shown. They would be similar to Itokawa on this diagram. (**b**) Ceres, Vesta, and Eros compared (NASA/JPL image)

the previous August. Dactyl was 100 km from the asteroid and 10–20 times smaller (Belton et al. 1996b). According to Chapman (1996), the main surprises at Ida were Dactyl (which enabled a density estimate for Ida) and the ejecta blanket on the large fresh crater Azzurra.
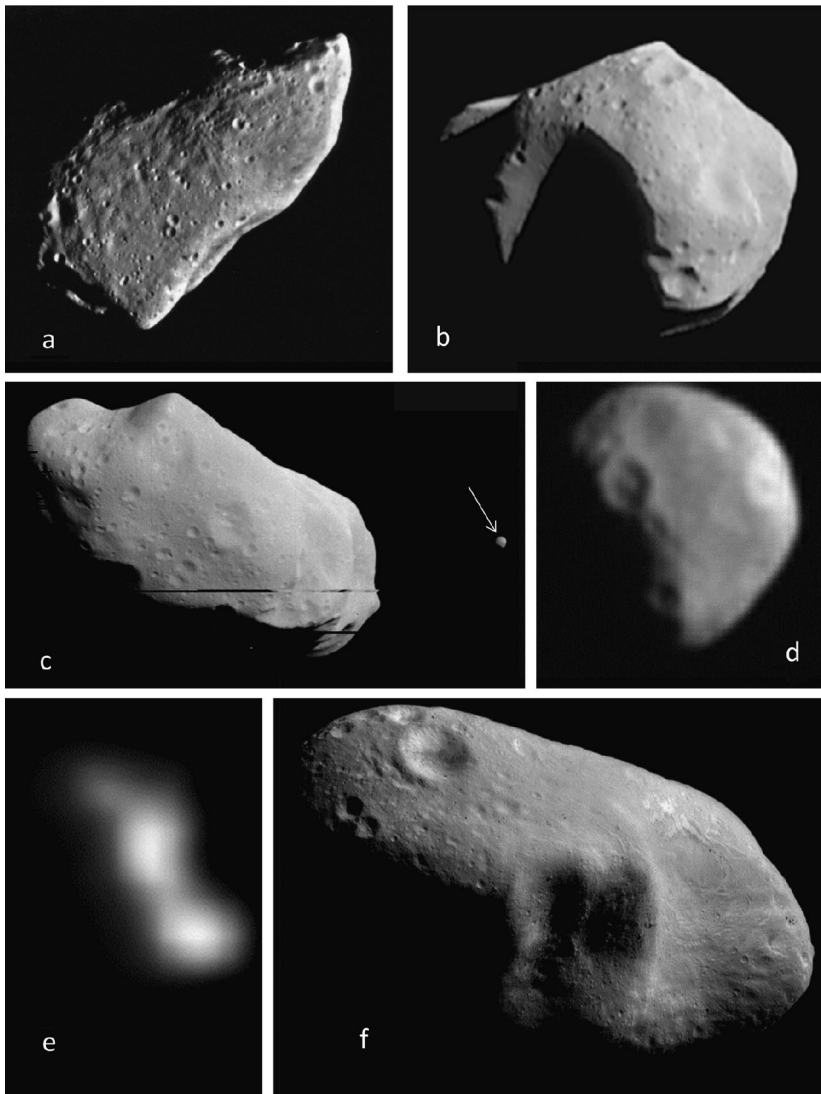
Fig. 4 Images of the asteroids that have been visited by spacecraft. (**a**) Gaspra (18.2 × 10.5 × 8.9 km) was imaged during the Galileo spacecraft fly-by in Oct 29, 1991, (**b**) Mathilde (66 × 48 × 46 km) was imaged by the NEAR spacecraft during a fly-by June 27, 1997. (**c**) Ida (59.8 × 25.4 × 18.6 km) was imaged by the Galileo spacecraft during a fly-by on Aug 28, 1993. Also in the field of view, and indicated by an *arrow*, is Ida's moon, Dactyl. (**d**) Ida's moon Dactyl (1.6 × 1.4 × 1.2 km) was discovered in images taken during the Ida fly-by. (**e**) Braille (2.1 × 1.0 × 1.0 km) was imaged during a fly-by of Deep Space 1 on July 29th 1999, (**f**) Eros (34.4 × 11.2 × 11.2 km) was imaged by the NEAR spacecraft prior to orbiting the asteroid for one year. (**g**) Annefrank (6.6 × 5.0 × 3.4 km) imaged during a fly-by by the Stardust spacecraft on Nov 2, 2002. (**h**) Itokawa (0.535 × 0.294 × 0.209 km) imaged by the Hayabusa spacecraft during its sample-collecting rendezvous Sept 15, 2005 to April 25, 2006. (**i**) Steins (6.67 × 5.81 × 4.47 km) imaged by the Rosetta spacecraft during a fly-by on Sept 5, 2008. (**j**) Lutetia (121 × 101 × 75 km) was also imaged by the Rosetta spacecraft during a fly-by July 10, 2010. (**k**) Vesta (573 × 557 × 446 km) was imaged by the Dawn spacecraft during it 15 month orbit July 16, 2011 to Sept 5, 2012. (**l**) Toutatis (1.70 × 2.03 × 4.26) was imaged by the Chang'e 2 spacecraft during a fly-by Sept 12, 2012. (**m**) Ceres (equatorial radius 479.6 ± 2.4 km, polar radius of 453 ± 4.5 km) imaged by the Dawn spacecraft shortly after going into orbit in March 6th, 2015
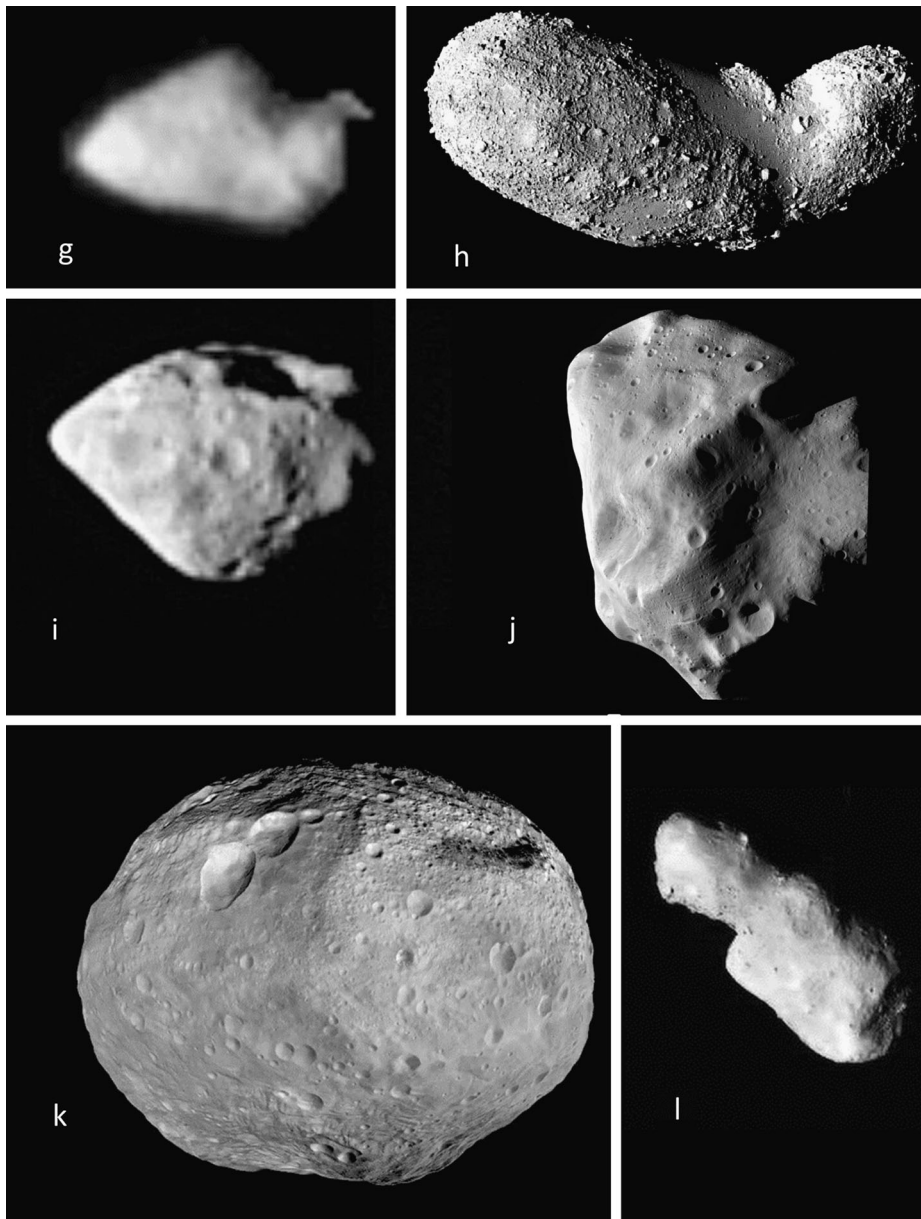
Fig. 4 (*Continued*)

While the NEAR spacecraft orbited the Sun, a NASA technology development mission, Deep Space 1, encountered asteroid Braille on July 29, 1999 (Fig. 4e). The mission was designed to demonstrate ion propulsion, solar cell improvements, new navigation and self-repair software, a beacon to minimize tracking costs, a miniature integrated camera and spectrometer (with a range of 1.25 to 2.6 μm), and two magnetometers mounted on booms (Richter et al. 2001). Because of a software glitch, thought to have been caused by a cosmic

m
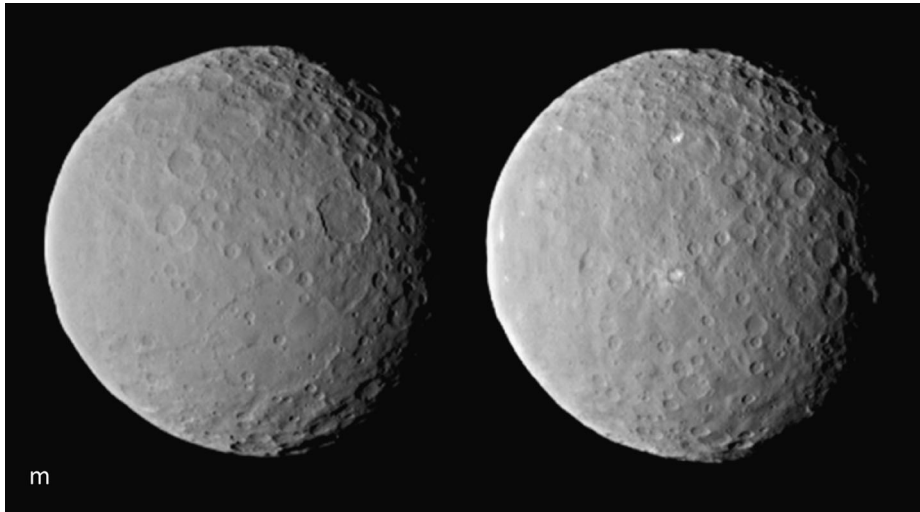
Fig. 4 (*Continued*)

ray particle event, only two images of the asteroid were obtained at a distance of 13,500 km on the outward journey (Buratti et al. 2004).

Shoemaker-NEAR arrived at Eros on 23 December 1998 programed to orbit the asteroid, but its engine shutdown prematurely and it flew by, its closest approach being 3800 km. Nevertheless, scientific data were obtained during the fly by Veverka et al. (1999b). The spacecraft returned to Eros (Fig. 4f) on 14 February 2000 and successfully went into orbit for a year, touching down on the surface on 12 February 2001 (Veverka et al. 2001). During its year in orbit, the spacecraft obtained 160,000 images, at wavelengths of 0.4 to 1.1 μm with its multispectral imager, and 70 images during the final descent. The spacecraft also deployed a near-infrared spectrometer with a range of 0.8 to 2.6 μm to determine the mineralogy of the surface (Veverka et al. 2000), a laser rangefinder to determine surface topography (Zuber et al. 2000), a magnetometer to detect magnetic fields (Acuña et al. 2002) and an X-ray/gamma-ray spectrometer to determine surface elemental composition (Trombka et al. 2000). Radio science enabled the determination of mass, density, rotation rate and location of its poles (Yeomans et al. 2000).

Also a NASA Discovery Program mission, the Stardust spacecraft flew by asteroid Annefrank (Fig. 4g), on its way to comet Wild 2, on 2nd November 2002. The spacecraft obtained 72 images of the S-class asteroid at 11,415 km to 3078.5 km distance with a passband of 0.47 to 0.94 μm and phase angle of 40 to 140 deg (Newburn et al. 2003; Duxbury et al. 2004a; Duxbury et al. 2004b). No filters were available. From the images, phase curves, albedo, size, shape and the orientation of the asteroid were obtained.

The first mission to an asteroid not organized by NASA was the Japanese Space Agency's Hayabusa mission to asteroid Itokawa (Fig. 4h). Planned as sample return mission, the spacecraft carried an X-ray spectrometer for elemental analysis and a near-infrared spectrometer (range 0.8 to 2.1 μm) for mineralogical analysis (Abe et al. 2006a, 2006b). It also carried a conical collector to collect samples from the cloud produced by a projectile fired from the spacecraft. The spacecraft arrived at Itokawa on 12 September, 2005 where it spent six weeks hovering at 20 km while performing remote sensing observations. It descended to the surface on the 19th and 25th November 2005. During the descent phase,

images were taken from 80 to 65 m above the surface. Hayabusa touched down on and sampled a 60×100 m smooth area that lies between the "head" and "body" of the otter-shaped asteroid (Yano et al. 2006). This region was named the Muses Sea in a tongue-in-check gesture to the pre-flight name for Hayabusa that was Muses C. The process was not entirely successful, but after an adventurous return flight, about 1000 individual mineral grains were found on the recovered spacecraft (Nakamura et al. 2014).

The next asteroid encounter was the Rosetta spacecraft's flyby of main belt E asteroid Steins (Fig. 4i) on 5th September 2008 when it passed within 803 km. The main instrument deployed at Steins was a camera system called OSIRIS which consists of a wide angle camera with 11 filters covering a range of 0.24 to 1.1 μm. A narrow angle camera with nine filters failed 10 min before closest approach (Keller et al. 2010). The twelve filters on the wide angled camera covered a range of 0.25 to 1 μm.

Two years after its encounter with Steins, on July 10th, 2010, Rosetta passed within 3170 km of the asteroid Lutetia (Fig. 4j), chosen because of it large size and puzzling spectrum. The OSIRIS instrument obtained 462 images covering 50 % of the surface, mainly the northern hemisphere (Sierks et al. 2011), while the visible, infrared, and thermal imaging spectrometer (with a range of 0.4 to 3.5 μm) attempted to identify surface minerals and determine surface temperature and thermal inertia (Coradini et al. 2011).

The Dawn mission, launched on September 27th, 2007, was also flown as part of NASA's Discovery Program of small deep space science missions (Russell and Raymond 2011). Its task was to orbit the two largest asteroids, Vesta and Ceres, both "dwarf planets" under recent changes in IAU nomenclature, with instruments for panchromatic and multispectral imagery; visible, infrared, γ-ray, and neutron spectrometry. Radio science will enable gravimetry (Rayman et al. 2006). Dawn arrived at Vesta (Fig. 4k) on 17th July, 2011, and went into orbit. For 22 days it mapped the surface from ∼2700 km using the panchromatic camera, at a resolution of ∼260 m/pixel, and the visible/IR spectrometer, with a resolution of ∼700 m/pixel, using three geometries to obtain topography. During this phase, the mission obtained 1179 stereoscopic panchromatic images covering 80 % of the surface, including the southern pole which, unlike the northern pole, was fully illuminated by the Sun during this "survey" phase (Jaumann et al. 2012). The spacecraft then dropped to a 700 km circular orbit from September to early November, 2011, where it obtained 2500 clear filter images with a resolution of about 70 m/pixel. The result of the mapping operations were global maps in fifteen sections, five equatorial, eight mid-latitude (four north and four south) and two polar (Roatsch et al. 2012). The orbit was then dropped to 210 km to continue mapping for 70 days. Finally, the spacecraft returned to it 700 km mapping orbit where it obtained additional images. The spacecraft was meant to leave Vesta after 12 months, but due to technical problems did not leave until September 5th, 2012.

As part of China's lunar exploration program, Chang'e 2 orbited the moon at 100 km from 9th October, 2010, until 8th June, 2011, ending this period with an orbit taking it within 15 km of the surface. The spacecraft was then transferred to the L2 point in the Earth-Moon system. On April 15th, 2012, Chang'e 2 left L2 for an encounter with Toutatis (Fig. 4l) on 13th December, 2012. The spacecraft carries an imaging spectrometer, gamma/X-ray spectrometers, microwave detectors, a space environment monitoring system, and a laser altimeter (Wang et al. 2010; Li et al. 2010).

The Dawn spacecraft recently went into orbit around Ceres where is will perform a similar suite of investigations as it performed at Vesta. Initial images show a heavily cratered surface with arcuate grooves emanating from the south polar region and a number of conspicuous bright spots (Fig. 4m).

There are several additional mission to asteroids currently in progress. In addition to Dawn being currently en route to Ceres, NASA's OSIRIS-REx mission is a sample return mission that has been selected to rendezvous with C class asteroid Bennu (Drake and Lauretta 2011). It will arrive at the asteroid in 2018, hover for 505 days at 5 to 0.7 km, collect samples, and return them to Earth in 2023. The spacecraft carries a suite of cameras, a LIDAR system, a visible/IR spectrometer, a thermal imaging spectrometer, and an X-ray imaging spectrometer. The samples will be collected by a mechanism that briefly touches the surface, and uses a blast of nitrogen to send the dust into a cage like structure.

The Japanese space agency, JAXA, launched the Hayabusa 2 mission on 3rd December 2014 to reach C asteroid 1999 JU3 in 2018, orbit for 18 months, and return samples to Earth in 2020 (Yoshikawa 2011). The scientific instruments on Hayabusa 2 are an optical navigation camera, a near-IR spectrometer, a thermal IR mapper, a LIDAR instrument, and a sample collector similar to Hayabusa's. The subsurface material will be exposed by a 2 km/s impactor (Okamoto et al. 2013). The mission includes several small JAXA landers and a German lander equipped with a camera, a radiometer, a magnetometer, and a hyperspectral microscope (Jaumann et al. 2013).

4 Physical Properties

4.1 Orbits

The orbital elements for the explored asteroids are listed in Table 2 and are shown projected onto the ecliptic as Fig. 5a–d. As is common in describing asteroid orbits, eccentricity is plotted against semimajor axis in Fig. 5e. Three of the asteroids that have been visited by spacecraft are near-Earth asteroids, Itokawa, Eros, and Toutatis, Toutatis being notable for its high eccentricity and thus large semimajor axis. The remainders are main-belt asteroids. Gaspra, Vesta, Annefrank, Steins and Lutetia lie between the 4:1 and 3:1 resonances with Jupiter, Mathilde lies between the 3:1 and 5:2 resonances while Ida and Ceres orbit just outside the 5:2 resonance. Toutatis has the highest eccentricity, Itokawa and Mathilde have the next highest (~ 0.27), the remainder are < 0.25. Braille is in a Mars-crossing orbit.

The NEA population is in a steady-state as objects are ejected from the solar system by planetary perturbations while being fed into near-Earth orbits, mostly from the main belt. However, the size distribution for this young NEA population is too shallow for the feeding mechanism to be collisional fragmentation, so it is thought that Yarkovsky drag might be responsible for populating the Earth's vicinity (Morbidelli et al. 2002). Yarkovsky drag is the slowing down of the asteroid's orbital velocity by emission of heat, and thus momentum, at ninety degrees to the asteroid-Sun axis as it rotates away from the subsolar point (Bottke et al. 2006). Clockwise rotation slows down an asteroid so it moves closer to the Sun. anticlockwise rotation causes it to move further out. Many NEAs show the effect of Yarkovsky drag on their orbits (Farnocchia et al. 2013).

Eros is an Amor asteroid (perihelion distance between 1.0 AU and 1.3 AU) while Itokawa and Toutatis are Apollo asteroids (perihelion distance ≤ 1.0 AU, semimajor axis ≥ 1.0 AU). Toutatis is also a Potentially Hazardous Object. This category of asteroid are defined as those with a minimum orbit intersection distance of ≤ 0.05 AU and an absolute magnitude of 22.0. Toutatis is also one of a number of asteroids, the Alinda asteroids, with orbits that have been described as chaotic, the result of a 3:1 resonance with Jupiter and a 1:4 resonance with the
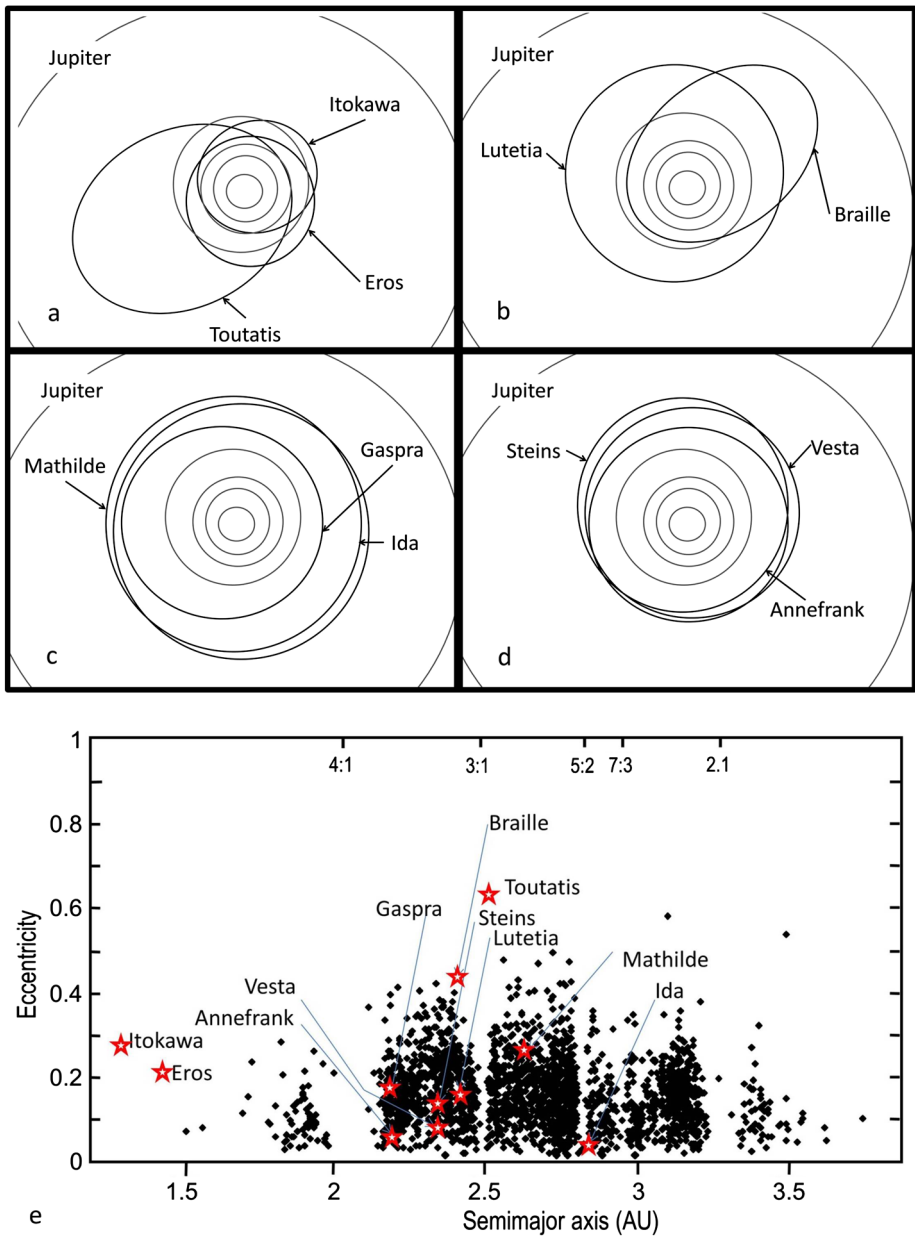
Fig. 5 (**a–d**) The orbits of the explored asteroids projected onto the ecliptic plane. (**e**) The orbits presented as an eccentricity versus semimajor axis plot with the explored asteroids superimposed

Earth. This situation results in frequent close approaches to the Earth (Krivova et al. 1994; Zausaev and Pushkarev 1994; Siregar and Soegiartini 2012).

Gaspra is a member of the Flora family, the largest of three families in the inner asteroid belt (the others being the Nysa and Vesta families). The family was first recognized by
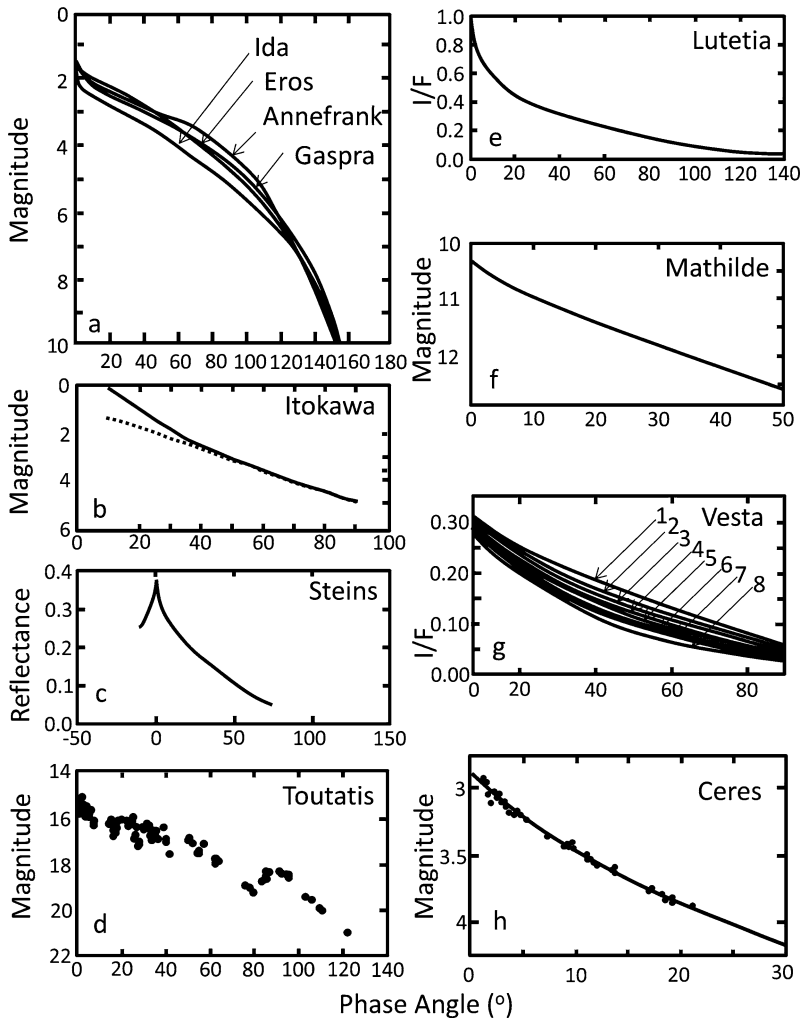
Fig. 6 Phase curves for the explored asteroids. (**a**) Annefrank, Gaspra, Ida and Eros as summarized by Hillier et al. (2011). (**b**) Itokawa from Lederer et al. (2005). (**c**) Steins from La Forgia et al. (2012). (**d**) Toutatis from Spencer et al. (1995). (**e**) Lutetia from Capaccioni et al. (2013). (**f**) Mathilde from Clark et al. (1999). (**g**) Vesta from Longobardo et al. (2014). (**h**) Ceres from Helfenstein and Veverka (1989). (The reader should refer to the original articles for several important details omitted from these sketches)

Hirayama in 1919. Its members have a large distribution in orbital elements caused by the chaotic diffusion in narrow mean motion resonances, the Yarkovsky nongravitational force, and the gravitational impulses received at close approaches with large asteroids. Thus the Flora family will dynamically disperse on the few 10^8-year time scale and its age must be significantly less than 10^9 years (Nesvorný et al. 2002).

The Koronis family, of which Ida is a member, is a family of S-class asteroids in the outer belt, a region dominated by C-class objects. The Koronis family is thought to have originated in the breakup of a 120–170 km object roughly 2 byr ago (Marzari et al. 1995).

4.2 Photometric Properties

The plot of the apparent brightness of a planetary surface as a function of solar-object-Earth or spacecraft angle (the solar phase angle, α) is referred to as the phase angle curve. Examples of curves for the asteroids that have been visited by spacecraft, sometimes including ground based data, are shown in Fig. 6. In general, brightness decreases as the cosine of the phase angle increases (Lambert's Law). The conspicuous increase at zero phase angle (the opposition effect) is probably caused by the disappearance of shadows on the asteroid. The curve can be fitted to various theoretical and empirical curves. Lumme and Bowell (1981a, 1981b) and Hapke (1981, 1984, 1986) have described rigorous treatments based on radiation transfer theory. By way of example, the Hapke equation for absolute reflectance l/F is given as:

$$\frac{l}{F} = \left[\left\{ \frac{\omega}{8} \left[(1 + B(\alpha)) P(\alpha) - 1 \right] + \left(\frac{r_o}{2} \right)(1 - r_o) \right\} \right.$$
$$\times \left\{ 1 - \sin\left(\frac{\alpha}{2}\right) \tan\left(\frac{\alpha}{2}\right) \ln\left[\cot\left(\frac{\alpha}{4}\right)\right] \right\}$$
$$\left. + \frac{2}{3} r_o \left(\frac{(\sin(\alpha) + t(\pi - \alpha)\cos(\alpha))}{\pi} \right) \right] S(\alpha, \theta)$$

where ω is the single-particle scattering albedo, α is the solar phase angle, and θ is the surface roughness parameter. B, P, and S are empirical constants that allow for the backscattering, the phase function of individual particles, and reflectance. By fitting this equation to the phase curve it is possible to deduce geometric albedo (i.e. physical albedo, reflectance at $\alpha = 0°$ divided by reflectance of a perfect reflector), bond albedo (i.e. spherical albedo, fraction of incident light scattered in all directions), and a parameter that describes the surface roughness (Table 3). The Bond albedo (A) is related to the geometric albedo (p) by the expression $A = pq$, where q is the so-called phase integral.

A comparison on the Bowell and Hapke treatments was given by Bowell et al. (1989). These authors concluded that, while both were successful, there remained difficulties. Recently Shepard and Helfenstein (2007) found that the Hapke treatment was unsuccessful in characterizing a number of known regolith simulant surfaces and suggested that the fault lies with the inability of radiative transfer models to adequately account for discrete media and the effects of porosity, and its assumption that individual particles are the primary scattering units. Li et al. (2014) also pointed out that Vesta has photometric properties similar to S asteroids, and thus that phase curves are not an effective means of determining surface properties.

The parameters in the International Astronomical Union H-G photometric system are H, the absolute magnitude, and G, the slope of the phase angle curve (see the appendix in Bowell et al. 1989). As an example, Keller et al. (2010) find that for Steins H = 12.90 and G = 0.45. Some authors fit the curve to a relationship such as $A = A_0(1 + m\alpha)$, where A is the observed amplitude, A_0 is the amplitude at zero phase angle, α is the phase angle and m is a constant governed by surface roughness. For S asteroids it is typically 0.03. As we see below, Longobardo et al. (2014) considered simply the slope of the phase curve in comparing asteroid surfaces.

Figure 6a compares phase curves for Annefrank, Gaspra, Ida, and Eros (the figure taken from Hillier et al. 2011). The Stardust mission observed Annefrank with a phase angle of 47.2–134.6°, while ground data are available for 2.3–18.3. The phase curve below 90°

Table 3 Spectral class, geometric and Bond albedo at visible wavelengths, for the explored asteroids*

Asteroid	Class[b]	References for spectra	Geometric albedo	Bond albedo	Alb Ref	H	G	H-G ref
Annefrank	S	37	0.279 ± 0.092	0.123 ± 0.039	37	13.7	–	JPL
Braille	V, Q	1, 2, 3	0.34 ± 0.03	0.14	38	15.7	–	JPL
1 Ceres (1943 XB)	G, C	1, 20	0.090 ± 0.003		56	3.34	0.12	JPL
Eros	S, S(III), S(IV)	4, 5, 6, 7, 8	0.290 ± 0.02	0.12 ± 0.02	39	11.16	0.46	JPL
Gaspra	S, S(I)	9, 10, 11, 12	0.23 ± 0.06	0.12 ± 0.03	40	11.46	0.29	50
Ida	S, Q	13	0.206 ± 0.032	0.081 ± 0.017	41	9.94	–	JPL
Dactyl	S	13	0.198 ± 0.050	0.073 ± 0.021	42			
Itokawa	S, S(III)/S(IV)	14, 15, 16	0.53 ± 0.04	0.07 ± 0.01	43	18.61–19.42	0.25	51
Lutetia	M, E, Xk, Xc	17, 18, 19, 20, 21, 22, 23, 24, 25	0.19 ± 0.01	0.073 ± 0.002	44	7.35	0.11	JPL
Mathilde	C	26, 27	0.047 ± 0.005	0.012	45	10.28	0.12	52
Steins	C, D, prob E	28, 29, 30, 31, 32	0.40 ± 0.07	0.241	46, 47	12.5	–	JPL
Toutatis	S(IV)	33, 34, 35, 36	0.13	–	48	15.30	0.10	JPL
Vesta	V	53	0.38 ± 0.04	0.18 ± 0.01	49	3.2	45–68[a]	54, 55

*Geometric albedo is the fraction of light reflected in the direction of the light source. Bond albedo is the fraction of light reflected in all directions. H and G describe the phase angle curve, H is magnitude and G is slope (Bowell et al. 1989; JPL, JPL asteroid database).

[a] G value depends on region, dark regions 67–68, bright regions 41–45, average 56–60.

[b] See text for a discussion of class assignments, some of which are from the present work. References for spectra and albedo: 1: Binzel et al. (2001a, 2001b), 2: Lazzarin et al. (2001), 3: Buratti et al. (2004), 4: Bell et al. (2002), 5: Veverka et al. (2000), 6: Clark et al. (2002a, 2002b), 7: Chapman and Morrison (1976), 8: Murchie and Pieters (1996), 9: Helfenstein et al. (1994), 10: Zellner et al. (1985), 11: Mottola et al. (1993), 12: Goldader et al. (1991), 13: Veverka et al. (2006a, 2006b), 15: Binzel et al. (2001a, 2001b), 16: Abell et al. (2007), 17: Lazzarin et al. (2004), 18: Perna et al. (2010), 19: Rivkin et al. (2011a, 2011b), 20: Tholen (1989), 21: Bus and Binzel (2002), 22: DeMeo et al. (2009), 23: Vernazza et al. (2009), 24: Vernazza et al. (2011), 25: Sierks et al. (2011), 26: Clark et al. (1999), 27: Binzel et al. (1996), 28: Barucci et al. (2007), 29: Barucci et al. (2008), 30: Fornasier et al. (2007), 31: Fornasier et al. (2008), 32: Groussin et al. (2011), 33: Howell et al. (1994), 34: Bus and Binzel (2002), 35: Davies et al. (2007), 36: Reddy et al. (2012), 37: Hillier et al. (2011), 38: Buratti et al. (2004), 39: Domingue et al. (2002), 40: Helfenstein et al. (1994), 41: Helfenstein et al. (1996), 42: Helfenstein et al. (1996), 43: Lederer et al. (2005), 44: Sierks et al. (2011), 45: Clark et al. (1999), 46: Groussin et al. (2011), 47: Jorda et al. (2012), 48: Lupishko et al. (1995), 49: Li et al. (2013), 50: Wisniewski et al. (1993), 51: Nishihara et al. (2005), 52: Mottola et al. (1995), 53: McCord et al. (1970), 54: Longobardo et al. (2014), 55: Tedesco et al. (2004), 56: Li et al. (2006).

yielded an albedo on 0.41, a roughness of 20°, backscattering −0.19 (Newburn et al. 2003; Hillier et al. 2011). Wisniewski et al. (1993) and Helfenstein et al. (1994) reported photometric data for Gaspra. The latter authors reported a geometric albedo of 0.22 ± 0.06, in good agreement with the ground based estimate. Pre-Galileo photometery for Ida was reported by Li et al. (1993). The Ida phase curve (19.5 to 109.8°), determined from ground based and Galileo data, was discussed by Helfenstein et al. (1996). They also reported a geometric albedo of $0.21^{+0.03}_{-0.01}$. Helfenstein et al. (1996) also showed the phase curve for Dactyl between 19.5 and 46.6° which was very similar to Ida's. The data for Eros are from Domingue et al. (2002) who reported Hapke parameters and calculated a Geometric albedo of 0.29 ± 0.02 and a Bond albedo of 0.12 ± 0.02.

Lederer et al. (2005) reported photometric data for Itokawa and produced the phase curve shown in Fig. 6b. This asteroid has a higher geometric albedo than average main belt S-class asteroids; this is consistent with results of other observers.

The phase curve of Steins (Fig. 6c) was reported by La Forgia et al. (2012) who performed a Hapke analysis (parameters shown on the curve) and reported that the asteroid regolith was made of large, highly scattering iron-poor opaque silicate particles with high macroscopic roughness, consistent with radar data for other E asteroids. If surface is enstatite, then grain sizes of 30–130 mm were indicated and a correlation between grain size and wavelength indicated a range of grain sizes.

The phase curve for Toutatis (Fig. 6d) was published by Spencer et al. (1995) from 0.2 to 121° using data from 25 sites at the asteroid's close approach in December 1992 and found that H = 15.3 and that the slope parameter, G, was 0.10 ± 0.10. The data were subjected to a full Hapke analysis by Hudson and Ostro (1998), deriving all the Hapke parameters and concluding that the surface of Toutatis was covered with a fine particulate regolith.

The phase curve for Lutetia (Fig. 6e) was reported in an LPSC abstract by Capaccioni et al. (2013) who had not yet made a full analysis.

For Braille there appears to be no phase curve in the literature, but Buratti et al. (2004) reported that the geometric albedo of Braille was unusually high 0.34 ± 0.03 (at 0.63 µm), which is also consistent with its placement within the rarer classes of stony asteroids, and which suggests it has a relatively fresh, unweathered surface, perhaps due to a recent collision.

For Mathilde (Fig. 6f), Clark et al. (1999) reported phase angle curves for 1–16° (ground based) and 40–136° (from NEAR spacecraft). They found a geometric albedo of 0.047 ± 0.005 (the lowest yet reported for any solar system object).

Fornasier et al. (2011) recently added high phase angle data to the phase curves of Vesta by Lagerkvist et al. (1995) and Hasegawa et al. (2009). They determined an albedo of 0.36 ± 0.02 at 649 nm and 0.34 ± 0.02 at 535 nm. Longobardo et al. (2014) report phase curves for bright, dark and whole disk regions on Vesta (Fig. 6g). These authors defined the phase slope as the reflectance decrease from 20° to 60°, relative to the reflectance at 20° for a specific wavelength and found the results in Table 4. As defined, the slope of the phase curve decreases from $\sim 70\,\%$ to $\sim 60\,\%$ to $\sim 40\,\%$ in going from C to S to Steins and Lutetia asteroids and these values are similar to the Vesta dark units, average, and bright units, respectively. They also considered the relationship between phase slope and wavelength and found little dependence, except perhaps for Stiens. Li et al. (2014) also pointed out that at 0.38, Vesta has the highest asteroid albedo.

Phase curve for Ceres from Helfenstein and Veverka (1989) are shown in Fig. 6h. The limited phase angle made interpretation of this curve difficult, but better information on surface properties will soon be available from the Dawn data.

Table 4 Phase slopes for Vesta and several other asteroids in decreasing phase slope order (Longobardo et al. 2014)

Asteroid	Type	Wavelength (μm)	Phase slope (%)	Refs[a]
Mathilde	C	0.70	69	1
Vesta dark units	V	0.75	68	2
		1.20	67	3
Eros	S	0.56	66	4
		1.49	62	4
Ida	S	0.56	62	5
Annefrank	S	0.63	62	2, 6
Vesta average	V	0.75	56–60	2
		1.20	56	7
Steins	E	0.63	57	8
Lutetia	C, D, or prob E	IR[b]	50	2
Vesta bright units	V	1.20	45	2
		0.75	41	

[a]1: Clark et al. (1999), 2: Longobardo et al. (2014), 3: Clark et al. (2014), 4: Clark et al. (2002a, 2002b), 5: Hillier et al. (2011), 6: Li et al. (2013), 7: La Forgia et al. (2012), 8: Capaccioni et al. (2013).

[b]The Lutetia phase slope is the same at all the five infrared wavelengths considered.

Table 5 Spin and orientation of spin axis of the explored asteroids

Asteroid	Rotn rate (h)		RA and Dec		
	Value	Rf	RA	Dec	Rf
5535 Annefrank (1942 EM)	15.12	1	unk	unk	–
9969 Braille (1992 KD)	226.4	2	unk	unk	–
1 Ceres (1943 XB)	9.074	26	300	53	25[a]
433 Eros (1898 DQ)	5.27	3	11.4	17.2	3
951 Gaspra (1916 S45)	7.042	5	9	28	6, 7[a]
243 Ida (1988 DB1)	4.634	8	348.76	87.10	9
Dactyl	> 8	10	unk	unk	–
25143 Itokawa (1998 SF36)	12.132	11	90.53	−66.30	12
21 Lutetia	8.165	13	342	48	15[a]
253 Mathilde (1949 OL1)	417.7	16	unk	unk	–
2867 Steins (1969 VC)	6.047	17	99	59	18
4179 Toutatis (1989 AC)	175	19	Tumbling		20
4 Vesta	5.398	21–23	308	48	24

[a]These authors reported the pole vector in ecliptic coordinates and here have been converted to RA and Dec for easy comparison.

1: Schmidt et al. (2007), 2: Oberst et al. (2001), 3: Miller et al. (2002), 4: Souchay et al. (2003), 5: Wisniewski et al. (1993), 6: Magnusson et al. (1992), 7: Barucci et al. (1992), 8: Binzel et al. (1993), 9: Davies et al. (1996), 10: Veverka et al. (1996), 11: Nishihara et al. (2005), 12: Demura et al. (2006), 13: Zappala et al. (1984), 14: Dotto et al. (1992), 15: Lagerkvist et al. (1995), 16: Torppa et al. (2003), 17: Mottola et al. (1995), 18: Lamy et al. (2008), 19: Jorda et al. (2012), 20: Spencer et al. (1995); Hudson and Ostro (1995), 21: Stephenson (1951), 22: Gehrels (1979), 23: Blanco and Catalano (1979), 24: Thomas et al. (1997), 25: Saint-Pé et al. (1993), 25: Chamberlain et al. (2007).

4.3 Rotation Rate, Orientation, and Shape

Rotation rates, orientation, and shapes can be determined from light curves (Fig. 7), from radar data (when the asteroid comes close enough to Earth), spacecraft imaging, and laser ranging. These asteroid data are summarized in Table 5. Rotation rate can be affected by gravitational interactions between the asteroid and other asteroids or planets (Scheeres et al. 2000) and by interactions with the Sun through the YORP effect (Rubincam 2000). The dominant force determining shape of most asteroids is fragmentation. If the asteroid is small, the YORP effect (Rubincam 2000; Farnocchia et al. 2013), will move surface material and affect shape. For large asteroids, the dwarf planets, isostatic adjustment, spin rate, and internal structure will determine the shape.

Annefrank (Fig. 7a) was observed for 26 minutes by Stardust and periods of ∼ 12, 15 and 23 hours were suggested by the light curves, of which 15 h was considered most likely (Schmidt et al. 2007). Annefrank was found to be at least $6.6 \times 5.0 \times 3.4$ km, with its shortest dimension normal to its orbit plane, highly angular, with flat appearing surfaces, covered with smaller, rounder bodies (Duxbury et al. 2004a; Duxbury et al. 2004b).

The rotation period of Braille (Fig. 7b) was determined from light-curve observations from four ground-based observatories and found to be 226.36 h (Oberst et al. 2001). Combining the light curves with a model based on low-resolution images suggests that Braille is $2.1 \times 1 \times 1$ km with photometric properties similar to the asteroid 4 Vesta, most notably a comparably high albedo.
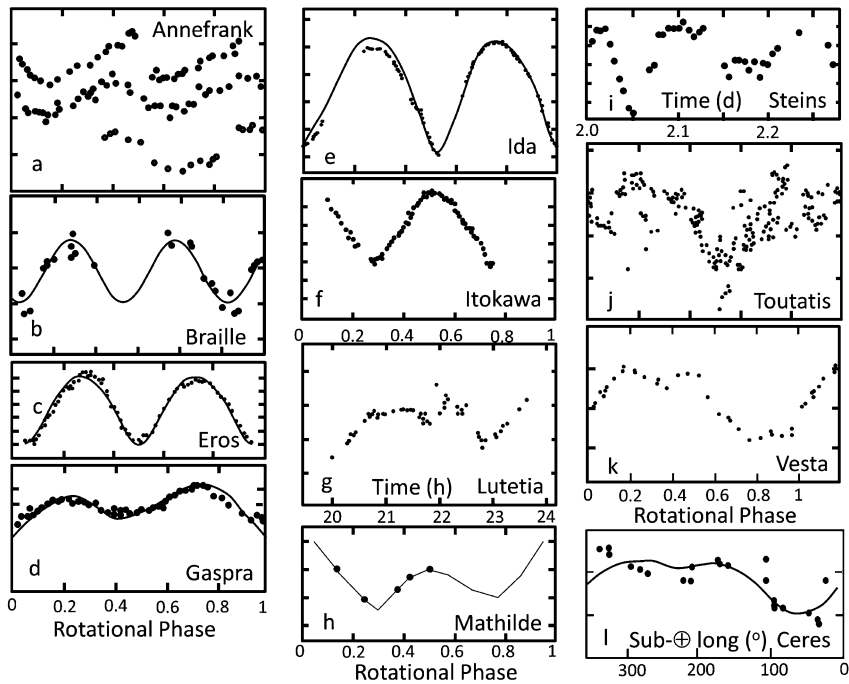
Fig. 7 Light curves for the explored asteroids, either converted to rotational phase after a period has been determined, or as a function of observation time. (**a**) Annefrank data from Schmidt et al. (2007), the three data sets correspond to different months. Three periods are possible, 12, 15, and 23 h of which the authors prefer 15 h. (**b**) Braille data from Oberst et al. (2001) with a 9.4 d sine wave compared with the prediction based on a calculated model (*solid line*). The period indicated was 226.4 h. (**c**) Eros data from Roach (1942) give a period of 5.33 h. (**d**) One of several light curves for Gaspra published by Barucci et al. (1992) in comparing the shape derived from light curves with the first images. The period is 7.042 h. (**e**) A representative light curve for Ida from Binzel et al. (1993). (**f**) A representative light curve for Itokawa from Kaasalainen et al. (2003) from which they determined a pole position of $\gamma = 355°$; $\beta = -84° \pm 5°$, a rotation period of 12.132 ± 0.0005 hours and shape aspect ratios $a = b = 2:0$ and $b = c = 1:3$. (**g**) The light curve for Lutetia taken from Lagerkvist et al. (1995). Several other authors have published light curves for Lutetia and the consensus period is 8.17 h. (**h**) The light curve for Mathilde shown is from Mottola et al. (1995) who summarized earlier results and found a period of 17.4 d. (**i**) This is one of twenty-six light curves determined for Steins by Lamy et al. (2008) who suggest a period of 6.04 h. (**j**) Spencer et al. (1995) gathered light curves for Toutatis and suggested a period of 7.3 d, however the scatter suggests that the asteroid is tumbling and will have different periodicities about three axes. (**k**) The light curve for Vesta reported by Stephenson (1951) from which he calculated a period of 5.342 ± 0.002 h. (The reader should refer to original articles for several important details omitted from these sketches). (**l**) The light curve for Ceres from Chamberlain et al. (2007)

For Eros, landmark observation and Doppler ranging give a rotation period of 5.270 h (Miller et al. 2002), in comparison with the ground based light curves of Roach (1942; Fig. 7c) produced a rotation period of 5.33 h. An accurate shape model was produced by laser ranging (Fig. 8) which gave a maximum size of 32.7 km (Zuber et al. 2000), compared with 31.4 km from visual images (Veverka et al. 2000) and 36 km from radar observations (Ostro et al. 1990). As originally indicated by the radar data, Eros is an elongated, curved shape with two large depressions (Psyche and Humerous) thought to be old eroded craters. The obliquity of Eros is very large, 89.0°, which means that the asteroid's spin axis is close to the ecliptic plane (Souchay et al. 2003). The rotation details of Eros are now sufficiently well known that it is possible to calculate the nutation of the obliquity.
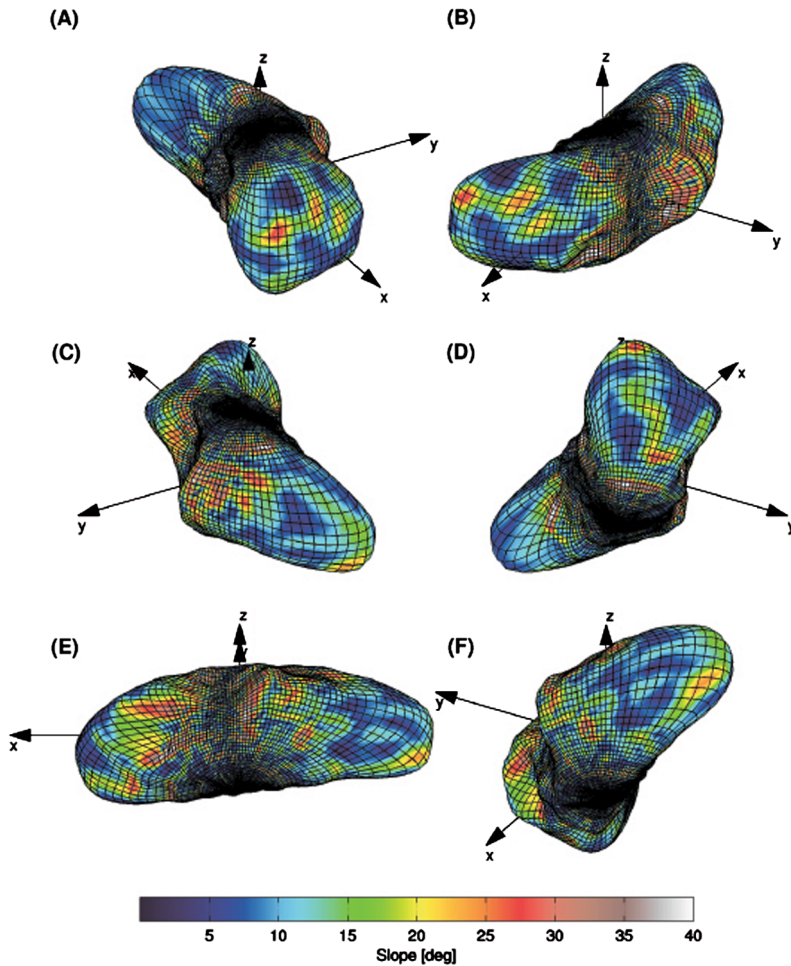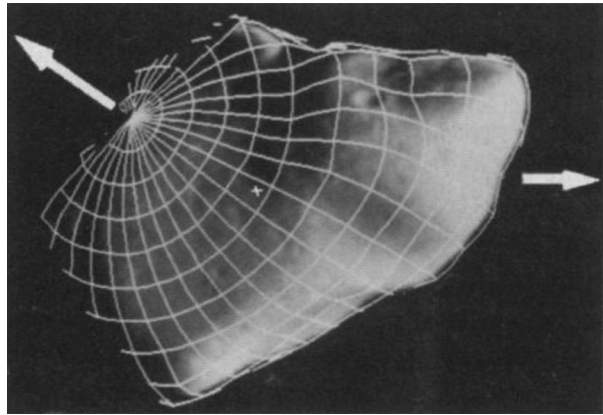
Fig. 8 Six perspective views of a three-dimensional shape model of 433 Eros from laser range finding as reported by Zuber et al. (2000). The mesh represents the scaled shape, and the surface facets are color–coded according to the surface slope with respect to a constant-density gravity field derived from the shape model. The asteroid is viewed at the following (elevation, azimuth) pairs: (**A**) 30°N, 60°E; (**B**) 30°N, 120°E; (**C**) 30°N, 0°E; (**D**) 30°S, 60°E; (**E**) 30°S, 300°E; and (**F**) 30°S, 0°E. This is a modified version of Fig. 3 in Zuber et al. (2000).

Gaspra is another asteroid whose rotation period determined from light curves has been checked against more accurate determinations by spacecraft (Fig. 7d). Barucci et al. (1992) compared the shape of Gaspra calculated from ground-based light curves with the shape observed by Galileo and concluded that light curves were now capable of making accurate shape predictions (Fig. 9). Gaspra has prograde rotation with a period of 7.04 h, with the rotation pole at a right ascension of $9.5 \pm 0.9°$ and declination of 26.7 ± 1.2 (J2000). The mean radius, axial ratios, and pole orientations from Galileo agree well with groundbased data (Magnusson et al. 1992; Wisniewski et al. 1993).

As with Gaspra and Eros, the predictions of rotation period and shape of Ida based on light curves (Fig. 7e) were confirmed by spacecraft data (Simonelli et al. 1996). There was excellent agreement in the rotation period (4.633632 ± 0.000007 h), the shapes and ampli-

tudes of the synthetic and observed light curves (Binzel et al. 1993; Thomas et al. 1996; Helfenstein et al. 1996). Ida's volume is $16,100 \pm 1900$ km^3, surface area 3900 ± 300 km^2, and maximum and minimum dimensions of 55.8 km and 15.8 km, somewhat crescent shaped with a "waist". The spin pole aligns with the model maximum principle moment of inertia axis within 2°. The mean density is 2.6 ± 0.5 g/cm^3, and surface acceleration between 0.3 and 1.1 cm/s^2 (Thomas et al. 1996).

There have been many studies of the light curve of Itokawa, mostly prompted by it being the Hayabusa target (Lambert and Tholen 2001; Lowry et al. 2001; 2005; Dermawan et al. 2002; Kaasalainen et al. 2003; Ohba et al. 2003; Nishihara et al. 2005). The example shown in Fig. 7f is from Kaasalainen et al. (2003). All report the same rotation rate and elongated shape. For example, the rotation rate estimate from Nishihara et al. (2005) is 12.1324 ± 0.0001 hours while Ohba et al. (2003) suggested that Itokawa was a triaxial ellipsoid with $a/b = 2.1$ and $b/c = 1.7$. These values were essentially borne out by the images from the Hayabusa mission.

Because of its small size and well-known characteristics, there has been interest in whether the YORP effect on the rotation rate of Itokawa can be detected (Scheeres et al. 2007; Lowry et al. 2014). Ďurech et al. (2008) placed an upper limit of $\sim 1.5 \times 10^{-7}$ rad d^{-2} on the YORP effect on Itokawa, which is inconsistent with the theoretical value of -2 to -3×10^{-7} rad d^{-2}. This prompted Scheeres and Gaskell (2008) to propose that the offset in Itokawa's center of mass and center of figure by 15 m would reverse the sign of the rate change, a conclusion that was not confirmed by Breiter et al. (2009).

Many light curve analysis for Lutetia (Fig. 7g) were reported by several authors which allowed the determination a synodic rotational period of 8.17 ± 0.01 hours (Zappala et al. 1984; Dotto et al. 1992; Lagerkvist et al. 1995). A determination of its shape, pole coordinates and a prograde sense of rotation are reported in Magri et al. (1999). Torppa et al. (2003), on the basis of available observations, determined new pole coordinates and a model shape (sharp and irregular) with rough global dimensions $a/b = 1.2$ and $b/c = 1.2$.

The slow rotation of Mathilde was described by Mottola et al. (1995) who used 52 days of ground based observations, from February to June 1995, to calculate a rotation period of 17.406 ± 0.010 days and a light curve amplitude of 0.45 ± 0.02 mag (Fig. 7h). A slight deviation from single periodicity, with secondary period of 33 days, was interpreted as evidence for a complex rotation state. Spacecraft images indicate that Mathilde has principal diameters of $66 \times 48 \times 44$ km with a mean radius of 26.4 ± 1.3 km, somewhat smaller than the value of 30 km suggested by previous telescopic data (Veverka et al. 1999a, 1999b).

For Steins (Fig. 7i), 26 light curves indicate a period of 6.04681 ± 0.00002 hours (Lamy et al. 2008). The global shape observed in spacecraft images resembles a top with dimensions along the principal axes of inertia of $6.83 \times 5.70 \times 4.42$ km. It is conspicuously more regular than other small asteroids like (233) Eros and (25 153) Itokawa. Its mean radius is 2.70 km and its equivalent radius (radius of a sphere of equivalent volume) is 2.63 km. The north pole is oriented with a RA of $99 \pm 5°$ and Declination of $59 \pm 5°$, so Steins has a very large obliquity of 172° and a retrograde rotation (Jorda et al. 2012).

Keller et al. (2010) likened the shape of Steins to that of binary near-Earth asteroid 1999 KW4, which Scheeres et al. (2006) and Ostro et al. (2006) attributed to spin-up by the YORP effect. The typical time scale associated with YORP is 250 My for a 5-km main-belt asteroid (Rubincam 2000). However, the rotation period of 6 hours is too long to induce shape changes, and one would have to invoke a faster rotation rate in the past. YORP induced torques can cause material to slide towards the equator to form the cone.

Toutatis has made several close passages by Earth and each has been used to obtain high quality light curves and radar data. A representative light curve is shown in Fig. 7j, which was obtained by data from 25 observatories during the September 1992 close approach, is shown in Spencer et al. (1995). A period of 7.3 days is indicated but the scatter on the curves suggests other periodicities are present, and the asteroid is tumbling (Harris 1994; Pravec et al. 2005). Because of the large number of near-Earth passages and the complex spin state of Toutatis, the effect of gravitational interactions and YORP effects have been investigated and both found to influence its spin state (Rubincam 2000; Scheeres et al. 2000). Harris (1994) argues that the dampening time for complex spinning is so large, that most asteroids larger than 0.4 km are tumbling, although this will only be apparent in the light curve if the asteroid is elongated. The shape model determined by radar observations of Toutatis also during the 1992 approach are shown in Fig. 10 (Ostro et al. 1995). The time delay on the reflected radar signal provides a measure of distance and the Doppler shift provides in indication of movement towards or away from the Earth, so by plotting time delay against radial velocity and a grey scale to reflect differences from the mean, an indication of shape as the asteroid tumbles can be produced. The radar images suggest Toutatis is a bifurcated object with lobes of differing size, the longest dimension of the asteroid being along the lobe-lobe line. The radar data also indicated non-principle axis rotation of period of 1 to 2 days. These shape results are borne out by 76 images of Toutatis returned by the Chang'e 2 spacecraft (Fig. 4l). Huang et al. (2013) found that the maximum physical length and width of Toutatis are $(4.75 \times 1.95$ km$) \pm 10$ %, respectively, and the orientation of the pole was RA $= 250 \pm 5°$ and Dec. $= 63 \pm 5°$, with respect to the J2000 ecliptic coordinate system.

Examples of early light curves for Vesta are those published by Stephenson (1951), Gehrels (1979), Blanco and Catalano (1979) and others. An example of one of the curves is shown in (Fig. 7k). The presence of only one minimum and one maximum indicated the near spherical shape of Vesta and gave a rotation rate of 5h 20m 29.3s with an ecliptic longitude and latitude of the north pole at $126 \pm 5°$ and $65 \pm 4°$.

Images of Vesta from the Hubble Space Telescope enabled improved estimates of the size, shape, and rotation rate of Vesta prior to Dawn's arrival (Thomas et al. 1997; Trombka et al. 1997; Drummond and Christou 2008; Li et al. 2011). Vesta's shape can be fitted by an ellipsoid of radii $280 \times 272 \times 227 (\pm 12)$ km. Using the mass determination for Vesta reported by Schubart and Matson (1979), and the Hubble estimate for volume, Thomas et al. (1997) derive a density of 3.8 ± 0.6 g/cm^3. For this density Vesta's shape is close to that of a Maclaurin spheroid with variations of ~ 15 km. Three independent methods now yield a pole position for Vesta of RA $= 305.8 \pm 3.1$, Dec. $= 41.4 \pm 1.5$ (Li et al. 2011). When the Dawn spacecraft provided new data on mass, volume, and gravitational field,
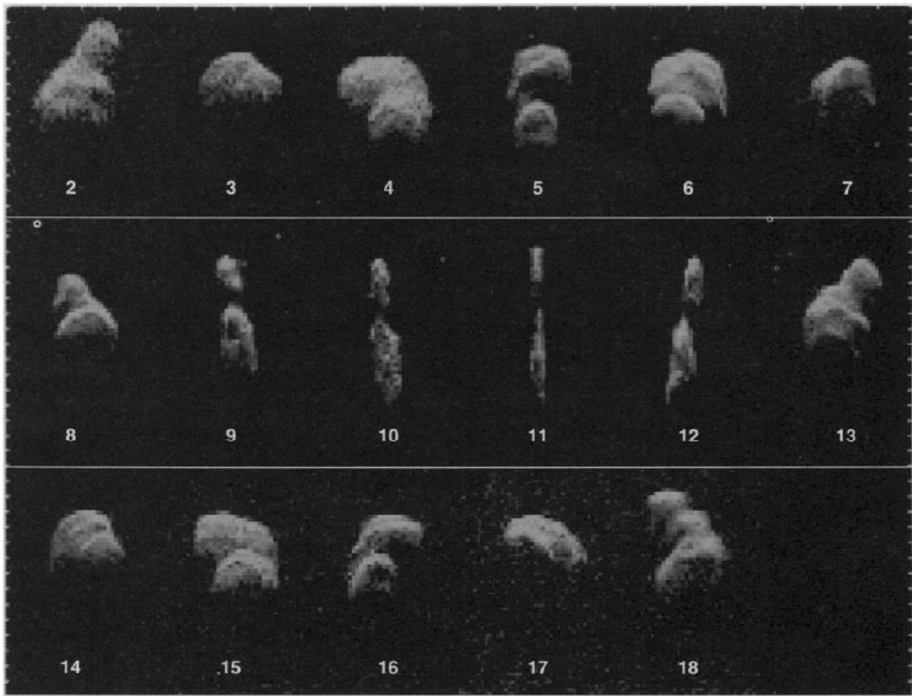
Fig. 10 Toutatis radar images. Goldstone low-resolution images plotted with the same time delay increasing toward the *bottom* and Doppler frequency increasing toward the *left*. Numbers indicate the date in December 1992. On the vertical sides, *ticks* are 2 μs apart. Two horizontal sides have *ticks* separated by 1 Hz for Goldstone and 0.28 Hz for Arecibo; those intervals correspond to a radial velocity difference of 18 mm s^{-1}. Gray scales were designed to show the extent of the delay Doppler distributions. (Ostro et al. 1995)

it was inferred that Vesta has a metallic core 107–113 km in radius (Russell et al. 2012; Raymond et al. 2014). Prior to the Dawn mission the pole position was determined from HST observations to be at an RA and Dec of $301 \pm 5°$ and $41 \pm 5°$ (Thomas et al. 1997; Drummond et al. 1988) or $305.8 \pm 3.1°$ and $41.4 \pm 1.5°$ (Li et al. 2010), but after Dawn our best estimates are $309.03300 \pm 0.00003°$ and $42.22615 \pm 0.00002°$ (Konopliv et al. 2014).

The light curve for Ceres at 335 nm was recently published by Li et al. (2006) and their curve, which agrees with the data of earlier workers, is shown in Fig. 7l. These authors found that the light curve could not be matched by the rotationally symmetric shape of Ceres and concluded that it was governed by the presence of albedo variations on the surface and concluded there were eleven surface albedo features, 40–350 km in size, present. They numbered the regions, except for one that had previously been detected and named "Piazzi" by Parker et al. (2002). The shape of Ceres less flattened that would be expected for a homogeneous body suggests that Ceres is differentiated, with a water-rich mantle and rocky core (Thomas et al. 2005).

By way of a summary, the rotation rate and size data are shown in Fig. 11, superimposed on a diagram for all asteroids by Pravec and Harris (2000). Most of the present asteroids with periods of 4 to 20 hours plot along the main field of asteroids, however three are slow rotators, Braille, Toutatis and, especially, Mathilde. Rotation rate is a major factor in performing exploration activities near asteroids and to date all the asteroids have been relatively slow
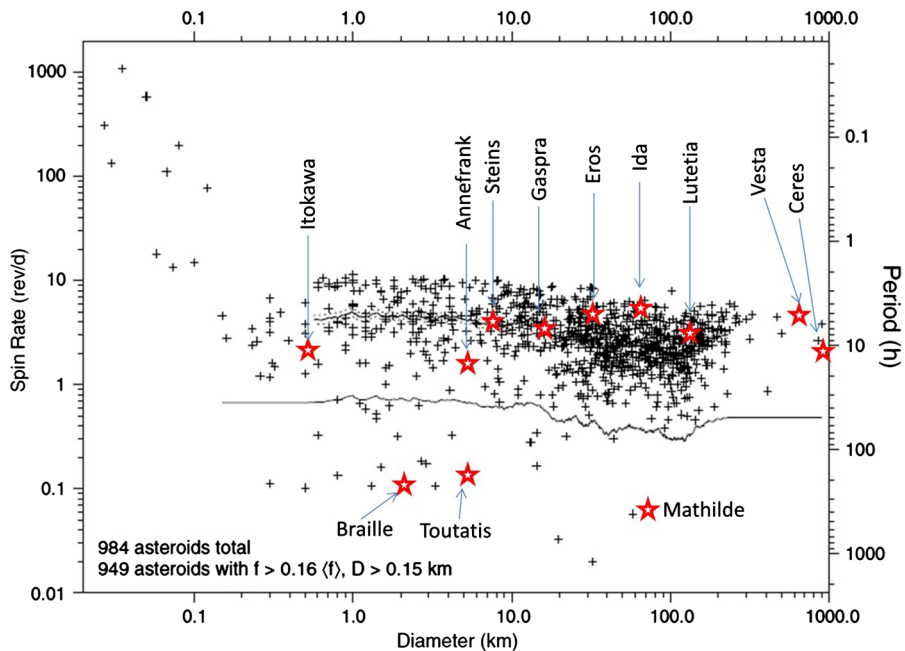
Fig. 11 Plot of spin rate versus diameter for asteroids (from Pravec and Harris 2000). A five point floating average is indicated, and repeated a decade lower for clarity. Superimposed on this plot are data for the asteroids that have been explored by spacecraft

rotators. There will be a major challenge if the Asteroid Retrieval Mission (KISS 2012) attempts to capture a 3–5 m asteroid since it will probably be rotating rapidly.

4.4 Mass, Volume, Density, Gravity and Magnetic Field

A summary of the physical properties of the explored asteroids is given in Table 6. Masses are best determined from the orbital dynamics of a nearby spacecraft, or moon in the case of Dactyl. Volume can then be determined from images and the all-important density can be determined from these. As a point of reference, the density of meteorites ranges from 2.5 g/cm^3 for the water-bearing CI chondrites to ~ 8.0 g/cm^3 for iron meteorites, the most common values being ~ 3.3 g/cm^3 for differentiated meteorites (including the HEDs which are thought to come from Vesta) and ~ 3.4 g cm^{-3} for the ordinary chondrites (which are subdivided into the H, L, and LL chondrites and constitute the largest classes of meteorites falling on Earth). Where spectroscopic data suggests a linkage between a given class of asteroids and a given class of meteorites, differences in density can be ascribed to macroscale porosity of the asteroid which, in turn, has been used to infer whether the asteroid was a monolith or a rubble pile.

The Galileo encounter with Gaspra was not close enough to enable the mass of the asteroid to be determined, but taking self-gravity and rotation into account Thomas et al. (1994) calculate acceleration due to gravity to be 0.38 cm/s^2 near the equator and 0.57 cm/s^2 at the north pole, assuming that the average density was 3.5 g/cm^3. Thus g on Gaspra is about 1/2000 of the terrestrial value. Fluctuations were experienced in the magnetic field around Gaspra which, if caused by a magnetized Gaspra, would indicate magnetization of

Table 6 Physical properties of the explored asteroids[*][†]

Asteroid	Mass (kg)	Volume (km³)	Density (g/cm³)	Rf	Accel. due to gravity (cm/s²)	Rf	V_{esc} (m/s²)	Rf	Magnetic field (T)[a]	Rf
5535 Annefrank (1942 EM)	unk	unk	unk	–	unk	–	unk	–	unk	–
9969 Braille (1992 KD)	7.8×10^{12}	2.00	3.9	1	0.01–0.05	13	0.7–1.0	13	$\leq 9.3 \times 10^{-5}$	1
1 Ceres (1943 XB)	9.0×10^{20}	4.36×10^{17}	2.06	14	29	14	510	14	unk	–
433 Eros (1898 DQ)	6.7×10^{15}	2.51×10^{3}	2.67	2	0.04–0.35	13	5.1–8.9	13	unk	–
951 Gaspra (1916 S45)	8.4×10^{15}	2.40×10^{3}	3.5 ass	3	0.38–0.57	3	7.8–11.3	13	$0.04–1.4 \times 10^{-4}$	4
243 Ida (1988 DB1)	4.2×10^{16}	1.62×10^{4}	2.6	5	0.31–1.11	5	10–17	13	$2.5–6.5 \times 10^{-5}$	6
Dactyl	unk	unk	unk	–	unk	–		–	unk	–
25143 Itokawa (1998 SF36)	3.6×10^{10}	1.8×10^{-2}	1.95	7	0.001–0.003	13	0.1–0.2	13	unk	–
21 Lutetia	1.7×10^{18}	5.0×10^{5}	3.4	8	0.8–2.0	13	43–55	13	unk	–
253 Mathilde (1949 OL1)	1.0×10^{17}	7.8×10^{4}	1.3	9	0.15–0.31	13	14–17	13	unk	–
2867 Steins (1969 VC)	1.37×10^{14}	7.6×10^{1}	1.8 ass	10	0.08–0.13	10	1.7–2.0	13	unk	–
4179 Toutatis (1989 AC)	1.92×10^{14}	7.6×10^{1}	2.5 ass	11	0.05–0.2	11	1.2–1.8	11	unk	–
4 Vesta	2.71×10^{20}	7.74×10^{17}	3.3	12	8.0–13.0	13	300–340	13	unk	–

[*] Abbreviations: Rf, references; Accel., acceleration; ass, assumed; eq, equator; po, pole; unk, unknown; bd, below detection.

[†] For comparison, Earth's values are: Mass, 5.97×10^{24} kg; volume, 1.08×10^{21} km³; density, 5.51 g/cm³; acceleration due to gravity, 981 cm/s²; magnetic field, $0.25–0.65 \times 10^{-4}$ T.

[a] It is unclear whether the magnetic field measured is caused by the asteroid or by perturbations in the interplanetary magnetic field.

1: Richter et al. (2001), 2: Yeomans et al. (2000), 3: Thomas et al. (1994), 4: Kivelson et al. (1993), 5: Thomas et al. (1996), 6: Blanco-Cano et al. (2003), 7: Abe et al. (2006a, 2006b), 8: Pätzold et al. (2011), 9: Veverka et al. (1999a, 1999b), 10: Jorda et al. (2012), 11: Scheeres et al. (1998), 12: Viateau and Rapaport (2001), 13: This work, calculated from data in the table, 14: Hilton (2002).

the asteroid comparable to the observed magnetization of iron meteorites or mostly highly magnetized ordinary chondrites (Kivelson et al. 1993). This could be to impact induced magnetization (Meadows 1972; Chen et al. 1996) or an internal dynamo in the Gaspra precursor (Weiss and Elkins-Tanton 2013). Alternatively, Blanco-Cano et al. (2003) suggested that there were details in the Galileo magnetometer results that were inconsistent with a magnetized asteroid and they suggested that the solar wind perturbations were caused by the effects of a conducting surface.

From its gravitational interactions with Dactyl, and Galileo images of Ida, the mass of Ida is known to be $4.2 \pm 0.5 \times 10^{16}$ g and its density is 2.6 ± 0.5 g/cm^3 (Belton et al. 1996a, 1996b). Dactyl's mass is unknown. The surface gravity of Ida varies between 0.31 and 1.11 cm/s^2, being greatest in the regions of highest and lowest relief; at high relief the rotation of the asteroid lowers the value and at low relief the underlying mass is least (Thomas et al. 1996). As with Gaspra, Galileo detected disturbances in the solar wind attributable to a magnetized Ida, but the cause of the magnetization is unclear, impact and a molten core have been advocated as mechanisms for magnetizing planetary surfaces (Hood and Huang 1991; Chen et al. 1996; Blanco-Cano et al. 2003).

Radio science enabled a determination of the mass of Mathilde of $1.033 \pm 0.044 \times 10^{17}$ kg and the volume could be derived from the images (Yeomans et al. 1997). The average density of Mathilde is remarkably low, 1.3 ± 0.3 g/cm^3, a value consistent with a rubble pile structure for the interior. If Mathilde's composition is similar to that of CM meteorites, the porosity of the interior must be ~ 50 % (Veverka et al. 1999a, 1999b).

The mass and density of Braille are 7.80×10^{12} kg and 3.9 g/cm^3 (Table 1 in Richter et al. 2001). The encounter of asteroid Braille by Deep Space 1 also detected evidence for substantial levels of magnetization, although major corrections had to be made for the magnetic field of the spacecraft (Richter et al. 2001). Arguments for the cause of the asteroid's magnetism are the same as for Gaspra and Ida.

Radio science for the NEAR spacecraft at Eros yielded a mass of $6.687 \pm 0.003 \times 10^{15}$ kg which, coupled with a volume estimate based on images, implies a bulk density of 2.67 ± 0.03 g/cm^3. Escape velocities on the surface vary from 3.1 to 17.2 m/s (Yeomans et al. 2000). Unlike Gaspra, Ida and Braille, Eros has only extremely low levels of magnetization (Acuña et al. 2002; Anderson and Acuña 2002)

From Hayabusa data for Itokawa, Abe et al. (2006a, 2006b) calculated a mass of $3.58 \pm 0.18 \times 10^{10}$ kg and a density of 1.95 ± 0.14 g/cm^3. Assuming an LL chondrite grain density for solids in Itokawa, this implies a bulk porosity of ~ 40 %. Hayabusa did not carry a magnetometer and there is no information about a magnetic field at Itokawa.

The gravitational perturbation of Lutetia on the Rosetta spacecraft four hours before to six hours after closest approach was used to determine the asteroid's mass as $1.700 \pm 0.017 \times 10^{18}$ kilograms. Using the shape model of Lutetia determined from the images, the bulk density was found to be 3.4 ± 0.3 g/cm^3 (Pätzold et al. 2011). As with Steins, the magnetometer on Rosetta was not able to detect any evidence for magnetization on Lutetia (Richter et al. 2012). The bulk density of Lutetia is comparable to the density of enstatite, the composition possibly consistent with its reflectivity spectrum (but see below), which suggests either considerable compression, even sintering, so that porosity is extremely small, say a few percent, or that the interior is differentiated (Weiss et al. 2012). In that the surface appears not to be magnetized, there is no direct evidence for a core.

The mass of Vesta was well-known before the Dawn encounter. Vesta's mass has been determined many times from the gravitational interactions with passing asteroids and its size has been determined from a variety of ground-based techniques; milar micrometry, radiometry, speckle interferometry, occultation, and HST imaging. The data were summarized by Viateau and Rapaport (2001). These authors determined that the mass of Vesta is
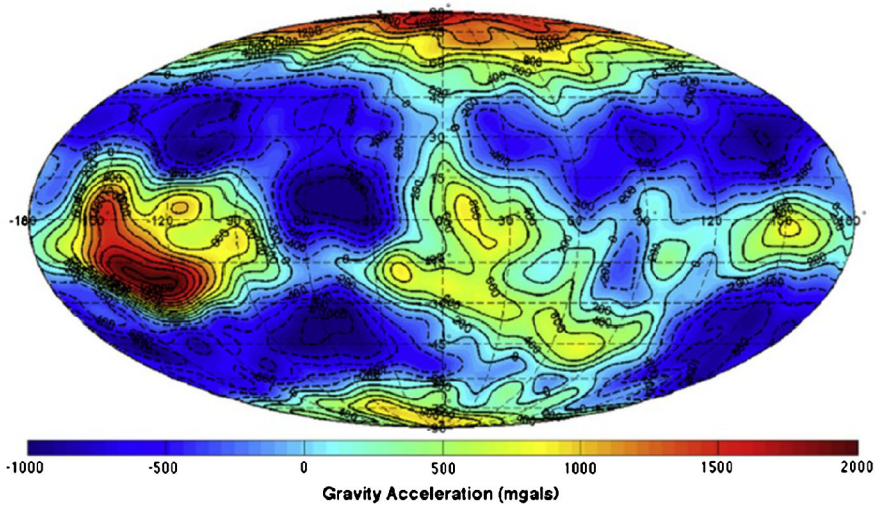
Fig. 12 The Vesta radial gravity solution. The J2 coefficient (which describes oblateness) has been removed. The maximum and minimum range is given by 2100 mgals at the large equatorial high near 126°W longitude and ∼ 1270 mgals also near the equator at 44°W (Konopliv et al. 2014)

$2.705 \pm 0.032 \times 10^{20}$ kg, and that its effective diameter ($D_{e} = 2(abc)^{1/3}$ where $2a$, $2b$ and $2c$ are the ellipsoid axes) is 531 ± 24 km. Thus the density of Vesta is 3.3 ± 0.5 g/cm^3. However, data from tracking the Dawn spacecraft have enabled the mass to be determined to better than one part in a million and a precise gravity field to be obtained (Fig. 12). The acceleration due to gravity varies from a large equatorial high of 2100 mgals (gal $= 1$ cm/s^2) near 126°W longitude to a low of -1270 mgals near the equator at 44°W. A large gravitational anomaly at 15°S, 140°W corresponds to a plateau called Vestalia Terra which is discussed below (Konopliv et al. 2014; Raymond et al. 2013).

While we have determinations of the size and shape of Annefrank (Duxbury et al. 2004a; Duxbury et al. 2004b), we do not have a determination of its mass and gravity field, presumably because it is too small and the Stardust spacecraft did not pass close enough. Similarly, the spacecraft did not carry magnetometers, so we have no information on magnetic field.

The mass of Steins is also unknown, but assuming a bulk density of 1.8 g/cm^3 (calculated from a grain density of 3.0 g/cm^3 and a porosity of 40 %), and a proposed shape model with a volume of 76 ± 11 km^3, Jorda et al. (2012) calculated accelerations due to gravity on Steins are 0.08–0.13 cm s^{-2}. Although Rosetta is equipped with a magnetometer, it did not detect any evidence for magnetization at Steins (Auster et al. 2010).

Toutatis is too small for a mass to be determined from its influence on the orbit of Chang'e 2, but from its dimensions, and assuming a density of 3.0 g/cm^3, we can calculate a mass of 2.3×10^8 kg. There is no information on whether Toutatis has a magnetic field.

Stellar occultation studies yields an equatorial radius for Ceres of 479.6 ± 2.4 km and a polar radius of 453 ± 4.5 km which corresponds to a density of 2.7 ± 0.1 g cm^{-3} (Millis et al. 1987). The shape of Ceres has been at the center of discussion concerning the interior structure. Thomas et al. (2005) argued that the flattening suggested by the stellar estimates of dimensions implies a differentiated interior, but there has not been agreement on this (Zolotov 2009; McCord and Sotin 2005). Anticipating the Dawn encounter, Konopliv et al. (2011) expect Ceres' gravity field to be much smoother than Vesta's because of its more
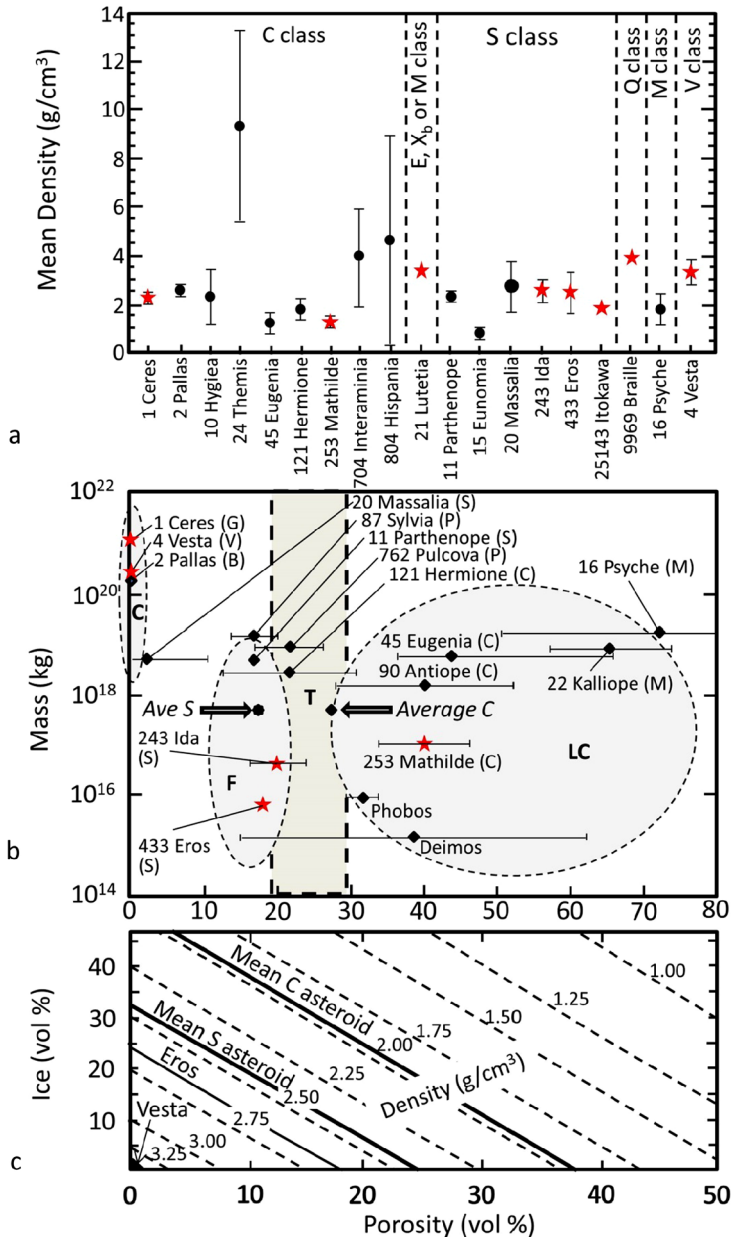
Fig. 13 The density and porosity of asteroids. Asteroids being discussed in the present paper are indicated by *stars*. (**a**) Density of 19 asteroids of various class (after Viateau and Rapaport 2001). Most asteroids have densities of 2–4 g/cm³, with S asteroids averaging about 1.5 times C asteroids. The only asteroid with the density of metallic iron is the C asteroid 24 Themis, but the uncertainty is large. (**b**) Mass plotted against porosity for 16 asteroids of various classes and Phobos and Deimos (Britt et al. 2002). The fields indicated C, F, T, and LC, refer to coherent asteroids, fragmentary asteroids, transitional asteroids, and loosely coherent asteroids (probably rubble piles), respectively. (**c**) Mass balance calculation for the density of asteroids assuming various amounts of pore space and ice or chemically bound water (Sears et al. 2015). The density of Ceres is close to the "mean C asteroid" in this plot

spherical shape. There is no evidence of a magnetic field on Ceres, although the relatively high magnetization of meteorites has caused Elkins-Tanton et al. (2011) to propose that there might be a magnetic field on the meteorite source asteroids and this would be consistent with Ceres being differentiated perhaps with an iron core.

The density data are summarized in Fig. 13a, which is an updated version of a figure taken from Viateau and Rapaport (2001). Although there is a lot of scatter and the uncertainties are sometimes large, we can generalize that C asteroids have densities of ~ 2.0 g/cm^3 while S asteroids have densities 2.5–3.0 g/cm^3. The difference in the asteroid observed density and the density of the presumed meteorite equivalent led Britt et al. (2002) to calculate macroporosities and from these to deduce internal structures (Fig. 13b). According to these authors, based on macroporosity, Vesta is a coherent asteroid, Ida and Eros are fractured asteroids, while Mathilde is a loosely coherent asteroid (possibly a rubble pile). These porosities assume water contents equal to those found in the meteorite analogues. If there is more water inside these asteroids than indicated by the meteorites (which are presumably surficial samples) then the estimated porosity would drop accordingly (Fig. 13c).

5 Geological Properties of the Explored Asteroids

5.1 Maps and Names

Blue et al. (2013) summarized the current status of naming surface features on asteroids and cites a USGS website where maps sanctioned by the IAU can be found (http://planetarynames.wr.usgs.gov/Page/Images). At the time of writing, the IAU recognizes names for features on Eros (41 named features), Gaspra (34), Ida (25), Dactyl (2), Itokawa (17), Lutetia (37), Mathilde (23), Steins (24), and Vesta (106). The geography of asteroids are discussed in, more-or-less, the order of their exploration because this also reflects increasing levels of detail that were possible. Summaries of the names of most features on asteroids, taken from the IAU/USGS website or specially prepared for this article (with help from Philip Stooke) are shown in Fig. 14. A summary the features that have been described on asteroids and some specimen literature references is shown in Table 7; detailed descriptions of these surface features appear below. An understanding of the nature of the surface of asteroids is critical to understanding their history and in preparing for future exploration efforts. A system of nomenclature facilitates these processes.

Gaspra consists of three main regions noted for their flatness (Fig. 14a; Belton et al. 1992). These have been named Dunne, Yeates, and Neujmin (the first two are persons associated with the Galileo mission, the third is the asteroid's discoverer). The large number of small (< 3 km) craters are, like Gaspra itself, are named after spa towns.

Mathilde's surface is noted for the presence of four craters with diameters comparable to the radius of the asteroid, Karoo (33.4 km), Ishikari (29.3 km), Damodar (28.7 km), Kuznetsk (28.5 km), the remaining 19 named craters (named after coal fields, given the low albedo of Mathilde) going down to 2.2 km in size (Fig. 14b).

The surface of Ida is dominated by craters and a ridge known as Townsend Dorsum (also named after a person associated with the mission) (Fig. 14c). The ridge seems to represent a resistant plane through the asteroid, perhaps an impact related fault (Thomas et al. 1996). The named craters are 0.8 to 11.8 km in diameter (named after caves, since Zeus was hidden in a cave on Mount Ida). Three regions are recognized, Paliza Regio, Pola Regio, and Vienna Regio (these being the asteroid's discoverer and the two cities he observed from).

Table 7 Representative references for descriptions of surface features on asteroids*

|	Craters	Regolith	Ejecta	Boulders	Grooves/ridges	Ponds	Pits/pitted terrain	Gullies
5535 Annefrank (1942 EM)	nd	nd	nd	nd	nd	nd	nd	nd
9969 Braille (1992 KD)	nd	nd	nd	nd	nd	nd	nd	nd
433 Eros (1898 DQ)	4	4	[4], [23], 12	4, 27, 28	32	4	4	
951 Gaspra (1916 S45)	1	16	[16]	[16]	25, 30			
243 Ida (1988 DB1)	2	15	15	15, 25, 26	31			
Dactyl	15	nd	nd	nd	nd	nd	nd	nd
25143 Itokawa (1998 SF36)	6	18	[6]	6, 29		6		
21 Lutetia	7–9	7, 9	7–9	7				
253 Mathilde (1949 OL1)	3	17	24	[17]				
2867 Steins (1969 VC)	10–12	10, 19	[10, 19]	nd			19	
4179 Toutatis (1989 AC)	13	13, 20	[13]	13				
4 Vesta	14	21	14	14			33	34

*A reference locates a description, square brackets are references that refer to the absence of these features. nd means that images are not sufficient for comment. No entry means no information known to the author.

1: Chapman et al. (1996a), 2: Chapman et al. (1996b), 3: Chapman et al. (1999), 4: Robinson et al. (1999), 5: Durda et al. (2002), 6: Fujiwara et al. (2006), 7: Sierks et al. (2011), 8: Jutzi et al. (2013), 9: Vincent et al. (2012), 10: Marchi et al. (2010), 11: Besse et al. (2012), 12: Keller et al. (2010), 13: Zou et al. (2014), 14: Jaumann et al. (2012), 15: Belton et al. (1996a, 1996b), 16: Belton et al. (1992), 17: Thomas et al. (1999), 18: Miyamoto et al. (2007), 19: Keller et al. (2010), 20: Hudson and Ostro (1998), 21: Russell et al. (2012), 22: Durda et al. (2012), 23: Chapman et al. (2002), 24: Thomas et al. (1999), 25: Sullivan et al. (1996), 26: Lee et al. (1996), 27: Thomas et al. (2001), 28: Veverka et al. (2001), 29: Saito et al. (2006), 30: Veverka et al. (1994), 31: Asphaug et al. (1996), 32: Procter et al. (2002), 33: Denevi et al. (2012), 34: Scully et al. (2012).
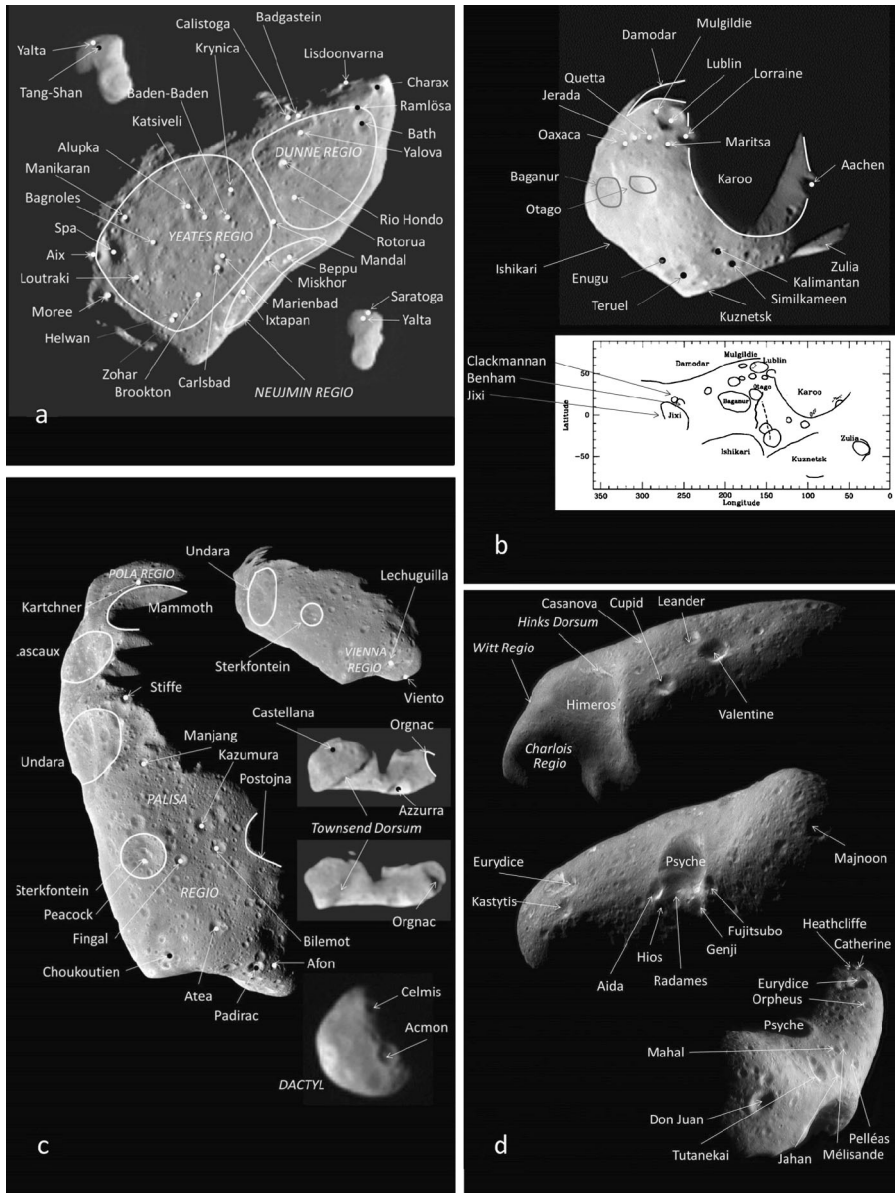
Fig. 14 Surface features of the explored asteroids. (**a**) Gaspra, (**b**) Mathilde, (**c**) Ida and Dactyl, (**d**) Eros. The maps for Gaspra, Ida, Dactyl and Mathilde were taken from the IAU website in February 2014 and include all the named features at that time. The maps for Eros were assembled for the present work with considerable help from Philip J. Stooke, University of Western Ontario, and exclude Avtandil, Bovary, Casanova, and Finsen Dorsum which are not visible in these views. (**e**) Itokawa, (**f**) Steins, (**g**) Lutetia, (**h**) Vesta. The maps for Itokawa, Steins, and Lutetia, Toutatis were taken from the IAU website in February 2014 and include all the named features at that time. The maps for Vesta were assembled for the present work with considerable help from Philip J. Stooke, University of Western Ontario, and include only a selection of named features, Vesta being too large and the number of named features too many, to be included on global images. (**i**) Ceres. Eventually, the features on Ceres will named after various deities associated with agriculture. (NASA/JPL, image PIA 19063)
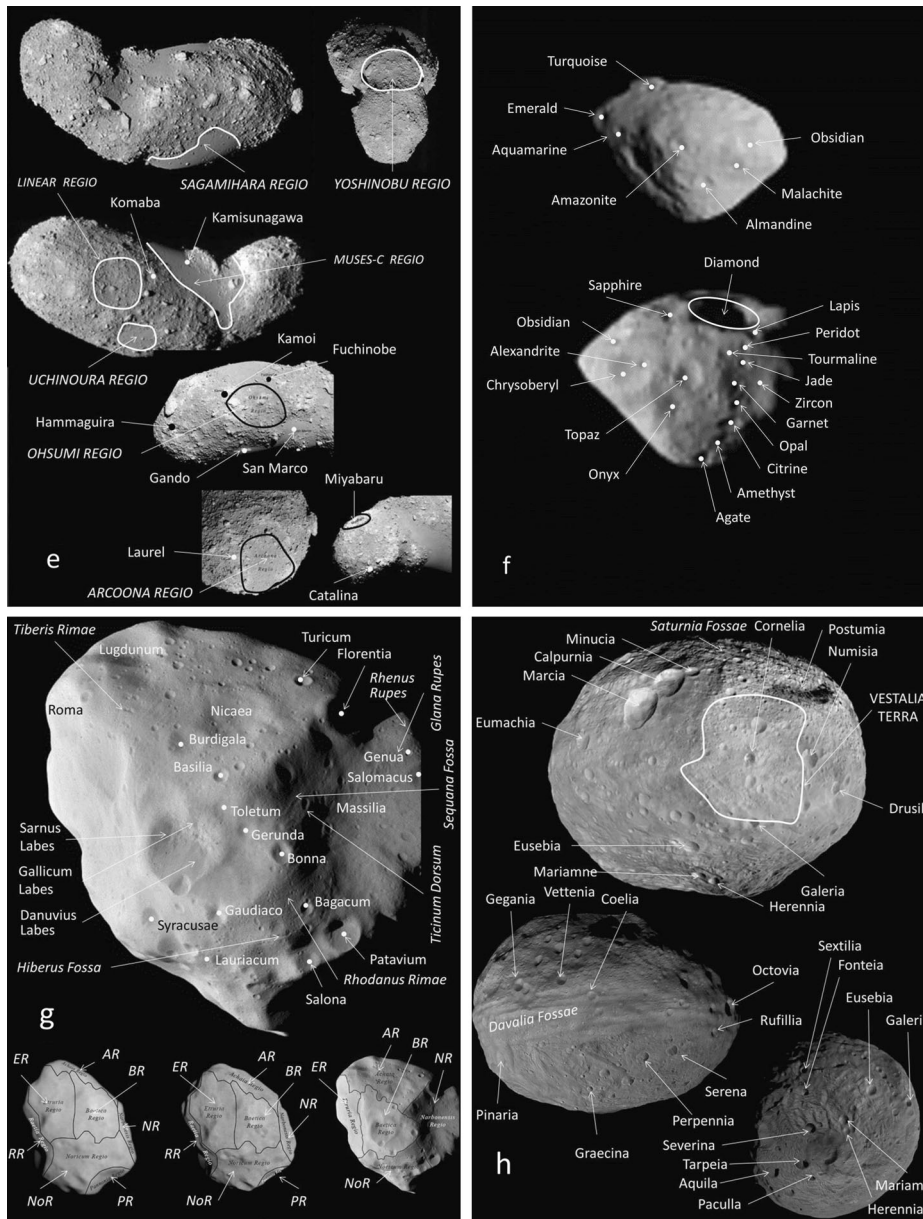
Fig. 14 (*Continued*)

Thomas et al. (1996) distinguish two regions, separated by a "waist" made up of numerous depressions. The two regions are distinguished by their crater populations. Region 1 (which includes the Pola regio) contains only small (< 6 km) craters, while region 2 (Paliza and Vienna regio) contains the larger craters. Asphaug et al. (1996) suggest that Vienna Regio is actually a crater. Two craters on Dactyl have been named Celmis and Acmon (after two of the three Dactyls, the inhabitants of Mount Ida).

i
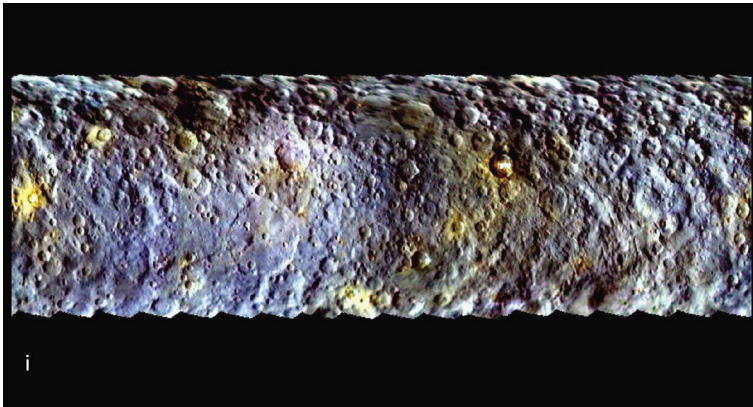
Fig. 14 (*Continued*)

The major surface features on Eros are an 11 km diameter crater called Himeros and a 7 km depression once called Shoemaker Crater but now recognized as the Charlois region on the convex side of this banana-shaped asteroid (Fig. 14d). On the concave side there is a 5.3 km diameter crater Psyche (Veverka et al. 2000; Thomas et al. 2002a). The craters on Eros are named after famous lovers. A second region is recognized, Witt region. Thus the two identified regions on Eros are named after the co-discoverers of the asteroid. On the 1 km to 100 m scale, Eros is marked by a series of randomly oriented groove and ridge patterns on a heavily cratered surface (Veverka et al. 2000, 2001; Procter et al. 2002; Thomas et al. 2002b). Two systems of ridges, Hinks Dorsum (previously Rahe Dorsum) and Finsen Dorsum (previously Calisto Fossae), constitute a plane through the asteroid that is usually interpreted a fault (Veverka et al. 2000; Thomas et al. 2002a; Procter et al. 2002; Robinson et al. 2002) and Greenberg (2008) argues is a plane of material resistant to impact, perhaps an igneous dike.

On the tiny asteroid Itokawa, seven regions and ten craters have been named after cities associated with space exploration and the mission (Fig. 14e). MUSES-C regio, Sagamihara regio, and Uchinoura regio are conspicuously smooth regions of fine-grained deposits, while the Ohsimu regio, LINEAR regio, Yoshinobu regio, Miyabaru regio, Arcoona regio are boulder strewn regions, some boulders being large enough to give unofficial names. Saito et al. (2006) state that 20 % of the surface of Itokawa is "smooth" and 80 % is "rough". The named craters (< 10 to 40 m) are randomly distributed around the asteroid in both types of region.

The large number of small craters on Steins are shallow and degraded, with a depth-to-diameter ratio of ~ 0.12 (Keller et al. 2010). Most conspicuous is a 2.1 km crater called Diamond which is located near the south pole from which a series of circular indentations and irregular ridges extend (Fig. 14f). A chain of seven craters (a catena) maybe cogenetic and connected with the formation of the crater, perhaps by loose surface material filling a fracture and draining. Opposite the catena is a groove surrounded by small pits and craters. A region on Steins is named after the discoverer, Nikolai Stepanovich Chernykh, while the craters are named after gemstones, in homage to the diamond shape of the asteroid.

On the basis of crater densities, cross-cutting and overlapping relationships, and features such as faults, fractures and grooves, Sierks et al. (2011) identified seven regions on Lutetia; Baetica, Achaia, Etruria, Narbonensis, Noricum, Pannonia, and Raetia (named after Roman
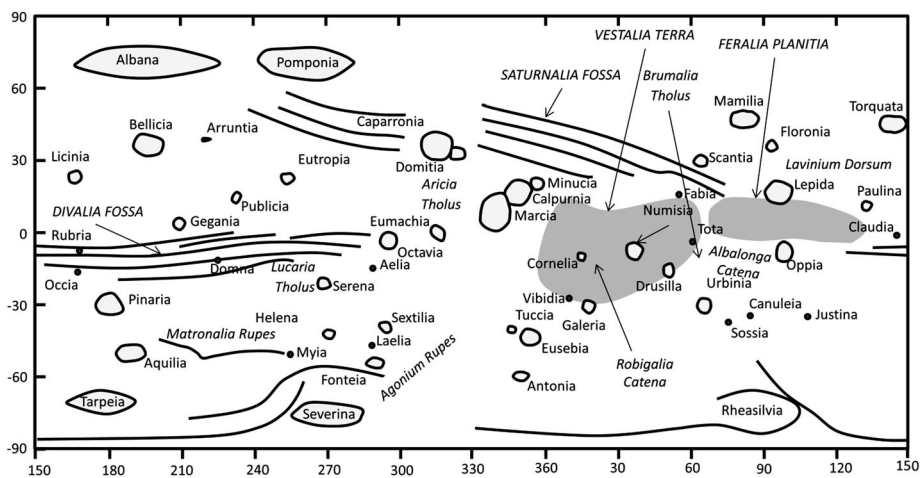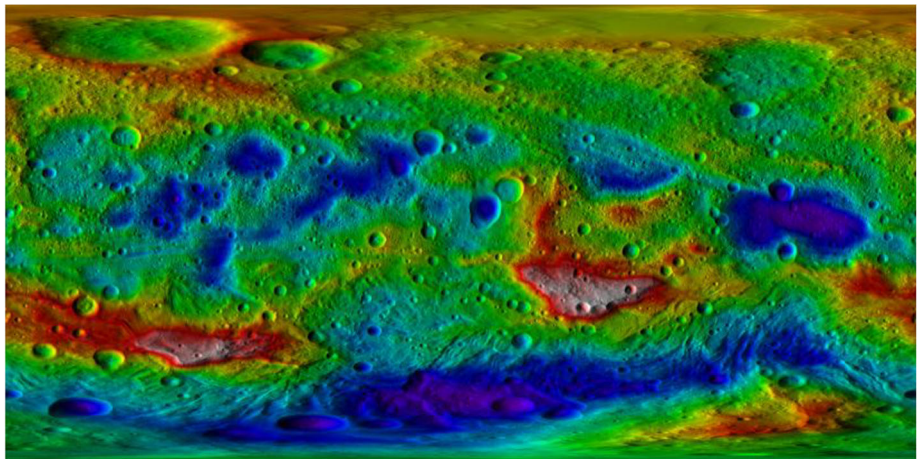
Fig. 15 (**a**) Topographic map of Vesta relative to a 285 × 285 × 229 km ellipsoid, *purple* is 22.47 km below the reference surface and *white* is 19.48 km above the reference surface. The map was constructed from 17,000 images from Dawn's framing camera. (**b**) Below is a sketch map of Vesta from the USGS/IAU indicating the accepted names. (**c**) Albedo map of Ceres identifying the regions with distinct albedo (Li et al. 2006). Regions 1–6 are bright regions, 7–11 are *dark regions*. The three *strips* refer to different wavelengths, 535 (*top*), 335 and 223 nm

provinces, Lutetia being the name for the Gallo-Roman city on the site of present-day Paris) (Fig. 14g). The dominant feature is probably a 21 km cluster of craters in the Baetica region in which there have been landslides and possibly the exposure of bedrock. The adjacent Noricum region is notable for its high crater density relative to Baetica (craters on Lutetia are named after Roman cities), suggesting that Baetica is covered with regolith produced as crater ejecta. There are curvilinear features on Lutetia (named after Roman rivers), which cut through craters and debris aprons. The polar region has a thick regolith that appears to have flown there down a gravity gradient (Sierks et al. 2011).

Vesta is a large asteroid with a great diversity of surface features (Fig. 14h); craters (87 currently with names), crater chains (catena, 2), a ridge (dorsum, 1), grooves (fossae, 2),
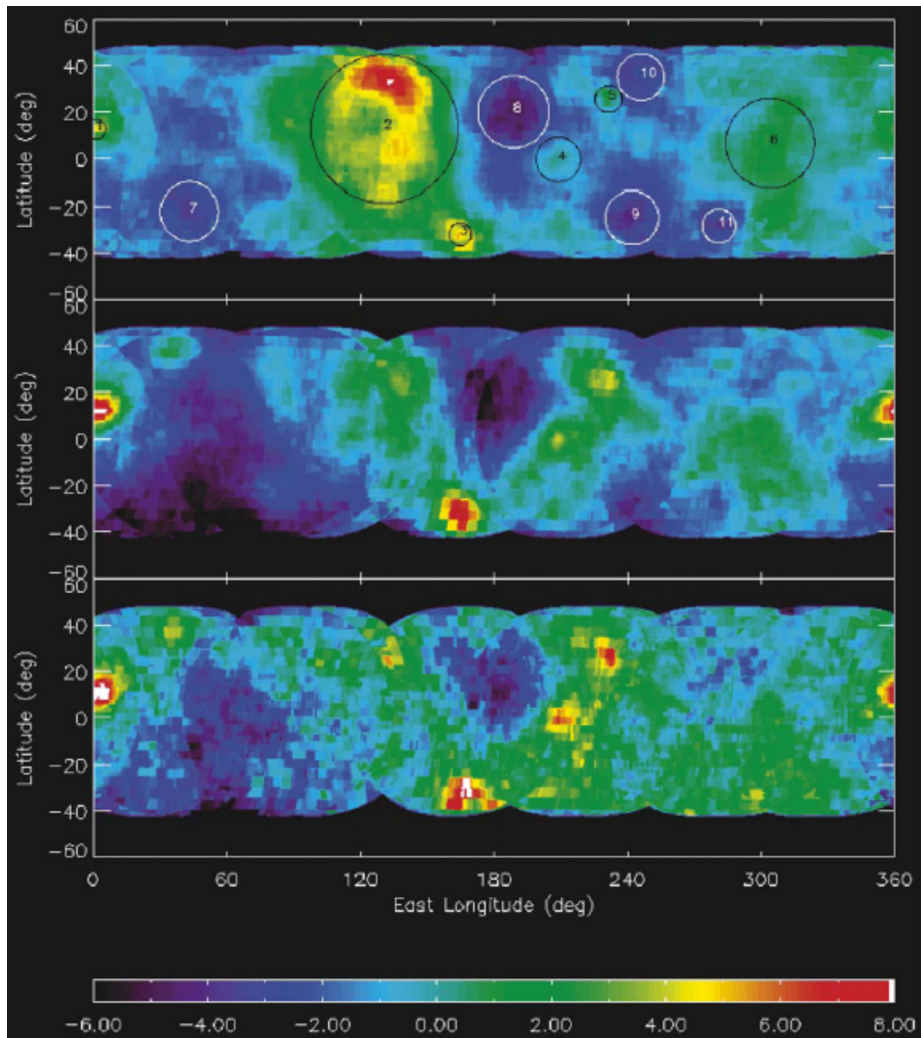
Fig. 15 (*Continued*)

a plain (terrae, 1), scarps (rupes, 2), hills (domes, tholi, 3), all with names associated with ancient Rome (the craters—with rare exceptions—named after Vestal Virgins) (Fig. 15). Details of its mapping procedure were described by Preusker et al. (2012).

Vesta's major geographical features are two overlapping south polar craters, Rheasilvia (500 km wide 19 km deep) and Veneneia (450 km and 15 km deep), with Rheasilvia being the more recent (Schenk et al. 2012). A central peak in Rheasilvia is twice the height of Hawaii and almost 80 % the size of Olympus Mons, the largest volcano in the solar system (Russell et al. 2012). The ejecta around the two polar craters form some of the highest mountains on Vesta.

Concentric with these two massive basins are sets of long narrow depressions, Divalia Fossa which are parallel to the equator and centered on Rheasilvia, and Saturnalia Fossa which are about 10° to the equator and centered on Veneneia. Buczkowski et al. (2012) de-

scribe these features in some detail and conclude that they are graben, the result of downward displacement of blocks as a result of parallel faulting, whose formation was associated with the impacts. They are distinct from the grooves and fractures commonly seen on smaller asteroids which are also thought to be impact-related.

Merging with a rim area of the Rheasilvia basin is a region of elevated topography (∼ 20 km higher than its surroundings and about 275 km across) is called Vestalia Terra (Jaumann et al. 2012). It is associated with a gravitational anomaly (and has been referred to as a mascon) but its origin is unclear. It might reflect an early igneous event or be related in some way to differences in impact gardening (Raymond et al. 2013). Adjacent to Vestalia Terra is Feralia Planitia, at 270 km (and 15 km deep) one of the larger basin-like features on Vesta (Garry et al. 2012).

As of the time of writing, the only geographical description of Toutatis is that it consists of two lobes with a number of unnamed craters and boulders (Zou et al. 2014).

Ground and Hubble-based observations have identified eight dark patches on Ceres, one of which is named after Piazzi, the others are identified by A-F (Fig. 15c) (Parker et al. 2002; Carry et al. 2012). Recent observations by Dawn have given the first glimpse of the dwarf planet and these were reported at the 2015 Lunar and Planetary Science Conference (Russell et al. 2015; Nathues et al. 2015; Zambon et al. 2015). A map was recently produced (Fig. 14i) which shows a cratered covered surface and several arcuate grooves that emanate from a large basin. The many features will be named after agricultural deities. There are also intriguing bright spots located in several craters that might be exposed ice or evaporite minerals. Rivkin and Volquardsen (2010) recently reported rotationally resolved spectra for Ceres and concluded that the surface is essentially homogeneous, although they may have detected differences associated with the bright areas.

5.2 Surface Features

5.2.1 Craters

The principles of impact cratering and its importance in understanding the history of planetary surfaces has been described at length in books such as that of Melosh (1989) and Osinsky and Pierazzo (2013). Some examples of craters on the present asteroids are shown in Fig. 16. Craters provide information on the age of a planetary surface through their degradation and through their number density. Other information is provided when they bring fresh material to the surface and when there are interactions with surface constituents, such as water, which is noteworthy in the case of Vesta.

On a plot of cumulative frequency vs. size, the crater data plot along curves with negative slope whose steepness (typically with a value of −3) is determined by the size distribution of incoming objects and whose placement is related to the age of the surface, the age increasing as the curves move to the right until the surface is "saturated", i.e. so heavily cratered that new craters are being formed at the rate they are being destroyed by subsequent impacts (Fig. 17a). The details of the method have been explained in numerous textbooks (e.g. Hartmann 1983) and a detailed example of calibrating these curves in the case of an asteroid was given in footnote 24 of Belton et al. (1992). The overall crater populations for the various asteroid surfaces suggest the same production function (i.e., same projectile power-law size distribution). A kink in the curve is usually interpreted as an erasure event that removed the smaller craters. An erasure event might be a large impact that buried existing smaller craters under ejecta.
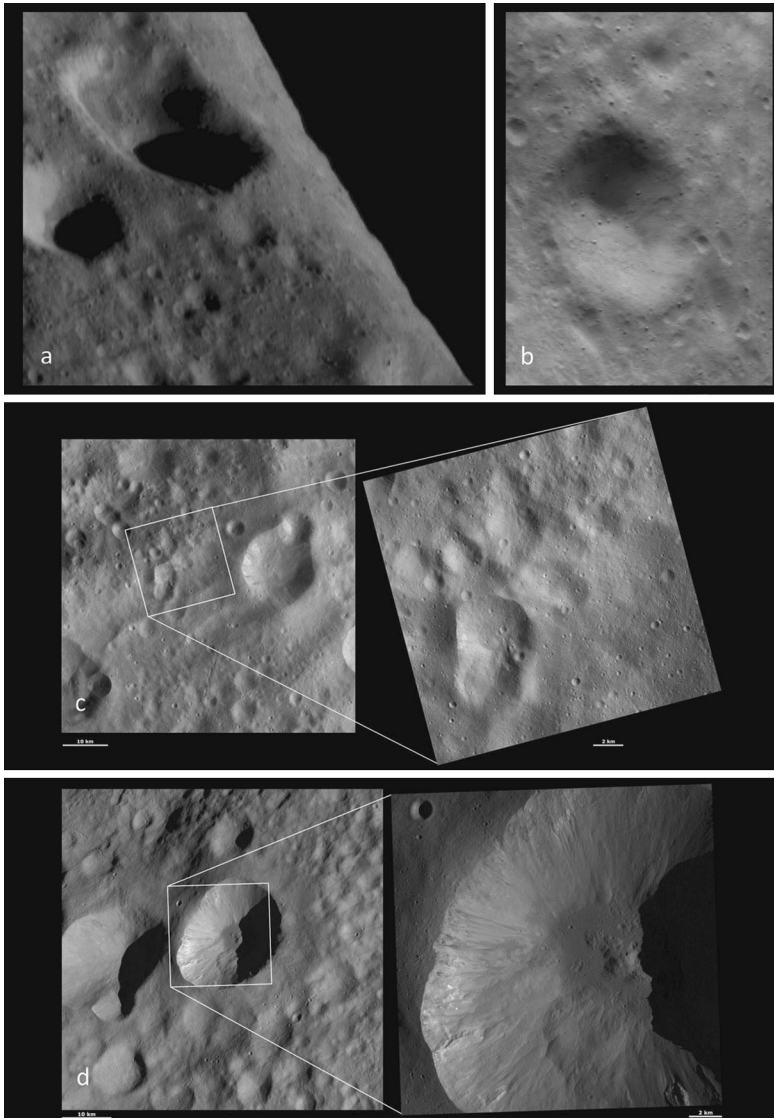
Fig. 16 Craters on asteroids. (**a**) Two relatively old craters (2.2 km and 1.6 km) on Eros' rim taken from an altitude of 100 km with a field of view 3 km Image (NASA/JHUAPL, image 20000830). (**b**) A 950 m diameter crater on Eros which is "middle-aged", i.e. still has a bowl shape but cratered and subdued form, taken obliquely at an altitude of 52 km with vertical field of view of 2.2 km (NASA/JHUAPL, image 20000828). (**c**) Claudia crater on Vesta from an altitude of 700 km (resolution 63 km/pixel) and 272 km (resolution 19 m). Claudia is the small (0.7 km) crater but is important because, being small and near the equator, it is the center of the coordinate system chosen for Vesta. This field of view shows many typical Vesta craters, which are old and worn down until they are simply depressions. In contrast, the many small younger craters, like Claudia, have sharp outlines. (NASA/JPL, image PIA15872). (**d**) Licinda crater from an altitude of 700 km (63 m/pixel resolution) and 272 km (19 m/pixel resolution). Licinia crater is the large crater that does not entirely fit into the *left* image. Licinia has a small mound of material, surrounded by darker, smooth material, with many tiny craters on this smooth material. There are also lobes of material slumping onto this smooth material from the sides of the crater. Further up the crater's walls, there are fine-scale streaks of dark and bright material originating from just underneath Licinia's scalloped rim. (NASA/JPL, image PIA16049)
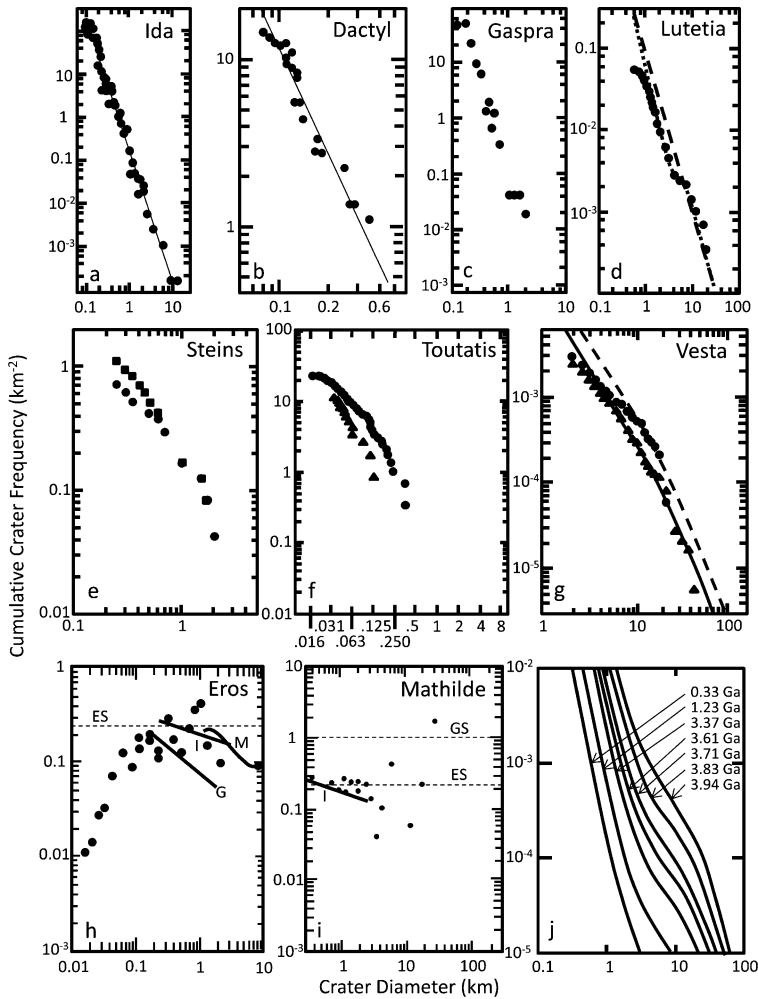
Fig. 17 Cumulative frequency curves for craters on the explored asteroids. (**a**) Data for Ida from Chapman et al. (1996a) suggest a surface age of ~ 2 billion years. (**b**) The data for Dactyl resemble the results for Ida (Chapman et al. 1996a). (**c**) Data for Gaspra from Chapman et al. (1996b) suggests a surface age of 200 Ma. (**d**) The Archaia region on Lutetia is large and flat and best suited to crater counting gives a surface age of 3.6 ± 0.1 billion years (*dotted line*, Sierks et al. 2011). (**e**) The cratering density of Steins varies with region, giving ages that range from a few million years to about a billion years (Marchi et al. 2010). (**f**) For Toutatis, crater densities are higher on the large lobe than the small lobe (Zou et al. 2014), but the asteroid and the crater numbers are too small for age determination. (**g**) Crater statistics for Vesta (Schenk et al. 2012). These authors did not attempt to estimate surface ages for Vesta but did report ages for the Rheasilvia impact (*solid line*) is 1.0 ± 0.2 Ga and the age for the Veneneia impact (*broken line*) is 2.1 ± 0.2 Ga. (**h**) Chapman et al. (1999, 2002) published their crater statistics as "R-plots", or spatial density, the differential cumulative frequency divided by D^{-3}, where D is the crater diameter. On such plots, saturation is horizontal (ES refers to equilibrium saturation). Here the R-plot for Eros, from Chapman et al. (2002), is compared with those for Ida (I), Mathilde (M), and Gaspra (G). (**i**) Mathilde has a small number of large craters and was not suitable for the determination of surface ages by crater counting. I refers to the data for Ida on this plot, GS and ES are geometric saturation and equilibrium saturation, respectively. (**j**) Diagram to illustrate how crater densities are used to estimate the age of a planetary surface. This application to Mars uses a calibration developed by Gerhard Neukum, DLR (Michael 2013). The reader is referred to the original publications for important details that are omitted from these sketches

We will now discuss the crater properties for each of our asteroids, in the order they were explored. Unfortunately, Annefrank and Braille were not observed well enough to determine the nature and number of craters on their surface, and Itokawa is too small for meaningful crater population studies.

Chapman et al. (1996) provides a detailed discussion of Gaspra's craters. Gaspra is smooth with fresh craters, young surface, seven large concavities are probably large old regolith covered craters. Greenberg et al. (1994) and Chapman et al. (1996b) have published statistics for Gaspra craters (Fig. 17b). Using the arguments similar to that of Belton et al. (1992) for calibration, these crater densities suggest a surface age for Gaspra of only 200 Ma.

In contrast to Gaspra, Ida has a much larger crater density and a much large range in levels of degradation, suggesting a much older surface, perhaps ∼2 Ga (Chapman et al. 1996a; Fig. 17c). There are also regional differences. The crater population of Dactyl has also been determined (Fig. 17d) and resembles Ida's. However, unusual features, such as a crater chain and possibly a crater with a central ejecta block, suggest that the impactor population may be different on Dactyl and have a large component of projectiles of local origin, that is, from the break up that formed the Koronis family.

As mentioned above four or five large craters are comparable to the radius of Mathilde. Chapman et al. (1999) found that the small to intermediate-sized craters (1 = 2 to 5 km diameter) a range of degradation states similar to Ida and approach saturation (quasi-equilibrium between the creation and the destruction of craters by subsequent impacts). The crater size distribution for Mathilde is shown in Fig. 17e. Since the impact history on Mathilde is dominated by a few large impacts, determining an age from the cratering statistics has not been practical.

The surface of Eros is dominated by craters. In fact, the overall shape of the asteroid is the result of several large cratering events (Robinson et al. 2002). The depth-diameter ratio of Eros' craters is typically ∼0.13, with the freshest craters approaching the lunar ratio of ∼0.2. The event that created the large (7.6 km) Shoemaker crater caused many large blocks of ejecta to be strewn the surface of Eros (Thomas et al. 2001). These Shoemaker ejecta blocks have been the subject of size distribution and theoretical studies (Durda et al. 2012; Chapman et al. 2002; Dombard et al. 2010). The internal shape of the craters is not influenced by internal strata in the asteroid, unlike on lunar mare regolith where lava flows underlie the surface regolith. The density of small craters below 200 m in diameter, compared to that expected for a saturated surface, is less than expected and this probably reflects their obliteration by regolith (Robinson et al. 2002) rather than a sweeping of small projectiles out of the solar system by the Yarkovsky effect as suggested by Chapman et al. (2002) (see O'Brien (2009)). Chapman et al. (2002) also determined the crater statistics for Eros and their data are shown in Fig. 17f. These data indicate a surface age of ∼ 2 Ga and thus dates from the period when Eros was in the main belt, its expected lifetime on its present near-Earth orbit being a few tens of millions of years.

While, Itokawa is too small for crater density plots, the asteroid is very well-studied and ten craters have been named (Fujiwara et al. 2006). They range in diameter from about 90 m (Miyabaru) to less than 10 m (Gando and San Marco).

Marchi et al. (2010), Besse et al. (2012), and Keller et al. (2010) discussed the craters on Steins. Crater diameters range from 150 to 2100 m with depth-to-diameter ratios of 0.04–0.25, with a marked difference on the two sides of the asteroid. Marchi et al. (2010) calculate surface ages from crater densities of a few hundred Ma to over 1 Ga (Fig. 17g), while Keller et al. (2010) found ages of 0.4± 0.2 and 1.6± 0.5 Ga for the two sides. There is a notable lack of craters less than 0.6 km. This is thought to be related to the impact that created the largest crater, Diamond, which extensively damaged the "original" Steins. Crater

destruction, erasure, direct or indirect infill by seismic shaking, and even the YORP effect have been invoked to explain the lack of small craters.

Lutetia craters have been discussed by Sierks et al. (2011), Jutzi et al. (2013), Vincent et al. (2012). The cumulative frequency plot from Sierks et al. (2011) appears in Fig. 17h and, for craters larger than 5–8 km, resembles those of Ida and Mathilde. Depth-diameter ratios are typically 0.12 but vary from region to region. In the Beatica region (the north polar region) small craters are covered by a thick ejecta blanket. For the large flat Archaia region, the age of the surface from crater counts was found to be 3.6 ± 0.1 Ga. The kink in the curve probably reflects the loss of small craters by blanketing.

Vesta's surface is also characterized by abundant impact craters; some with ejecta blankets (Jaumann et al. 2012). There is a marked north-south dichotomy with craters being more abundant in the northern hemisphere than in the southern hemisphere. This is almost certainly because of burial of craters in the south by ejecta from two massive impacts at the South Pole (Marchi et al. 2012). The two large impact basins at the southern pole of Vesta were studied by Schenk et al. (2012) who determined their ages by counting craters at the bottom of the craters and found ages for both Rheasilvia and Veneneia to be ∼1 Ga (Fig. 17i). Post Rheasilvia craters have been studied by Kneiss et al. (2014).

Zou et al. (2014) find higher crater densities on the larger lobe of Toutatis than on the smaller lobe, but the cause is unclear, a difference in age or a difference in erasure (Fig. 17j).

Ceres is also covered with craters, some with a central uplift and some without. Nathues et al. (2015) point out that the crater diameter at which simple craters transition to craters with a central uplift is consistent with the model described by Bray and Schenk (2015) which is ∼5 km. In addition to the many craters, there is a 270 km basin on Ceres which appears to be infilled and smooth.

5.2.2 Regolith

The regolith is defined as a layer of fragmental debris of relatively low cohesion that overlies a solid surface (Fig. 18). As originally defined, it excluded crater ejecta referring only to that fine-grained material made by a constant flux of micrometeorites (Shoemaker et al. 1968). However, as detailed observations were made, particularly of the Moon, it became impossible to separate regolith from crater debris, both the fine-grained material and boulders (Cintala and McBride 1994). In view of their microgravity, and the energetics of impact, the paradigm was that small bodies could not retain regoliths (Housen et al. 1979), but this paradigm has been overturned by robotic missions to asteroids. Whether or not asteroids retain a regolith is of major interest for a number of reasons. They provide information on the history of the surface. They modify the effects of large impacts by enhancing energy absorption, thus the amount of melting is greater than for impact into solid surfaces. They have a major impact on surface operations of robotic and crewed mission, whether it is sample collection or the mobility of dust and its physical and electrical properties. Unfortunately, the surfaces of Braille, Annefrank and Dactyl were not observed with sufficient resolution to observe regoliths.

When the first images of an asteroid were seen it was notable that Gaspra's surface morphology appeared subdued (Fig. 4a). Ridges that define the asteroid's shape were smooth. This suggested a regolith many tens of meters thick. At the same time, brighter materials associated with craters and the crests of ridges had stronger 1-micrometer absorption features in their spectra, suggesting freshly excavated mafic materials, while darker materials with weaker 1-micrometer absorptions appeared concentrated in interridge areas. This was interpreted as evidence for a thin regolith on Gaspra, that had migrated downslope (Belton et al. 1992).
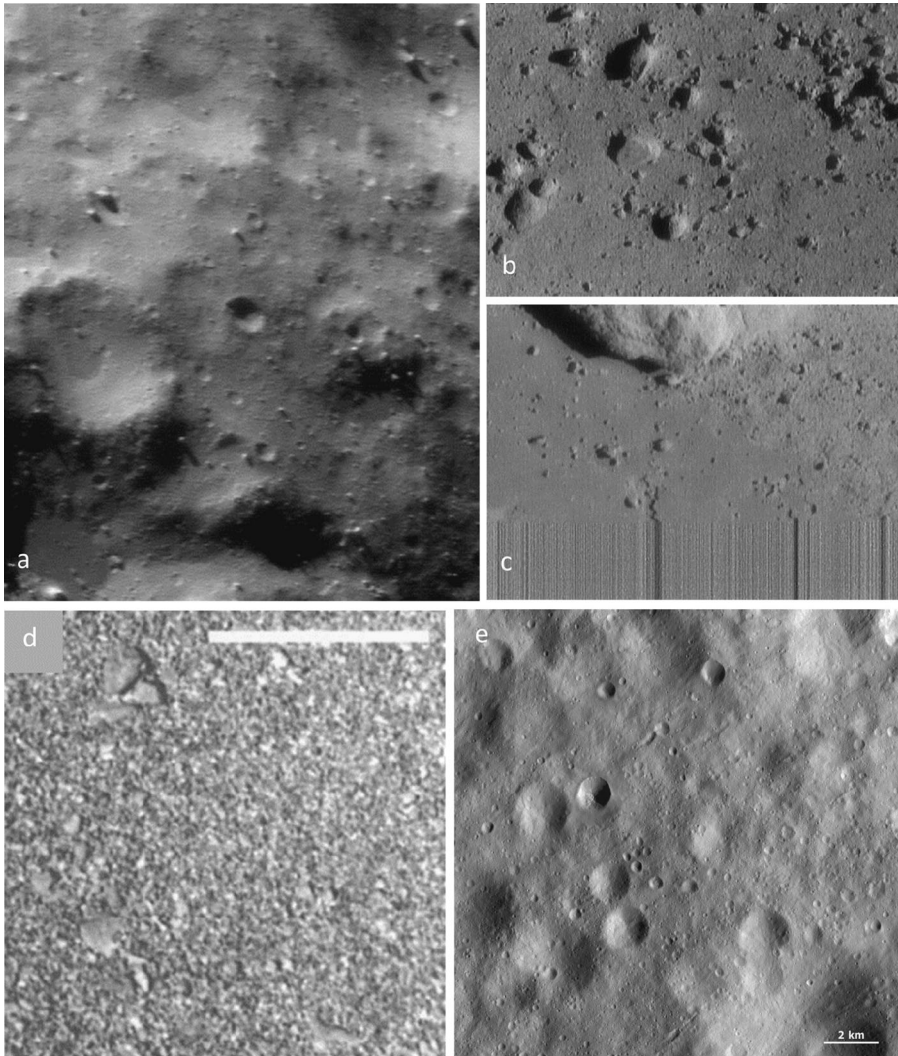
Fig. 18 Images of regolith. (**a**) The regolith of Eros as seen from 38 km altitude, and 1.1 km field of view, shows features as small as 6 m and a surface dominated by a blanket of regolith. Boulders litter the landscape, and the smallest craters are obscured. Many of the low spots are extremely flat, and appear infilled. The whole scene is about 1.1 kilometers (0.7 miles) across. (**b**) The last image of asteroid 433 Eros received from NEAR Shoemaker at a height of 120 m, and with a field of view 6 m, as it descended to the surface. At the *top* of image is a 4 m rock, at *bottom* is loss of signal. (**c**) From the same sequence, Eros at 250 m, field of view 12 m. The cluster of rocks at the *upper right* is 1.4 m across. (**d**) The regolith of Itokawa at the site of the Hayabusa sampling (Yano et al. 2006). The scale bar is 1 m. Centimeter to sub-cm grains are visible. (**e**) Vesta's surface covered by heavily cratered regolith, some buried craters appear as shallow, circular depressions. (Lucaria Tholus quadrangle, 169 km altitude, 16 m/pixel). (Eros: NASA/JPL/JHUAPL. Itokawa: ISAS/JAXA. Vesta: NASA/JPL PIA15822)

There was considerable evidence for an impact generated regolith on Ida (Fig. 4c; Belton et al. 1996a, 1996b), the argument now being that most ejecta from craters larger than about 1 km will reaccrete rather than being lost to space (Asphaug et al. 1998; Geissler et al. 1996).

The photometry also suggested a particulate regolith (Helfenstein et al. 1996). Morphologic features suggesting a regolith were, (1) downhill mass-wasting scares and albedo streaks, (2) positive relief features thought to be ejecta blocks, and (3) grooves, thought to be deep fractures covered by regolith (Sullivan et al. 1996). Estimates of regolith depths, based on chute depths, crater dimensions, and grooves, were 50–100 m. There are also subtle color variations on Ida, that are related to craters, that suggest younger ejecta laying over an older space weathered surface (Helfenstein et al. 1996; Geissler et al. 1996).

Thomas et al. (1999) point out that two of the large craters on Mathilde, Lublin and Karoo, show signs of downslope movement of regolith by either a chute mechanism (gravity driven) or sliding mechanism (stress driven). The surface of Mathilde (Fig. 4b) is very homogeneous in color and albedo, with no evidence for fresh ejecta from craters (Veverka et al. 1999a, 1999b).

Eros shows evidence for a substantial regolith (Fig. 18a–c). There is a deficiency of craters < 200 m (relative to predicted slopes of empirical saturation) due to a thick regolith and steep slopes that allow downward movement of regolith. There are also debris aprons, fine-grained "ponded" deposits (see below), talus cones, bright and dark streamers on steep slopes due to downslope movement of regolith, partially buried boulders, in filled and subdued craters. Most of Eros' craters are rounded, or smoothed, suggesting a widespread regolith that infills and drapes craters. Eros craters nearly completely lack concentric interior morphology suggesting a well-mixed regolith with properties changing gradually with depth to many meters to tens of meters everywhere on the asteroid. Robinson et al. (2002) state that there is evidence of a regolith in one form or another can be found in nearly every high-resolution image of Eros (Veverka et al. 2001; Thomas et al. 2002a).

An average thickness of the regolith of for Eros of 20-40 m was estimated by Robinson et al. (2002) by dividing the excavated volume of all craters larger than 1 km in diameter (89 km^3) by the surface area of the asteroid (1125 km^2), assuming a retention of 25–50 % (Thomas et al. 2001). However, there is considerable variation in regolith thickness due to the low gravity and high spin rate of the asteroid and randomness of impacts, and even around a given crater there may be a factor of two or more range in regolith thickness. An indication of regolith thickness can be gleamed by from the size of the craters that penetrate the regolith and excavate boulders. These considerations suggest infilling of a few meters to 150 m, with a median at 20–30 m.

Downslope regolith movement on Eros forms debris aprons and talus cones, and results in burial of craters and boulders (Veverka et al. 2001; Thomas et al. 2002a). Where slopes exceed 25° relatively fine-grained material generally forms smooth deposits on crater walls and are found in heavily degraded craters burying or embaying interior topography and they show higher albedo (by a factor of 1.5) than average Eros materials (Clark et al. 2002b; Bussey et al. 2002; Thomas et al. 2002a). These higher albedo deposits also show a slight increase in 550/760 nm ratio of about 1–2 % and in the 950/760 nm ratio an increase of about 5–8 % apparently because it is less space weathered than average Eros (Murchie et al. 2002; Clark et al. 2002b).

The surface of Itokawa is covered with unconsolidated mm-sized and larger gravels (Fig. 18d). However, the regolith is heterogeneously distributed, being coarse in certain areas and very fine grained in others (Miyamoto et al. 2007). It was argued that global scale mobilization of the surface in a dry, airless, microgravity environment caused the finer fraction to migrate to areas of potential gravity lows to form the Muses-C, Sagamihara, and Uchinoura regions.

Crater shape and depth to diameter ratio for Steins (0.12) are consistent with degradation and covering by a regolith that has experienced seismic shaking (Keller et al. 2010). Marchi

et al. (2010) observed a deficit of craters < 0.6 km which they interpreted as a result of ejecta blanketing during the formation of the 2.1 km Diamond crater near the south pole or to the movement of regolith by the YORP effect.

The surface of Lutetia is also covered in regolith, especially the north polar region, with slopes below the angle of repose almost everywhere (Sierks et al. 2011). Landslide flows (or possible rock outcrops) are brighter than the surrounding cratered terrains, suggesting either that the regolith texture of differs from elsewhere or that the older areas are space weathered. Similar variations of reflectivity were observed on Eros. Vincent et al. (2012) observe variations in the depth/diameter ratio of craters across the surface of Lutetia, averaging 0.12 with a range of 0.05 to 0.3, which they ascribe to variations in regolith thickness. The regolith is particularly thick in the Beatica region, which includes the north pole. Jutzi et al. (2013) have modelled this impact numerically and found that a 2.3 km diameter projectile impacting at a velocity of 5 km s^{-1} would produce a crater of roughly 34 km similar to that observed in the center of the region.

Radar measurements by Hudson and Ostro (1998) on the light curve and model indicated that the surface of Toutatis might be covered with a fine regolith layer and Scheeres et al. (1998) point out that the interacting periodicities in the rotation of Toutatis, an irregular non-prime axis rotator, would shake the asteroid and produce a globally uniform regolith. However, the resolution of the camera on Chang'e 2 was insufficient for direct observation of regolith features.

Prior to Dawn encounter, Hubble Space Telescope observations detected a 460 km impact basin on the southern hemisphere of Vesta (Thomas et al. 1997). Jutzi and Asphaug (2011) performed numerical analysis on the impact that would produce such a basin, assuming a 50 km impactor at 5 km s^{-1}. Since Vesta rotates rapidly (5.3 hr period), ejecta deposits will deposited irregularly and variably-shaped, multiply-folded, and abruptly-terminated hemisphere ejecta sequences will be produced. The Dawn spacecraft certainly found a thick regolith (Fig. 18e; Russell et al. 2012), but these predictions have not yet been tested in detail.

Regions of high and low albedo were detected on Vesta, in fact the range of albedos is among the largest observed on Solar System rocky bodies (McCord et al. 2012). The dark regions were generally associated with craters, either in the ejecta or crater walls, and are thought to represent exogenic material similar to CM chondrites. McCord et al. (2012) argue that the bright material is the uncontaminated indigenous Vesta basaltic soil. Impact mixing caused the dark material to disperse and mix with the light material creating broader, diffuse darker regions, and finally Vesta's background regolith. These early conclusions were confirmed by a more detailed study (Jaumann et al. 2014).

At the time of writing, there is inadequate data to discuss regolith on Ceres, although Nathues et al. (2015) refer to three kinds of terrain, "smooth", "lineated", and "rough".

5.2.3 Ejecta

The surfaces of Braille, Annefrank and Dactyl were not observed with sufficient resolution to observe ejecta blankets. Belton et al. (1992) found no ejecta blankets on Gaspra and at the time none were expected for asteroids of this size. Similarly, while there are many craters and evidence for a regolith, there do not appear to be any obvious ejecta blankets on Itokawa (Fujiwara et al. 2006). The same is true of Steins (Marchi et al. 2010; Keller et al. 2010) and Toutatis (Zou et al. 2014). On the other hand, ejecta blankets have been observed on Ida and Vesta (Fig. 19) and Lutetia.
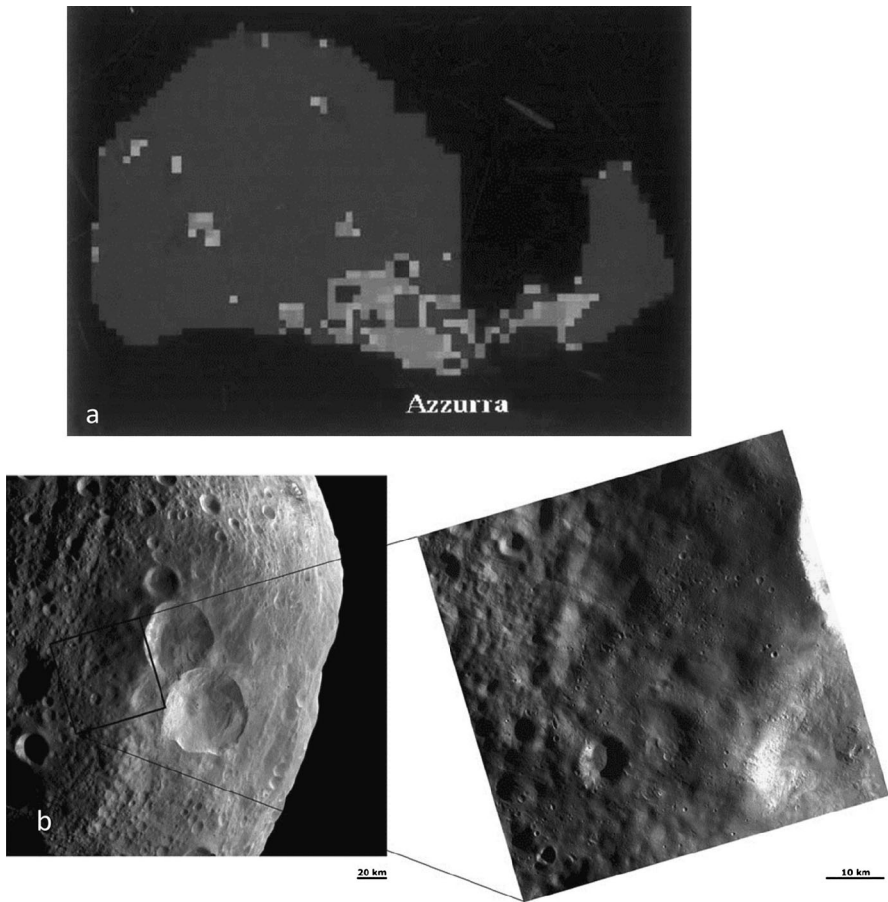
Fig. 19 (**a**) The ejecta surrounding crater Azzurra on Ida shows up on this image of blue/red ratios where the higher the ratio, the lighter the shade. (Chapman 1996). (**b**) The ejecta blanket of Vesta's "snowman craters" (Marcia, Calpurnia, and Minucia). *Left*, low resolution image (in which the ejecta blanket is more easily seen). *Right*, high resolution image. The ejecta blanket appears smoother than the neighboring regions but thins out and becomes rougher towards the *top left*. Some older impacts are seen through the ejecta blanket and the clusters of small, fresh craters on the ejecta blanket are likely secondary impacts. These images were taken at altitudes of 2740 km and 673 km, and fields of view were 260 m and 66 m per pixel, respectively. (NASA/JPL. Image PIA14958)

Ejecta blankets have been observed on Ida because the surface is older and the range of crater sizes is larger, and higher resolution images are available. Belton et al. (1996a) proposed two explanations for the bluer regions associated with young fresh craters, that they are ejecta blankets or that they are materials around the crater disturbed by the impact (Fig. 19a). There are no ejecta blankets on Ida as obvious as those on the Moon and numerical simulations by Asphaug et al. 1996 were more consistent with seismic shaking than ejection, but Belton et al. considered the issue unresolved. Chapman (1996) argued that the ejecta have the properties of less space weathering surfaces and concluded that the regions are ejecta blankets. Geissler et al. (1996) argued that when the rotation and irregular shape of Ida are taken into account, it is probable that the regions around craters are ejecta blankets.

Fig. 20 Estimated thickness profile of the ejecta blanket in the Baetica region of Lutetia. The *asterisks* indicate depths based on crater filling (assuming a crater depth diameter ratio of 0.12, typical of Lutetia). The *solid line* is the best fit power law (Vincent et al. 2012)
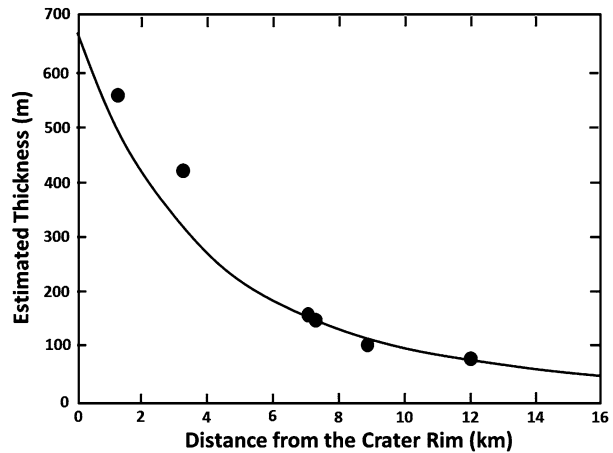
While Eros has a thick regolith, and there are numerous indications of regolith movement and ejected boulders, there does not appear to be any visibly obvious ejecta blankets (Robinson et al. 2002; Chapman et al. 2002). On the other hand, from a study of ejecta ballistics, taking into account the effect of Eros' rapid rotation and irregular shape, Durda et al. (2012) detected an ejecta blanket (in terms of boulder densities) with a sharp boundary around crater Valentine. They also found that ejected boulders bounce poorly, the coefficient of restitution (velocity after landing divided by velocity before) was only 0.09–0.18.

On Lutetia the smoothness of the polar (Baetica) region is attributed to ejecta from the 34 km crater in the center of the region (Sierks et al. 2011; Vincent et al. 2012; Jutzi et al. 2013). Erasure of craters via the shock associated with such an impact is shown to be less significant and does not reproduce the observed spatial distribution of erased craters or "ghost" craters. The depth of the ejecta blanket is estimated to be up to ∼ 600 m, based on the depth-to-diameter ratios of these buried craters. The thickness of the ejecta blanket in the Baetica region and how it decreases with distance from the center of the region was determined by Vincent et al. (2012) from apparent depth-diameter ratios of the craters (Fig. 20).

The two giant impacts at the southern pole of Vesta produced extensive ejecta deposits reaching ∼ 100 km from Rheasilvia's rim, sometimes further (Schenk et al. 2012; Jaumann et al. 2012). Erasure of craters is complete for about 50 km, after which incomplete burial is observed and crater density increases. There is indication that the ejecta is non-uniformly distributed, but it is unclear whether the ejecta blanket is asymmetric due to Vesta's rotation in the manner predicted by Jutzi and Asphaug (2011). However, the dimensions and the thickness of the ejecta blanket, 4–5 km deep, are consistent with the Jutzi and Asphaug (2011) calculations. An example of regolith on Vesta is shown in Fig. 18e.

Jaumann et al. (2012) note that ejecta blankets are often observed on the younger craters on Vesta and describe a particular area in the 45 km crater named Lepida (307°E, 16°N) where the largest craters that are completely filled have diameters of about 4 km, so assuming a depth/diameter ratio of 0.2 they inferred a thickness of ejecta (regolith) in this area of about 0.8 ± 0.1 km. An example is shown in Fig. 19b. They also note that topography plays a role in crater ejecta blankets, so that on slopes the blanket is strongly asymmetric, being wider upslope and narrower downslope. Vesta has significant relief and steep slopes, sometimes exceeding 40°, the angle of repose, so that bedrock can be exposed, as on Eros (Cheng et al. 2002).
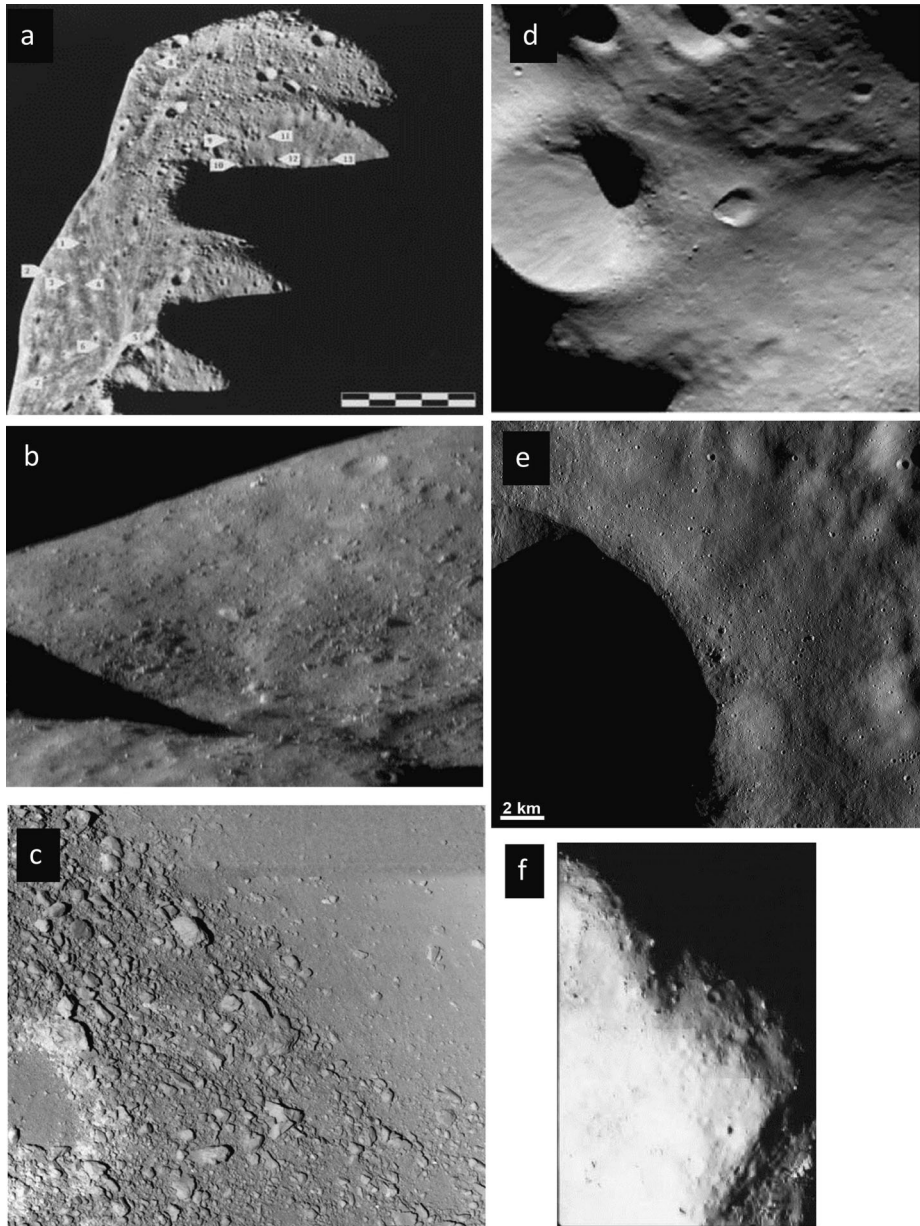
Fig. 21 (**a**) Thirteen boulders on Ida near the 11-km diameter craters Lascaux and Mammoth in the eastern region and 13 blocks. (Image 202562439, resolution 31 m/pixel; *scale bars* 5 km, Lee et al. 1996). (**b**) Boulder-strewn region on Eros seen from an altitude of 37 km. The largest boulder (near the center of the image) is about 60 meters across. The whole scene is about 1.5 km across. (NASA/JPL, Image PIA 03130.) (**c**) Close-up image between rough and smooth terrain on Itokawa showing boulders from *left top* to *right bottom*. At *left* is a crater with a disrupted rim. (University of Tokyo/JAXA). (**d**) Boulders on Lutetia near the crater Patavium (Küppers et al. 2014). (**e**) Boulders near a crater in the Bellicia quadrangle of Vesta. (Altitude 198 km, 19 m/pixel, PIA15516). (**f**) Boulders on the surface of Toutatis from an altitude of 29 km (Huang et al. 2013)

5.2.4 Boulders

Boulders are important because it is assumed that in order to produce them an impactor must penetrate the regolith and excavate bedrock (Fig. 21). They therefore provide an indication of the thickness of regolith as well as providing samples of the subsurface for remote sensing and sample return.

Belton et al. (1992) did not report any large ejecta blocks or boulders on Gaspra, and the same was true of Mathilde (Thomas et al. 1999). Mounds between the craters Karoo and Kuznetsk, could be boulders but may be artifacts of overlapping crater rims. However, these expected 100 m features are at or near the resolution limit. Similarly, the resolution of the Rossetta images of Steins is insufficient to enable boulders to be seen (Keller et al. 2010).

On the other hand, boulders (or positive relief features, PRL, which can reach 100 m in size, Fig. 21a) did seem abundant on Ida (Lee et al. 1996; Belton et al. 1996a, 1996b; Sullivan et al. 1996), such that Lee et al. (1996) and Chapman et al. (2002) were able to determine size distributions. Geissler et al. (1996) discuss the importance of rotation in determining the distribution of boulders on Ida.

Boulders are also commonplace on Eros (Fig. 21b), are non-uniformly distributed, and most seem to have been produced during the impact that created the Shoemaker crater. In fact, over 40 % of the volume of large blocks on Eros could fit inside Shoemaker crater (Thomas et al. 2001; Robinson et al. 2002; Veverka et al. 2001). The size-frequency distribution for Eros boulders is shown in Fig. 22a. The interiors of Humeros and Shoemaker are especially high in boulders, but on the < 50 m scale the asteroid surface is dominated by boulders and other features indicative of regolith accumulation and transport. From the abundance of boulders and from ejecta patterns from Shoemaker crater, it seems that Psyche is older than Shoemaker (Thomas et al. 2001). Nevertheless, while younger than Psyche and Humeros, the Shoemaker crater is not a young feature, and since most of the boulders seem to have been formed by the Shoemaker impact, few other impacts seem to have made large numbers of boulders (Robinson et al. 2002). A similar conclusion seems to apply to the Moon (Wilcox et al. 2002); most of the boulders in a given region were formed by just a few large impacts. Dombard et al. (2010) propose that it is the disintegration of boulders that produces the ponds, because many large ponds are associated with boulders.

In the rough terrains on Itokawa (Fig. 21c), there are numerous boulders with a variety of angularity and aspect ratios (Saito et al. 2006; Fujiwara et al. 2006). The boulder largest is named Yoshinodai, which is $50 \times 30 \times 50$ m and is 1/10 the size of Itokawa. Another is Pencil, which is partially buried. A third is known simply as "the black boulder". The total number of boulders > 5 m exceeds 500 and it was possible for Saito et al. (2006) to produce size distribution data (Fig. 22b). The size distribution of the boulders on Itokawa is inconsistent with them being ejecta fragments and it is thus assumed that they are the result of catastrophic disruption and that Itokawa is therefore a rubble pile.

Boulders are commonplace on Lutetia (Fig. 21d), and 200 blocks of up to 300 m in dimension were found around the central 21 km crater cluster in Baetica which means that the average boulder density is 0.4 boulders km^{-2} in that region (Sierks et al. 2011). Many partially buried. The steep size distribution of boulders on Lutetia resembles that of Eros (a power law equation with an exponent of -5). Boulders in the Pannonia region are also associated with crater which suggest that large impacts on Lutetia frequently expose bedrock. Again they are often partially buried.

Fig. 22 Statistics for boulders on asteroids. (**a**) A spatial density plot for Eros from Chapman et al. (2002). *Large symbols* represent boulders observed during a low altitude flyover the small symbols represent boulders observed from higher orbits, note there is a factor of 20 difference in the two populations (indicated with a *double-headed arrow*). *Error bars* on all three plots have been omitted for clarity.
(**b**) Cumulative frequency distribution for boulders on Itokawa from Saito et al. (2006). Boulder ranges from ∼ 40 to 5 m in size and have a slope on this plot of −2.8 suggesting less comminution than, say Eros, where the slope is −3.8.
(**c**) Cumulative frequency distribution for boulders on Toutatis from Zou et al. (2014). The boulders on Toutatis range in size from ∼ 100 m to ∼ 8 m and the small lobe has a greater number of large. (The reader should refer to original articles for several important details omitted from these sketches)
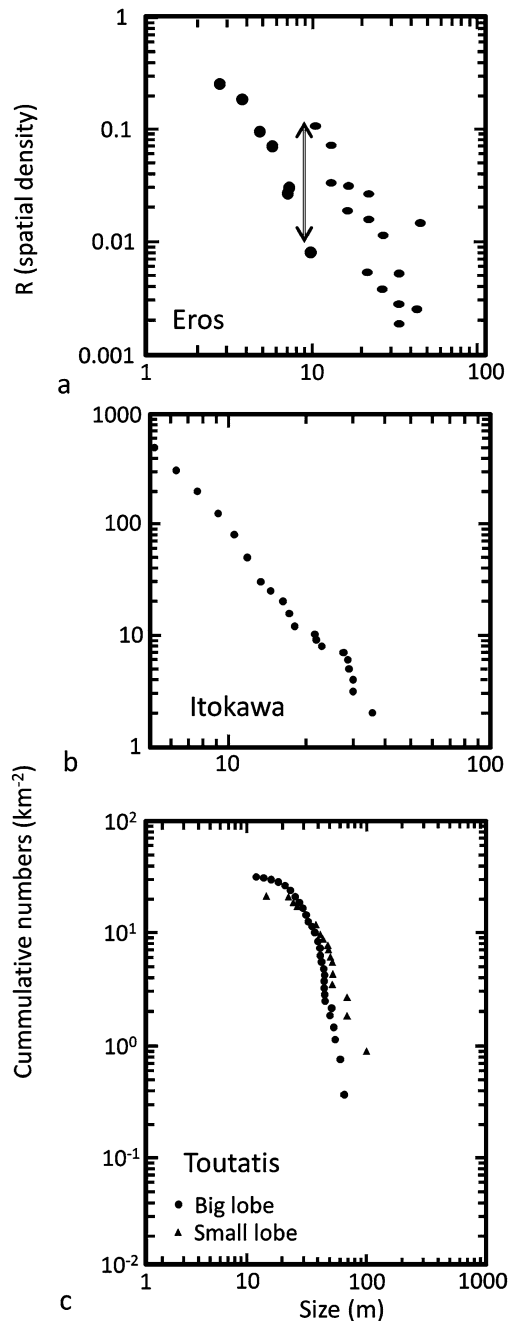
Jutzi and Asphaug (2011) predicted the existence of ejecta from the two massive south polar craters to be present on Vesta, and were concerned that they might be mistaken for other geological structures. Such global scale ejecta has yet to be reported, but on a local scale Jaumann et al. (2012) report large boulders (Fig. 21e) in some parts of crater ejecta

on Vesta, and these are often associated with slopes that are above the angle of repose and indicative of intact bedrock beneath.

There are many boulders on the surface of Toutatis (Fig. 21f), on both the large lobe (89 boulders, two larger than 50 m) and small lobe (24 boulders, three larger than 50 m). The largest boulder (89 m) was in the region where the two lobes were in contact. Zou et al. (2014) published both a map and size distribution data and pointed out that the slope of the frequency plot was steeper for boulders on the large lobe (Fig. 22c).

5.2.5 Grooves and Ridges

Most asteroid surfaces have groves of various sorts (Fig. 23). In general, they imply something about the integrity of the asteroid, because if they are cracks through the asteroid it is possible to infer, for example, that the asteroid has some coherence, rather than being a rubble or gravel pile.

The grooves on Gaspra appear to be extensional in some locations and compressional in others (Veverka et al. 1994). They probably represent expressions in the regolith of reactivated features in the deep interior (Sullivan et al. 1996). The impact that caused the Vienna Regio concavity on Ida could have resulted in fractures in the Pola Regio, where grooves have been observed (Asphaug et al. 1996). It is also possible that the 10 km crater Azzurra reopened these fractures and gave them a fresh appearance. This would suggest that Ida does not have a rubble pile interior but well-joined fault planes and welded blocks of pores smaller that the stress pulse.

The ubiquitous grooves on Eros that commonly occur in suborthogonal sets, and have linear or scalloped outlines similar to those of Gaspra, Ida, and Phobos and are likely to have a similar mode of origin, namely drainage of regolith into underlying fractures (Fig. 23a, b, Procter et al. 2002). The large scale of Rahe Dorsum and many grooves on Eros's surface suggests that the asteroid is a largely coherent, but fractured body.

The two major sets of grooves and ridges on Vesta, Divalia Fossa and Saturnalia Fossa, which lie at mid latitudes and are centered on the two polar impact basins, were described above. A close up view of part of one of them is shown in (Fig. 23c).

5.2.6 Ponds

One of the most intriguing features of the surface of near-Earth asteroid Eros are the so-called "ponds", smooth areas on the floor of craters (Fig. 24) (Robinson et al. 2001). Similar smooth areas have been observed on other asteroids, such as the Muses Sea on Itokawa (Fujiwara et al. 2006) The major properties of the Eros Ponds are that they (1) have distinctive flat floors sometimes showing non-central downside movement, (2) have sharp boundaries, (3) have uniform morphology, color and albedo, (4) typically have a radius $\sim 1/3$ the diameter and a ~ 5 % of the depth of the host crater diameter and that they are not concentrations of a uniform widespread ejecta, and (5) can be seen on other (noncrater) depressions (Robinson et al. 2002). Additionally, (6) the Eros depressions appear preferentially at locus of sub-solar point and they are more abundant in regions of lower gravity. There is a word of caution identified by Roberts et al. (2014a, 2014b) who question the flatness of the ponds and suggest that the apparent distribution of the ponds is an artifact of image resolution caused by the orbit of the Shoemaker-NEAR spacecraft and shape of Eros.

Initially it was suggested that the ponds were caused by the electrostatic levitation of dust which mobilized the finest grains and when deposited in the depressions produced the extremely flat ponds. However, seismic redistribution of regolith materials has been proposed
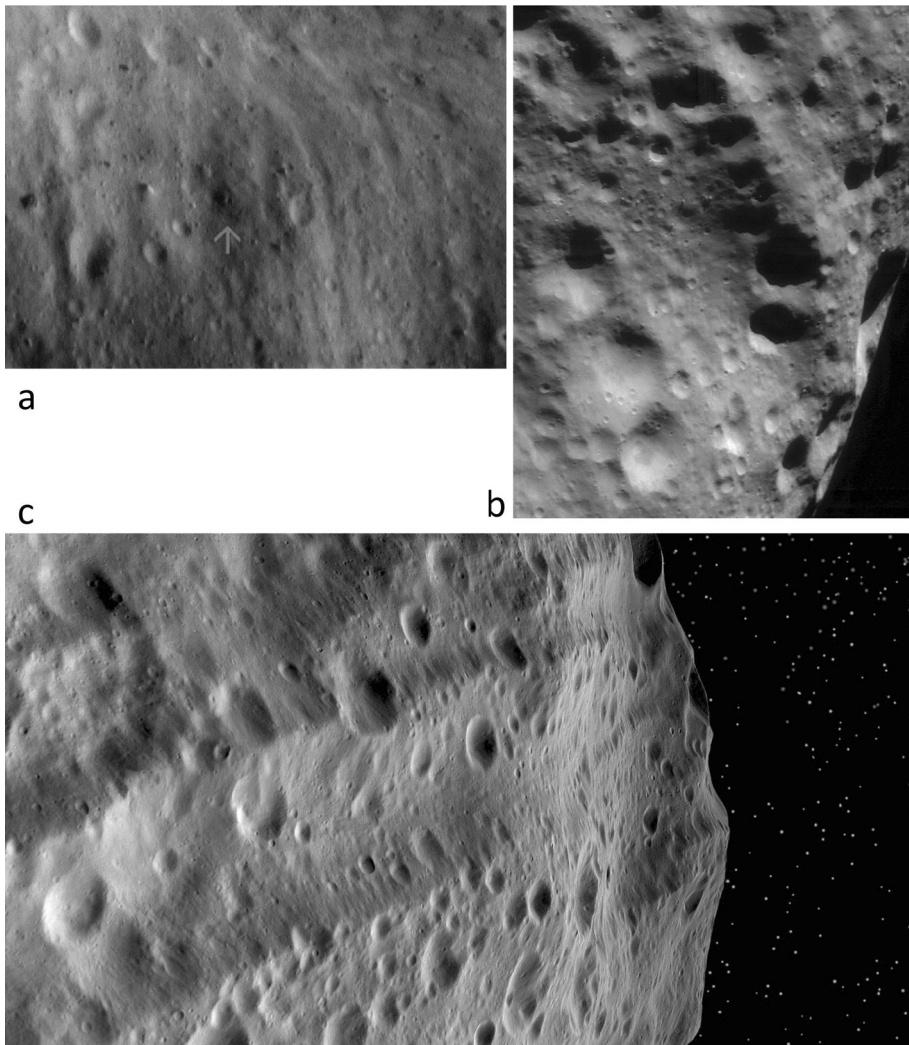
Fig. 23 Images of grooves and ridges. (**a**) This is a mosaic of four images—taken by NEAR Shoemaker on September 21, 2000, from about 100 kilometers (62 miles) above Eros—covers part of the asteroid's southern hemisphere, southwest of the large, 5.3-kilometer (3.3-mile) diameter crater. The ridge that trends from *upper left* to *lower right* is among the older features on Eros, as evidenced by the large number of superimposed impact craters. The whole scene is approximately 11 kilometers (7 miles) from top to bottom. (NASA/APL, image 20000816). (**b**) This region of Eros has also been cut by the shallow troughs, or grooves, that trend from the *top* to the *bottom* of the image. Also apparent is the obliteration of old craters and the formation of new (the *arrow* indicates a young crater with dark ring of material) and the presence of many boulders. The orbital altitude is 51 km and the field of view is 2.2 km. (NASA/JPL, image PIA 03110). (**c**) Huge grooves, part of the Divalia Fossa system and caused by the south polar impacts, are usually several hundred km long, ≤ 15 km wide and ≥ 1 kilometer deep. (Image is an artificially generated oblique from 210 km, 20 m/pixel, NASA/JPL PIA 15673)

to explain subdued topography and flat floored craters on the Moon (Schultz and Gault 1975) and was suggested to be an important process for asteroids (Cintala et al. 1978, 1979). This idea was adopted for the ponds on Eros (Cheng et al. 2002). As an extension of this, Dom-

Fig. 24 Crater ponds. Image of a crater on Eros that has been infilled with fine material (referred to as a "pond"). The image was taken from an altitude of 36 km with a field of view 900 m across. Many angular boulders are in the field, the smallest being about 6 m, and regolith has banked up against several of them. The dark object in the *upper center* of the image is the shadow of a large boulder. (NASA/JHUAPL)
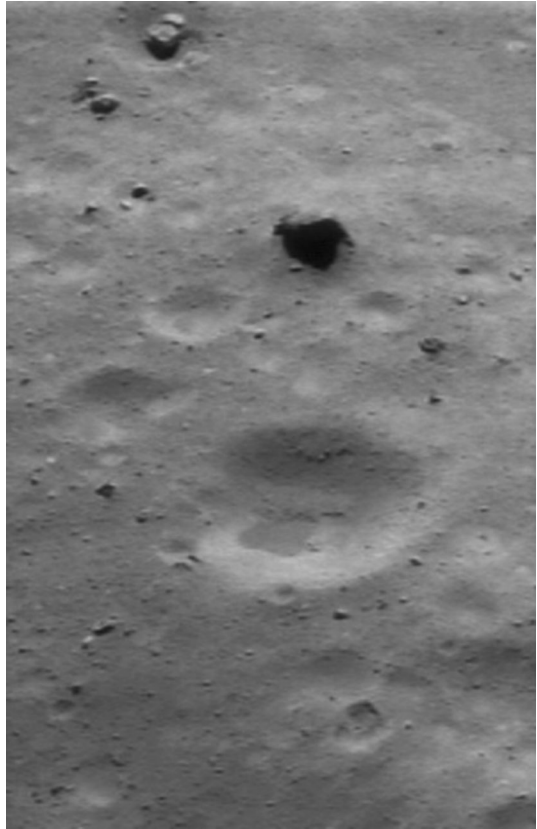

bard et al. (2010) have observed that the ponds are frequently associated with large boulders and that it is the comminution of the boulders during seismic shaking that feeds the ponds. Finally, with the recent discovery of water on Vesta's surface, and its predicted behavior during energetic events like impact, Sears et al. (2015) suggest a role for volatiles in the formation of the Eros ponds.

5.2.7 Pits and Pitted Terrain

The Dawn images of Vesta showed that in the floor of center of the major Marcia crater, and occasionally regions the ejecta, had a pitted texture (Denevi et al. 2012), reminiscent of similar features on Mars (Fig. 25; Tornabene et al. 2012; Boyce et al. 2012). Detailed examination of the martian features have led to the conclusion that these are volatile rich impact melts that were degassing at the time of solidification. Their presence on Vesta is therefore remarkable and is consistent with the discovery of water rich regions. Apparently, the surface of Vesta was water-rich at the time of the Marcia impact and its impact melts behaved like the melts on Mars.

A distinctly different kind of feature, also sometimes described as "pits", has been observed on Eros and Steins (Robinson et al. 2001; Keller et al. 2010). These "pits" are drainage features where a regolith-filled fracture has allowed drainage of the regolith at certain points. In the case of Steins the fracture is thought to have been produced by the
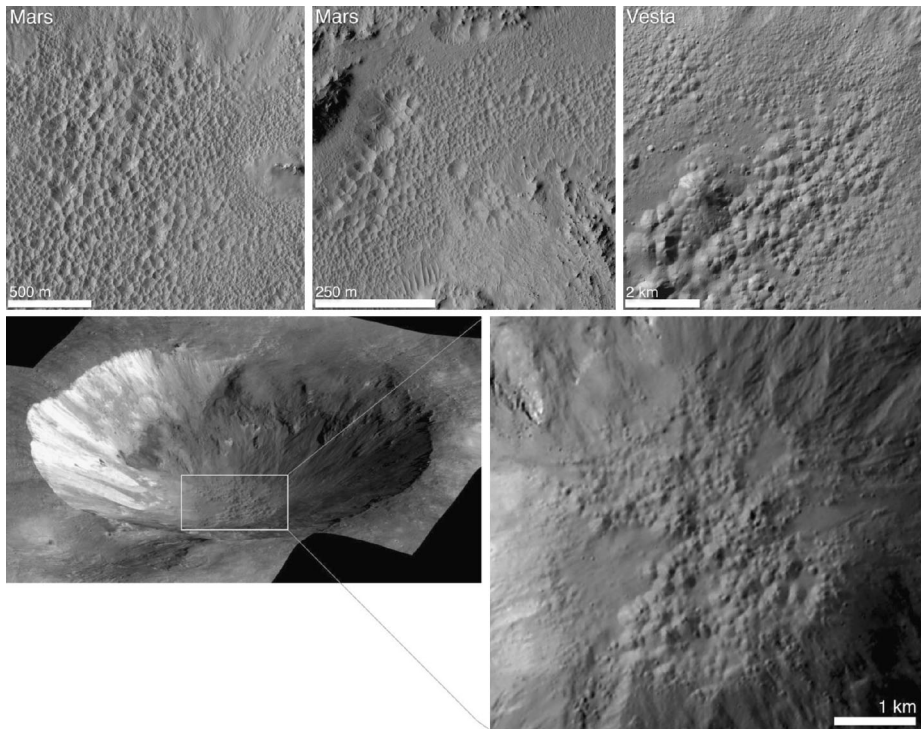
Fig. 25 *Upper sequence*: Pitted terrain on Vesta compared with similar terrain on Mars. *Left*, the floor of a Martian crater Tooting, which is 28 km in diameter. *Middle*, the floor of a Martian crater Zunil (10 km in diameter). *Right*, the floor of Marcia crater on Vesta (70 km in diameter). The morphologies of pits are similar on both bodies, with irregular shapes and sharp angles where pits share walls. *Lower sequence*: Perspective view of Cornelia crater (15 km in diameter) with close-up of crater floor

impact that produced the large Diamond crater and the sequence of pits is referred to as a catena (Keller et al. 2010). Drainage pits were first observed on Phobos and mechanically modelled by Horstman and Melosh (1989).

5.2.8 Gullies

The discovery of features resembling gullies on Earth and Mars inside large craters was interpreted by Scully et al. (2012) as evidence for liquid water flow on the surface of Vesta (Fig. 26). Since Vesta is an airless body, the water would have to be associated with impact and the presence of a transient atmosphere. The gullies are often on the walls of craters that have pitted terrain in their crater floors or, occasionally, in the ejecta, so these features could be part of a complex outcome of impact into water-bearing surfaces. The effects of impact into water-bearing surfaces have recently been explored in connection with terrestrial craters (Kirsimäe and Osinsky 2013; Stöffler et al. 2013). However, Scully et al. (2013, 2014) modified their earlier conclusion by argueing that only the long, thin, sinuous dendritic gullies were produced by the flow of liquid water. The short straight gullies they attribute to dry mass flow. This was taken one step further by Krohn et al. (2014) who argue that all gullies on Vesta are the result of dry flow.
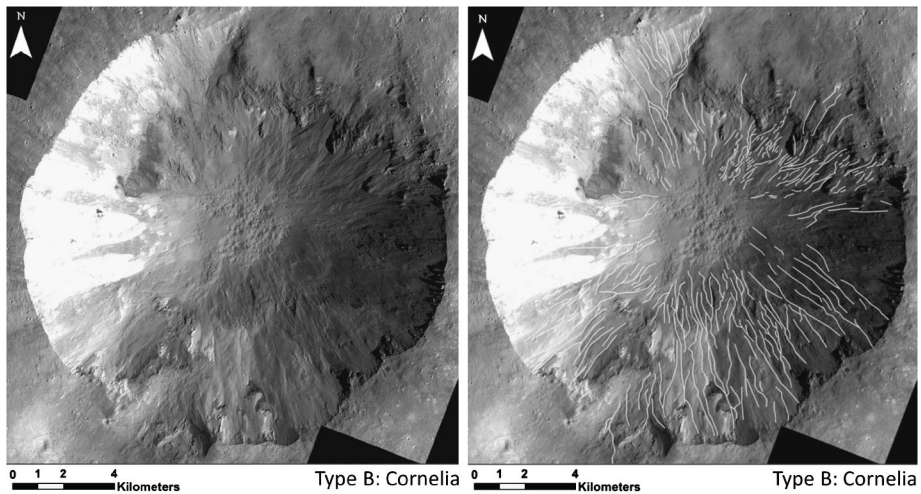
Fig. 26 Cornelia crater on Vesta contains features that resemble gullies on Earth and Mars. When straight, these are thought to be dry flows, but when long, thin and sinuous, they are thought to represent wet flows during transient conditions associated with impact (Scully et al. 2013, 2014)

6 Compositional Properties

6.1 Asteroids and Meteorites

It was, of course, the paper of McCord et al. (1970) that triggered the major research effort of matching asteroid spectra to those of meteorites when they suggested that the HED meteorites were coming from Vesta. The surface composition of an asteroid provides the primary indication of the compositional nature of the entire asteroid and therefore its taxonomy, but with a number of caveats. A basaltic, or non-chondritic composition, indicates global differentiation and perhaps the existence of a core, mantle and crust. Such is the case for Vesta (Russell et al. 2012). However, thermal models can be constructed that suggest that chondritic surface does not preclude a differentiated interior (Weiss and Elkins-Tanton 2013). A chondritic spectrum might suggest a link with chondrite meteorites, but this is complicated by the existence of a great many chondrite classes (Weisberg et al. 2006) with contrasting compositional and spectral properties. For instance, C chondrites have flat and relatively featureless spectra, superficially resembling the C asteroids (e.g. Rivkin et al. 2002), but any number of materials have flat featureless spectra. Nevertheless, there are small several features that have been used to infer the abundance of water or hydrated minerals (Rivkin et al. 2002). On the other hand, ordinary chondrites (the H, L, and LL classes) have major absorption features superficially resembling certain types of S asteroid (Burbine et al. 2002). Aside from the great variety of meteorite classes (Weisberg et al. 2006), there are also a great variety of asteroid spectra (Bus et al. 2002; asteroids have been sorted into over 25 taxonomic classes on the basis of their visible/near IR spectra), and matching asteroids with meteorites has proved extremely difficult.

Attempts to link meteorite classes with asteroids has emphasized the importance of probably another major caveat, which is that long-term exposure to space changes the nature of the asteroid surface, commonly called "space weathering" (Clark et al. 2002b), so simple comparison with of an astronomical spectrum with a laboratory spectrum is fraught with
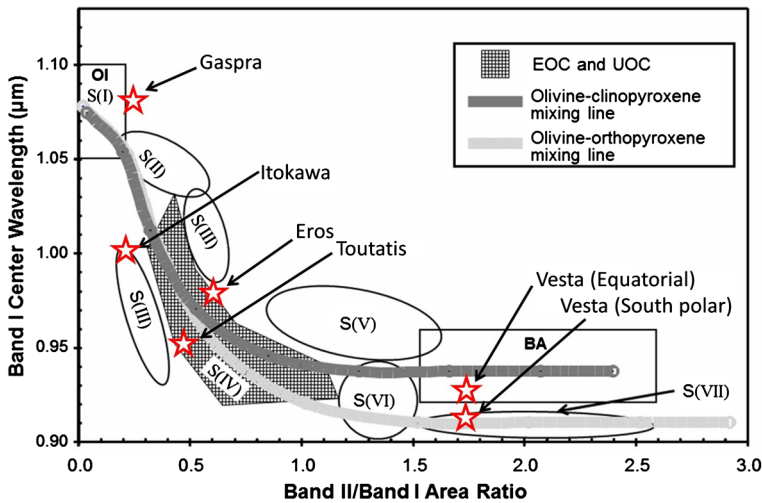
Fig. 27 BAR (band area ratio) plot for S and V asteroids (Gaffey et al. 1993a, 1993b, as modified by Geitzen et al. 2012). Asteroids with strong absorption bands (essentially the S and V classes) have two major absorptions, a ~ 1 µm band due to olivine and pyroxene and a ~ 2 µm band due pyroxene, thus a plot of the position of the 1 µm band (that can vary from 0.8 to 1.2 µm) against the area of the 1 µm band divided by the area under the 2 µm peak produced a plot (the BAR, or Band Area Ratio, plot) which enables discrimination of the S subclasses and the V class based on the relative proportions of olivine and pyroxene. The *lines* are from Geitzen et al. (2012), are mixing lines for olivine and pyroxene. Compositional differences can affect the positions of the 1 and 2 µm features (e.g. Klima et al. 2011), as can the structural state of the pyroxene, whether it is in the monoclinic form or orthorhombic form (Gietzen et al. 2012). Superimposed on this plot are data points for the present S and V asteroids, estimated by the author from published spectra (Gaspra, Helfenstein et al. 1994; Itokawa, Abe et al. 2006a, 2006b; Toutatis, Reddy et al. 2012; Vesta, De Sanctis et al. 2012a, 2012b) or taken from the literature (Eros, Bell et al. 2002)

problems. To add to the confusion, while space weathering is well understood for lunar samples, it is almost certain that the details of space weathering will not be the same with asteroids whose location in space and, usually, surface composition, are very different from the Moon's (McKay et al. 1989), and will vary with asteroid type. The analysis of peak shapes of S asteroids using the band area ratio (BAR) plot (Fig. 27), as opposed to spectral matching that relies heavily on the slope of the continuum, is essentially immune from the effects of space weathering and does enable major mineral identifications to be made with reasonable accuracy (Gaffey et al. 1993b). This information can translate to linkage with a class of meteorites, but often there is ambiguity, the same few major minerals appearing in very different rock types.

Another factor influencing the surface properties of near-Earth asteroids is tidal effects. If the asteroid is weakly coherent then close passage by the Earth could result in complete disruption (Richardson et al. 1998), but even if the body is not disrupted, some refreshing of the surface might occur (Binzel et al. 2010) and this may be influencing the radar data.

Finally, as meteorites continually demonstrate, and the Dawn mission showed for Vesta, asteroid surfaces are frequently contaminated with material from other asteroids (Wilkening 1973; McCord et al. 2012). The spectacular Almahata Sitta meteorite, that was observed as an asteroid (2008 TC$_3$) before it landed in the Sudan and became a meteorite (Jenniskens et al. 2009), is a breccia of highly diverse meteorite types; ureilites, a ureilite-related an-
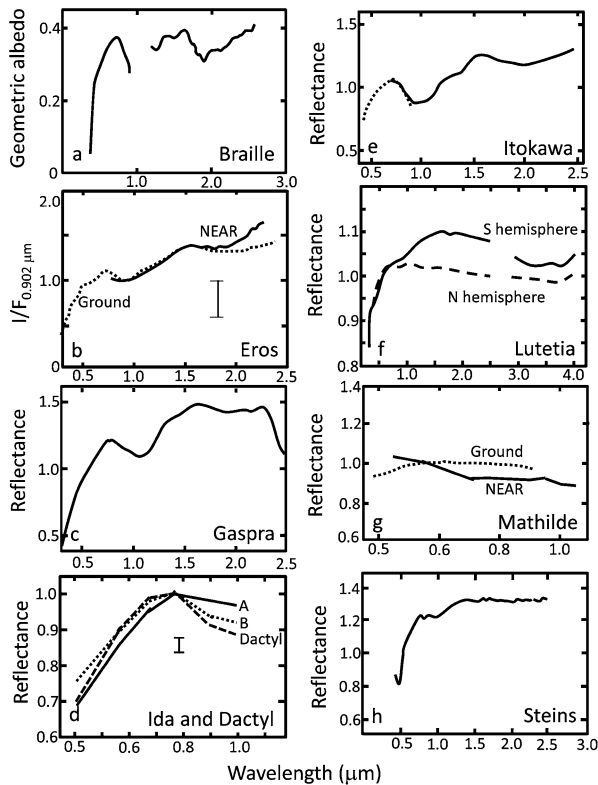
Fig. 28 Visible/near IR spectra for the explored asteroids. (**a**) Visible and near-IR spectra for Braille obtained from the Deep Space 1 spacecraft (Buratti et al. 2004). The authors noted the similarity to Q asteroids and suggested the asteroid was a mixture of olivine and pyroxene. (**b**) Ground-based and NEAR visible and near-IR spectra for Eros indicate an orthopyroxene:olivine ratio of 0.38 and intermediate between S(IV) and S(II) classification (Bell et al. 2002). The *error bar* is a typical uncertainty on the NEAR data. (**c**) Visible and near-IR spectra for Gaspra obtained from ground-based and Galileo observations (Helfenstein et al. 1994). (**d**) Visible spectra for Ida (terrains A, intercrater plains, and B, crater ejecta) and Dactyl determined by the Galileo spacecraft (Chapman 1996). The ejecta has a bluer spectrum consistent with less space weathering than most of the surface. (**e**) Ground-based visible (*dotted line*, McDonald Observatory) and near-IR (IRTF) spectra for Itokawa suggest a pyroxene:olivine ratio of 1:3 (Abell et al. 2007). (**f**) Ground-based visible and near-IR spectra for the northern and southern hemispheres of Lutetia (Rivkin et al. 2011a, 2011b). The spectra resemble C and X asteroids but the bands are too weak for mineralogical interpretation. (**g**) Visible spectrum for Mathilde obtained by ground-based and NEAR observations (Clark et al. 1999). The featureless spectrum is typical of C asteroids. (**h**) The visible and near-IR spectra for Steins which is classified as an E(II) asteroid with a 0.49 μm feature attributed to troilite (FeS) (Fornasier et al. 2008). (**i**) The visible and near-IR spectrum for Toutatis from Reddy et al. (2012). (**j**) The visible and near_IR spectra for the southern (A) and northern (B) hemispheres of Vesta, from Russell et al. (2013). (**k**) The visible and near-IR spectrum of Ceres from Rivkin et al. (2011a, 2011b). (The reader should refer to original articles for several important details omitted from these sketches)

desite, metal-sulfide assemblages related to ureilites, enstatite chondrites, ordinary chondrites, carbonaceous chondrites, and Rumuruti-like chondrites (Horstmann and Bischoff 2014).

However, to temper this pessimism, there have been some remarkable successes. Spectral reflectivity measurements suggested a link between Vesta and the HED meteorites, a link that has been strengthened by subsequent meteorite data and confirmed by the observations

Fig. 28 (*Continued*)
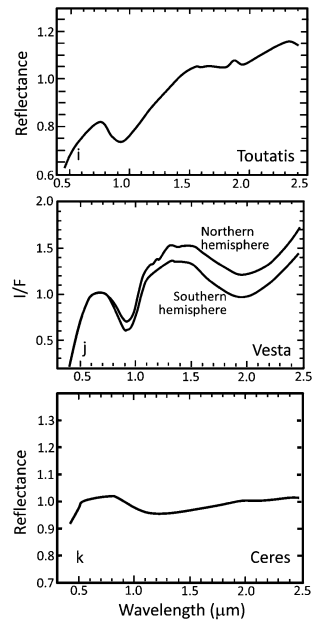
of the Dawn mission (Russell et al. 2013). Itokawa was suspected of being related to the LL chondrites on the basis of reflectivity spectra, corrected for space weathering, before grains from the asteroid were found to have LL chondrite compositions in the laboratory (Binzel et al. 2001a, 2001b; Nakamura et al. 2011).

With this brief discussion of asteroid spectroscopy in mind, we can now summarize the status of knowledge of the surface composition of the explored asteroids. As in many properties, there is a large range of visible/near IR spectra for the explored asteroids (Fig. 28), so that classes range from S, to E, to V, to C (Table 3).

6.2 Visible/Near IR Spectroscopy

The spectrum for Braille is shown in Fig. 28a. The spectrum is known in the visible and near-infrared, but there is a gap in the coverage around the 1 µm band. Using data in the visible range, Lazzarin et al. (2001) suggested that Braille was V-type to Q-type, and with a strong similarity to the H chondrites. Binzel et al. (2001a, 2001b) also obtained spectra in the visible and noted the strong (but incompletely covered) 1 µm band attributable to olivine and pyroxene. They favored a Q type classification. Buratti et al. (2004) used data in the near-infrared data (1.25–2.6 µm) from the spectrometer on Deep Space 1 and found a ~ 10 % absorption bands at ~ 2 µm in addition to that previously reported at ~ 1 µm. They suggested that the composition of Braille is roughly equal parts pyroxene and olivine and that the overall shape of the spectrum was Q-type. These properties are consistent with those of ordinary chondrites and in turn suggests a relatively fresh, unweathered surface. While it is possible to use the bands at 1 µm and 2 µm to infer and olivine-pyroxene composition, the gap around 1 µm makes it difficult to insert Braille on the BAR plot.

The data for Eros, shown in Fig. 28b, are from Bell et al. (2002) and are a combination of NEAR data (Veverka et al. 2000; Clark et al. 2002a, 2002b) and ground-based data (Chapman and Morrison 1976; Murchie and Pieters 1996). From the relative intensities of

the 1.0 μm and 2.0 μm the OPX/(OPX + OL) ratio is 0.38 ± 0.08 and on the BAR plot of Gaffey et al. (1993a, 1993b) Eros plots within the S(IV) to upper S(III) fields (Fig. 27). These values are similar to those of L or LL chondrite meteorites.

The spectra of Gaspra shown, in Fig. 28c, was published by Helfenstein et al. (1994) uses ground-based data of Binzel (unpublished), Zellner et al. (1985), Mottola et al. (1993) and Goldader et al. (1991). The spectra derived from Galileo data covered the range 0.3–1.0 μm and was essentially in agreement with the ground-based data except for a slightly shallower continuum (Helfenstein et al. 1994). The depth of the 1 mm band and relative shallowness of the 0.2 mm band suggest a fairly olivine-rich surface and my crude measurements from the published spectrum place Gaspra near or in the S(I) group on the BAR plot (Fig. 27).

The visible spectra of Ida and Dactyl obtained by the Galileo spacecraft were published by Veverka et al. (1996) and are shown in Fig. 28d. Both Ida and Dactyl are S asteroids, but there are differences between the two and there are differences across the surface of Ida. These differences concern the depth of the 1 μm band and the slope of the continuum. The interpretations offered by Veverka et al. (1996), and echoed by Chapman (1996), is that crater ejecta is less space weathered than the rest of the surface, particularly notable for the 10 km Azzurra crater and the Azzurra crater ejecta might be called taxonomy type-Q. In the case of Dactyl, these authors favor an interpretation that the spectral differences are mineralogically driven, and that perhaps Dactyl has higher pyroxene abundance. In any event, the spectral differences observed for Ida and Dactyl are small and within the range of spectra observed for the parent asteroid family (the Koronis family; Binzel et al. 1993; Rivkin et al. 2011a, 2011b). The spectrum, based on five-color photometry in the visible region, is not adequate for determining placement of Ida or Dactyl on the BAR plot.

The near-IR spectrum of Itokawa obtained by the Hayabusa spacecraft was published by Abe et al. (2006a, 2006b) and found to be very similar to the ground-based spectra from of Binzel et al. (2001a, 2001b) and Abell et al. (2007) (Fig. 28e). There are small differences in the depth and position of the 1 μm absorption, so that Itokawa is more heterogeneous than, for instance, Eros, but most authors agree that the Itokawa near-IR spectra are consistent with an LL composition. It plots on the S(IV)/S(III) boundary on the BAR plot (Fig. 27). Abell et al. (2007) noted evidence for clinopyroxene in the spectra which they suggested indicated that the surface had experienced partial melting, but Gietzen et al. (2012) point out that type 3 ordinary chondrites (otherwise known as the unequilibrated ordinary chondrites) contain low-Ca clinopyroxenes that could also explain these types of spectra.

Visible/near-IR spectra have been obtained for Lutetia by Lazzarin et al. (2004), Mueller et al. (2006), and Perna et al. (2010) and are shown in Fig. 28f. There are no discernable 1 and 2 μm features, and besides the UV edge, the spectrum for the northern hemisphere is flat while the southern hemisphere possibly has features in the 3 μm region. On the basis of three ground-based spectra over a rotational period, the first authors suggested that Lutetia was a C asteroid with uniform surface composition and with absorptions at 0.43 and 0.51 μm which they attributed to aqueous alteration and porphyrns, respectively. Perna et al. (2010) obtained 13 spectra at various rotational phases and confirmed the two absorptions reported by Lazzarin et al. (2004). However, they found the spectral difference between the northern and southern hemispheres (Fig. 28f). Rivkin et al. (2011a, 2011b) obtained ground-based spectra over the range 2–4 μm to look especially for the 3 μm water band which they found in the southern hemisphere but not the northern hemisphere. In summary, there are no indications of olivine and pyroxene bands in the spectrum of Lutetia, weak bands at 0.43 and 0.51 mm, and signs of water in the southern hemisphere. This fairly flat spectrum has

caused Tholen (1989) to assign Lutetia to the M class, Bus and Binzel (2002) to assign it to the Xb class, and DeMeo et al. (2009) to call it an Xc asteroid. Vernazza et al. (2009, 2011) concluded that Lutetia could be related to the enstatite chondrites, the E asteroid taxonomy, while on the basis of data from the Rosetta spacecraft Sierks et al. (2011) suggest that the data are equally consistent with CO3, CV3 and enstatite chondrites.

Clark et al. (1999) reported the visible spectra obtained for Mathilde by NEAR spacecraft and compared it with the ground-based spectrum reported by Binzel et al. (1996). Both are featureless spectra, but there is a 10 % difference that Clark et al. (1999) did not consider significant (Fig. 28g).

Visible/near-IR spectra have been reported for Steins by Barucci et al. (2007, 2008) and Fornasier et al. (2007; 2008) whose data are similar, especially with respect to the slope at 0.49μm, but differ concerning a small band at 0.96 um (Fig. 28h). The spectra are essentially flat in the near-Infrared, although there are variations in slope, and they resemble the spectra of enstatite chondrites, the enstatite achondrites (aubrites) having shallower slopes but are otherwise similar. Observations in the infra-red by the Spitzer Space Telescope provide information on the thermal properties and composition of Steins and consistent with an enstatite composition (Groussin et al. 2011).

Visible/near-IR data for Toutatis have been reported by Howell et al. (1994), Bus and Binzel (2002), Davies et al. (2007) and Reddy et al. (2012) and a sketch of a represent spectrum is shown in Fig. 28i. Howell et al. (1994) suggested that the surface of Toutatis consisted of high Fe pyroxene and that the body was differentiated. It plotted in a region that overlapped with S(II), S(III) and S(IV). A more recent analysis by Reddy et al. (2012) found that the asteroid plotted in the S(IV) field and has Fe-pyroxene and olivine equivalent to an L chondrite (Fig. 27).

On the BAR plot (Fig. 27) ground based spectroscopy places Vesta in the BA field, (basaltic achondrites, i.e. HED meteorites). Essentially all published results to date confirm the connection between the HEDs and Vesta (e.g. Drake 2001; Russell et al. 2012; McSween et al. 2013). In addition to the visible and near-infrared reflectance data, experimental petrology demonstrated that the eucrites were the product of approximately a 10 % melt, siderophile element partitioning suggested that this melt was the residue of an asteroidal-scale magma ocean. Mass balance considerations point to a parent body that had its surface excavated, but remains intact. Modern telescopic spectroscopy has identified kilometer-scale "Vestoids" between Vesta and the 3:1 orbit-orbit resonance with Jupiter (Binzel and Xu 1993). Dynamical simulations of impact into Vesta demonstrate the plausibility of ejecting relatively unshocked material at velocities consistent with these astronomical observations (Asphaug 1997). Hubble Space Telescope images show a 460 km diameter impact basin at the south pole of Vesta (Thomas et al. 1997) which was found to be two large basins by the Dawn imagery (Schenk et al. 2012).

The main purpose of Dawn-based vis/near-IR spectroscopy was to look for regional variations in composition on Vesta and these were reported by De Sanctis et al. (2012a). The authors found that while the spectra were very similar in the visible range, in the IR range there was a significant difference between the equatorial region and the South Polar Region (Fig. 28j). When the parameters needed for the BAR plot are crudely determined from the published spectra of De Sanctis et al. (2012a), both Vesta regions plot in or near the BA field, the equatorial region plots on the BA field but the south polar region actually plots in the S(VII) field (Fig. 27). According to Gaffey et al. (1993a, 1993b), the S(VII) asteroid spectra are "consistent with metal-basaltic assemblages (analogous to mesosiderite meteorites) or to feldspar-rich basalts or basaltic anorthosites (pyroxene-bearing feldspar-dominated assemblages)".

Before the Dawn mission it was presumed that the large polar basins would penetrate the mantle and this would be reflected in greater amounts of olivine in the basin. This has not proved to be the case. Orange material, seen occasionally in craters and on crater walls, was at one time thought to be olivine, but now appears to be impact melt (Le Corre et al. 2013). In fact, the only observations of olivine rich materials on the surface of Vesta are found in isolated instances in craters, crater walls, and the rims of the Rheasilvia and Veneneia basins (Ammannito et al. 2013a). Using the mixing curves of Gietzen et al. (2012), the S(VII) field could reflect the presence of orthopyroxene, as observed in the diogenite meteorites (Keil 2002). Thus several authors have suggested that the bottoms of the South Polar Basins are diogenitic (Ammannito et al. 2013b; De Sanctis et al. 2013), consistent with igneous stratigraphy and orthopyroxene-rich rocks underlying the basaltic (eucritic) crust but it is not clear exactly how this stratigraphy came about (McSween et al. 2013).

Ground based measurements by Hasegawa et al. (2003) suggested water on Vesta, but this has not been confirmed by the infrared spectrometers on Dawn, although it was confirmed by neutron spectroscopy (see below).

The main science issue presented by Ceres is its composition (Johnson and Fanale 1973; McCord and Gaffey 1974; Lebofsky et al. 1981; Larson et al. 1983; Rivkin et al. 2003; 2006). Absorption features are weak or absent (Fig. 28k), but Vilas (1994) has used the absorption at ∼ 0.8 μm to argue for the present in water in many C asteroids. The role of water in the history of Ceres is of much importance and models have been developed by Fanale and Salval (1989) and more recently by Schorghofer (2008). The strong absorptions in the ∼ 3.0 μm region have been the subject of considerable work, the 3.05 μm band being ascribed to water ice frost (Lebofsky et al. 1981), ammoniated clays (King et al. 1992), irradiated organics in ice (Vernazza et al. 2005), and carbonates (Rivkin et al. 2006). Related to composition of Ceres is the connection it has, if any, with the C chondrites which have low albedos, relatively flat spectra in the visible to 2.5 mm regions, and strong absorptions around 3.0 μm (e.g. Vilas and Gaffey 1989; Vilas and McFadden 1992; Calvin and King 1997). Another issue is whether it is internally differentiated (McCord and Sotin 2005), which, in a water-rich body like Ceres, means whether it has an internal structure reflecting the loss and redistribution of water and perhaps even a subsurface ocean. It is a controversial issue (Zolotov 2009), but recent estimates of the shape of Ceres suggests that it is not a uniform sphere suggestive of some internal differentiation (Thomas et al. 2005; Erard et al. 2005). While planetary scientists have deliberated on the presence and behavior of water on Ceres, there has been a similar discussion of the role of water in determining the properties of CM chondrites (McSween 1979) and two groups of authors have proposed classification schemes for the aqueous alteration of CM chondrites (Browning et al. 1996; Rubin et al. 2007).

6.3 Other Methods of Remote Sensing

The composition of the surface of Eros was measured using the X-ray/gamma-ray spectrometer and found to have hydrogen and major element concentrations comparable to L or LL chondrites (Peplowski et al. 2015).

Using data from the International Ultraviolet Explorer (Hendrix et al. 2003) found that much of the western hemisphere of Vesta was lighter than most of the eastern hemisphere, in contrast to the situation at visible wavelengths. By analogy with the Moon, Hendrix et al. (2003) attributed this to differing degrees of space weathering. However, if what they observed was the same darkening as observed by Dawn, then these differences may
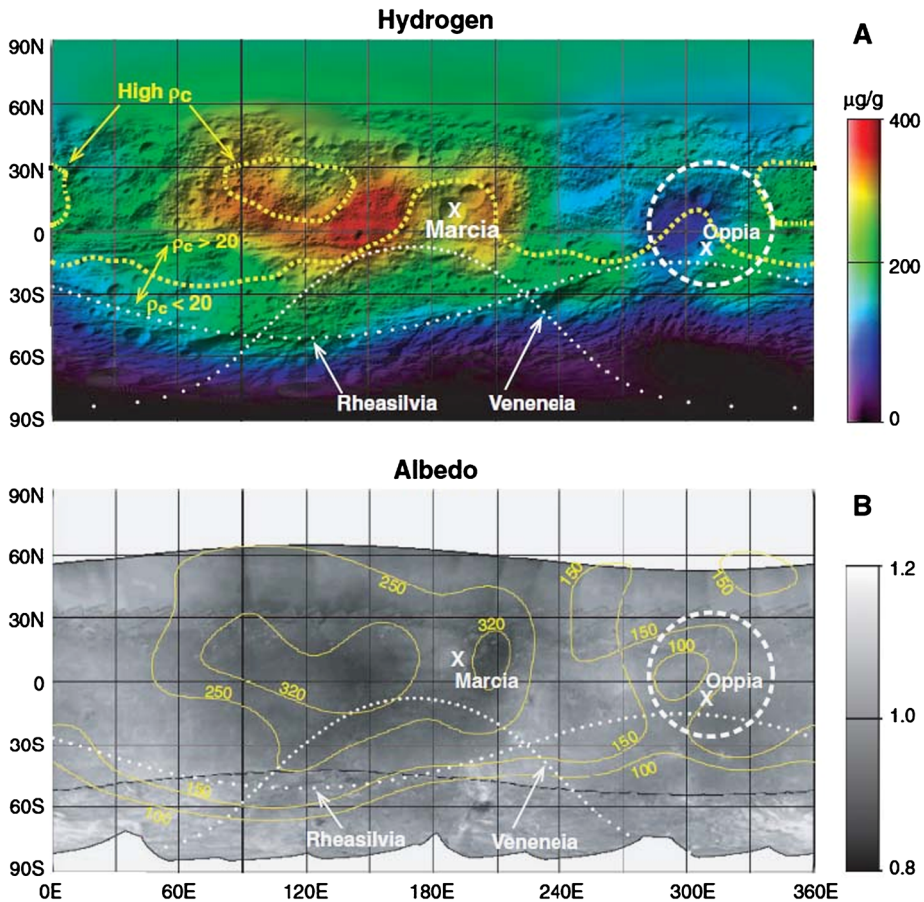
Fig. 29 (**a**) Distribution of hydrogen on Vesta as determined from the Dawn spacecraft's neutron spectrometer. (**b**) A map of the albedo of Vesta. The similar distribution suggests that both the dark material and H, most probably in the form of water, were placed on Vesta by the impact of carbonaceous, water-rich material resembling the CI and CM chondrites. The *dashed white line* indicates a circular depression in which crater Oppia is located. The *contours* marked ρ_c refer to crater densities (in craters per 10 km^2), the thin contours marked with numbers (250 etc.) indicate relative ages of the surface, the *dotted white lines* refer to the extents of the Rheasilvia and Veneneia basins (Prettyman et al. 2012)

be due to the presence on the surface of large amounts of material resembling CM chondrites.

The gamma ray and neutron detector on Dawn (which is sensitive to Fe, Ca, Al, Mg, and other rock-forming elements) indicate that Vesta is more compositionally uniform than the Moon, but variations were present that could be explained with the help of laboratory measurements on eucrites-diogenite mixtures (Prettyman et al. 2013). The results were in agreement with those of visible-near-IR spectroscopy. The Rheasilvia basin and ejecta blanket was found to be consistent with Mg-rich orthopyroxene, while Vesta's "dark" hemisphere, where exogenic hydrogen has accumulated, was thought to be richer in basaltic eucrite, representative of Vesta's ancient upper crust. There were no indications of any olivine-rich lithologies that might indicate exposure of the mantle.

Table 8 Particles collected by Hayabusa from the surface of Itokawa*

Description	Number	Predicted Number*		
	Itokawa	LL	L	H
Monomineralic				
Olivine	580	615	447	290
Low-Ca pyroxene	126	170	219	207
High-Ca pyroxene	56	48	43	37
Feldspar	186 (172 plagioclase, 14 K-spar)	101	90	79
Troilite	113	58	52	46
Chromite	13			
Ca-phosphate	13			
Metal	3	96	236	429
Total monomineralic	1087			
Polymineralic				
Mostly silicates, some with metal	447			

*Meteorite abundances determined by petrographic methods converted to expected numbers of grains by density-correction and normalization to 1087 (Itokawa data from Nakamura et al. 2011, 2014; meteorite data from Sears 1978).

As shown in Fig. 29, which is from Prettyman et al. (2013), neutron and gamma ray spectroscopy also detected water-rich regions on Vesta. In fact, $\sim 30\%$ of Vesta's surfaces contains $> 250\,\mu\text{m/g}$ of water. Correlated with the water is dark material (see the albedo map in Fig. 29), so the suggestion is that carbonaceous chondrites brought both the dark material and water to the surface of Vesta by impact (McCord et al. 2012; Jaumann et al. 2014). CI chondrites are up to ~ 20 vol% water and CM chondrites are up to ~ 10 vol% water. The Vesta pits, discussed earlier, also suggest the presence of water during the impact that produced the host melts.

6.4 Returned Samples

The only asteroid for which space missions have returned samples is Itokawa which returned over a thousand dust particles. On a Teflon spatula scrapped around the inside of the sample collector, Nakamura et al. (2011) found 1534 particles, 3–40 µm in size, with most $< 10\,\mu\text{m}$. The mineral identification of the particles is broadly consistent with ordinary chondrite mineralogy, with enhancement of feldspar and depletion of metal as expected for density sorting in the regolith or during collection (Table 8). By tapping the collector over a glass slide they recovered 40 particles with a size range of 30–180 µm.

The bulk composition of the Itokawa particles is probably meaningless because of small sample mass and selection effects in particle collection; however Ebihara et al. (2011) argue that the Fe/Sc and Ni/Co ratios of a 3 µg polymineralic grain were chondritic. The mineral assemblage is broadly chondritic so it is meaningful to compare the olivine and pyroxene compositions—one of the major characteristics of the individual chondrite classes—in which case Itokawa appears to have LL chondrite composition (Fig. 30a, Nakamura et al. 2011, 2014). However, not all grains have the same composition; about 15 % appear to be unusual and were referred to by Nakamura et al. (2011) as "unequilibrated". The other major

Fig. 30 Compositional data for samples of Itokawa collected by the Hayabusa spacecraft. (**a**) Composition of the two major rock forming minerals (ferrosilite in the pyroxene and fayalite in the olivine, as mole percentages) compared with data from the equilibrated ordinary chondrites, H, L, and LL classes. (Itokawa data from Nakamura et al. 2011, meteorite data from Sears 1978). (**b**) Oxygen isotope composition compared with equilibrated ordinary chondrites (H, L, LL) and terrestrial minerals (San Carlos olivine and Miyake anorthite). The *axes* refer to $^{17}O/^{16}O$ versus $^{18}O/^{16}O$ in units of parts per thousand deviations from a standard (Standard Mean Ocean Water). ECL, equilibrated ordinary chondrite line, TF, terrestrial fractionation line, Ol, olivine, Opx, orthopyroxene, Pl, plagioclase. The *line* parallel to TF is a regression line through the Itokawa mineral data which intercepts the ECL line in the LL chondrite region indicating the bulk Itokawa samples are compositionally identical to LL chondrites (Nakamura et al. 2011)
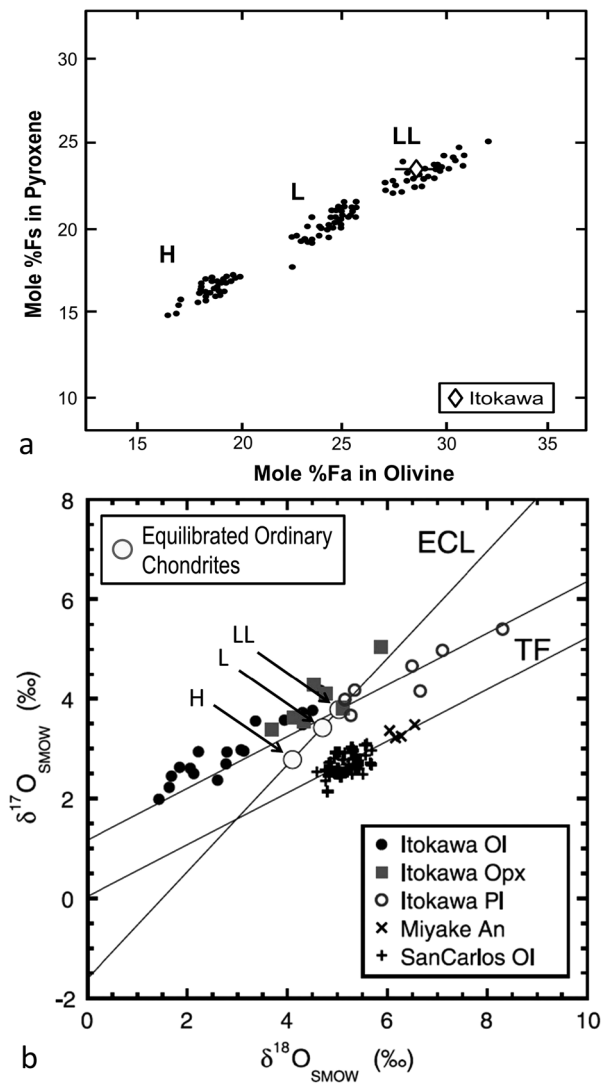
tool for taxonomy of meteorites is the oxygen isotopes (Fig. 30b). On the three-isotope plot, $\delta^{17}O$ against $\delta^{18}O$, data for olivine, pyroxene and feldspar plot along a mass-fractionation line (slope 0.5) indicating thermal equilibration between the minerals. However, the slope of this mineral line intercepts the slope of the equilibrated chondrite line (ECL) at the LL chondrites location, again suggesting an affiliation with the LL chondrites. These results confirm the conclusions based on visible/near IR spectroscopy (Binzel et al. 2001a, 2001b; Abe et al. 2006a, 2006b).

The homogeneous composition of most of the olivines and pyroxenes, and the slope 0.5 line produced on the three-isotope line produced by the major minerals, indicates a high degree of thermal equilibration consistent with parent body metamorphism. On the petrographic scale of Van Schmus and Wood (1967), Nakamura et al. (2011) suggest that the Itokawa samples are mostly type 6, but with a range of type 4 to type 6 to accommodate

the unequilibrated grains. The coexistence of apparently equilibrated minerals means that the pyroxene geothermometer and olivine-spinel geospeedometer can be applied and these indicate peak temperatures of ∼800 °C and slow cooling to ∼ 600 °C. The plagioclase structure also suggests closure temperatures of 655 to 660 °C (Tanaka et al. 2014). On the basis of a thermal model and assuming ^{26}Al is the heat source, Wakita et al. (2013) suggest that Itokawa came from an object > 20 km in radius and accreted at a period between 1.9 and 2.2 Myr after CAI.

The Itokawa grains also enable information to be gleamed about space exposure conditions, without the complications of lithification which are present in the case of gas-rich regolith breccia meteorites (Bischoff et al. 1983). Trapped solar wind gases are present, despite He loss, and cosmic ray produced ^{21}Ne suggest a surface exposure age of less than 8 Ma (Nagao et al. 2011). Five out of ten grains examined by Noguchi et al. (2011, 2014) showed evidence for evaporation and recondensation of elements during regolith working, forming the familiar nanoparticles of iron (sulfur-rich at the surface, sulfur-poor at depth) that are thought by some authors to explain the discrepancy between S asteroids and ordinary chondrites.

7 Discussion

7.1 Asteroids and the Stories They Tell

As discussed above, there are about 25 classes of asteroid according to their visible/near-IR spectra fingerprints. In about half the cases the spectra are fairly flat and features are weak. Considerable effort is spent in trying to interpret them in terms of mineralogy and meteorite matches (Rivkin et al. 2002). In about half the cases, the spectra have deep, albeit very wide, absorption features and the mineralogical interpretations are straightforward, at least to the first-order (Gaffey et al. 1993a). At greater levels of detail, which are often very important, there are considerable complications caused by the compositional and structural complexity of rock-forming minerals (Klima et al. 2007, 2011). Overlaid on this general picture is the certain knowledge that spectra are only describing the very surface layer. From our extensive studies of lunar regolith, we also know about space weathering and some variability in the asteroid spectra can be ascribed to differences in space weathering (Clark et al. 2002b), but this is also a surface process. What lies beneath can only be inferred.

Based on models for collision, fragmentation, and behavior of the fragments, it is expected that many asteroids should be rubble piles and the morphologies of small asteroids are sometimes interpreted to be consistent with this (Love and Ahrens 1996). On the other hand, spin rates for < 200 m objects are high and require monolithic internal structures (Pravec and Harris 2000). The brecciated nature of meteorites is sometimes interpreted as evidence for a rubble pile structure for the meteorite parent bodies (Taylor et al. 1987), although the length scales of a microscopic thin section, or even a hand specimen, are very different to those of an asteroid. Scaling from centimeter-scale observations to kilometer-scale processes is difficult. Interpretations of meteorite thermal histories, including cooling rates for stones and irons, have been used to infer internal structures for asteroids (Ghosh et al. 2006), and by-and-large seem to favor some kind of "onion skin" model, namely concentric zones of differing thermal history with internal heating due to ^{26}Al. Since most ordinary chondrites are highly magnetized (Morden and Collison 1992; Pesonen et al. 1993), it has been proposed that some S asteroids have chondritic crusts covering differentiated interiors so a magnetic field was created (Elkins-Tanton et al. 2011). On the other hand, the

present author and his colleagues have suggested that the chondrite classes can be produced by density and size particle sorting during fluidization on a thick regolith and that the interior of all asteroids (C and S) have essentially CM-like compositions (Huang et al. 1996; Akridge and Sears 1999; Sears 2005).

With this thumbnail sketch in mind, we can now discuss some ideas that have emerged (at least in the writer's mind) from the eight missions to asteroids.

7.2 What Has Been Confirmed?

The first image of asteroid Gaspra was intriguing. Before that time asteroids had been merely points of light. Before the missions, we had information about orbit, spin rate and orientation, size, and surface mineralogy if we had reflection spectra. We had telescopic (ground, air, and space borne) and spectral data, and at about the time the missions came on-line we had radar images and we could resolve compositional variations on Vesta and albedo variations on Ceres. In retrospect, it was probably also clear that asteroids would have dry cratered surfaces, although perhaps it was a surprise that some were so heavily cratered, which signified a great age of their surfaces (e.g. Sierks et al. 2011). Being so small it was assumed they would largely be irregular shape, as suggested by light curves (Kaasalainen and Torppa 2001). Ceres is the only spherical asteroid among the explored asteroids (albeit with some polar flattening, Thomas et al. 2005), although from some directions Vesta looks circular, the two major southern basins give it a decidedly non-spherical appearance (Fig. 3). Most of the physical properties of the asteroids (where known), their orbital parameters, their rotation rates, their spin orientations, were confirmed by the missions, and determined to greater precision than before.

The existence of space weathering has been confirmed, and perhaps better understood, as a result of the missions. Detailed studies of the returned Itokawa samples showed that individual grains were showing signs of weathering similar to those expected previously (Noguchi et al. 2014). Similarly, it was observed that space weathering on a V asteroid was unlike that for S asteroids, as expected (Pieters et al. 2012).

Reddy et al. (2013) made a detailed comparison of what had been learned from the Dawn mission to Vesta compared with data from the Hubble Space Telescope and ground-based observations. Dawn improved our knowledge of the rotational period, pole position and obliquity, and the mission doubled the known range of topographic features on Vesta relative to earlier measurements. The Dawn mission also improved our knowledge of surface geography and essentially confirmed much simpler details expected on the basis of ground-based observations (Fig. 31a). The final conclusion of Reddy et al. (2013) was that by-and-large ground-based astronomy was "valuable support" for future missions.

The Dawn images of Ceres are compared with images from the Hubble Space Telescope in Fig. 31b. A detailed comparison by the science team has yet to be published, and precise alignment of the two images is uncertain, but one can imagine several linkages between the dark regions observed by HST and surface features on the dwarf planet.

Radar is capable of providing images of asteroids that come close enough to the Earth. As mentioned above, one of the explored asteroids has been observed with radar, Toutatis. While still lacking the intricate detail of an optical image, the radar images are remarkably similar to the spacecraft images at a small fraction of the cost (Fig. 32). The radar images obtained do resemble the spacecraft images in their overall irregular shape, the presence of large boulders on the surface, sometimes bifurcation and, in one instance, a moon.

Fig. 31 (**a**) Comparison of features on Vesta as observed by the Dawn spacecraft with previous maps derived from ground and Hubble based observations (Reddy et al. 2013). (**b**) Comparison of Dawn images of Ceres by combining images at 440, 550, and 920 nm (NASA/JPL, Image PIA19063) with previous albedo maps based on ground-based observations (Carry et al. 2012)
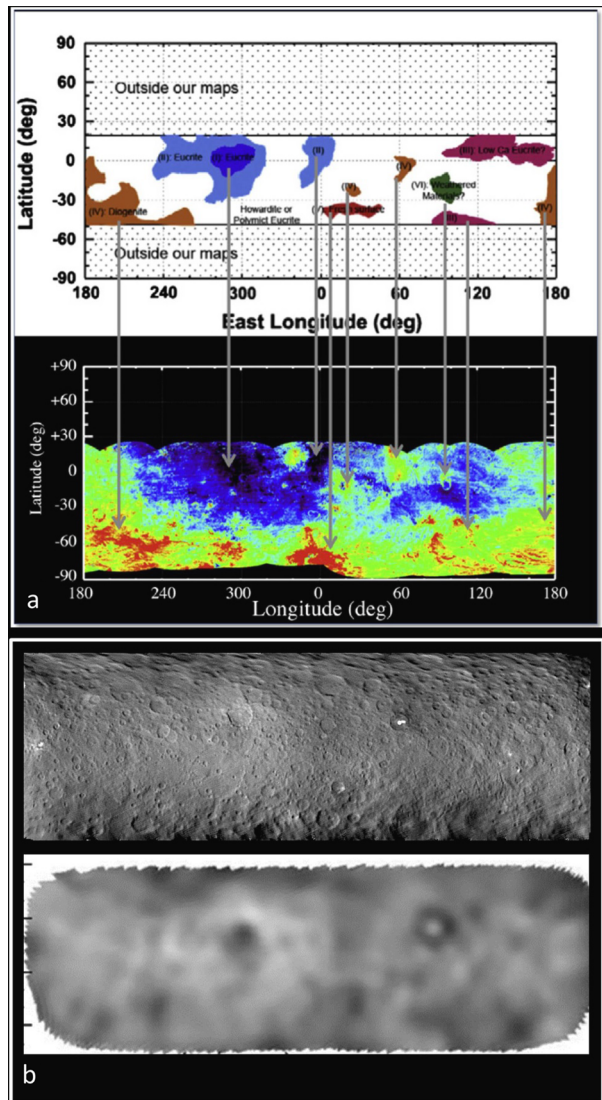

7.3 What Is New?

7.3.1 The Existence of Regolith

Probably the most important contribution to planetary science to emerge from the asteroid missions was that all of the asteroids, regardless of their size, are covered in regolith (see regolith discussion above). Prior to the missions, there was a strong argument that small objects like 10 km asteroids could not retain a regolith (Chapman 1976; Housen et al. 1979). The presence of regolith has important implications for impact mechanics and the thermal history of the asteroid (e.g. Akridge and Sears 1998). A thick insulating layer of regolith means greater heat retention inside the asteroid and a shallowing of the thermal
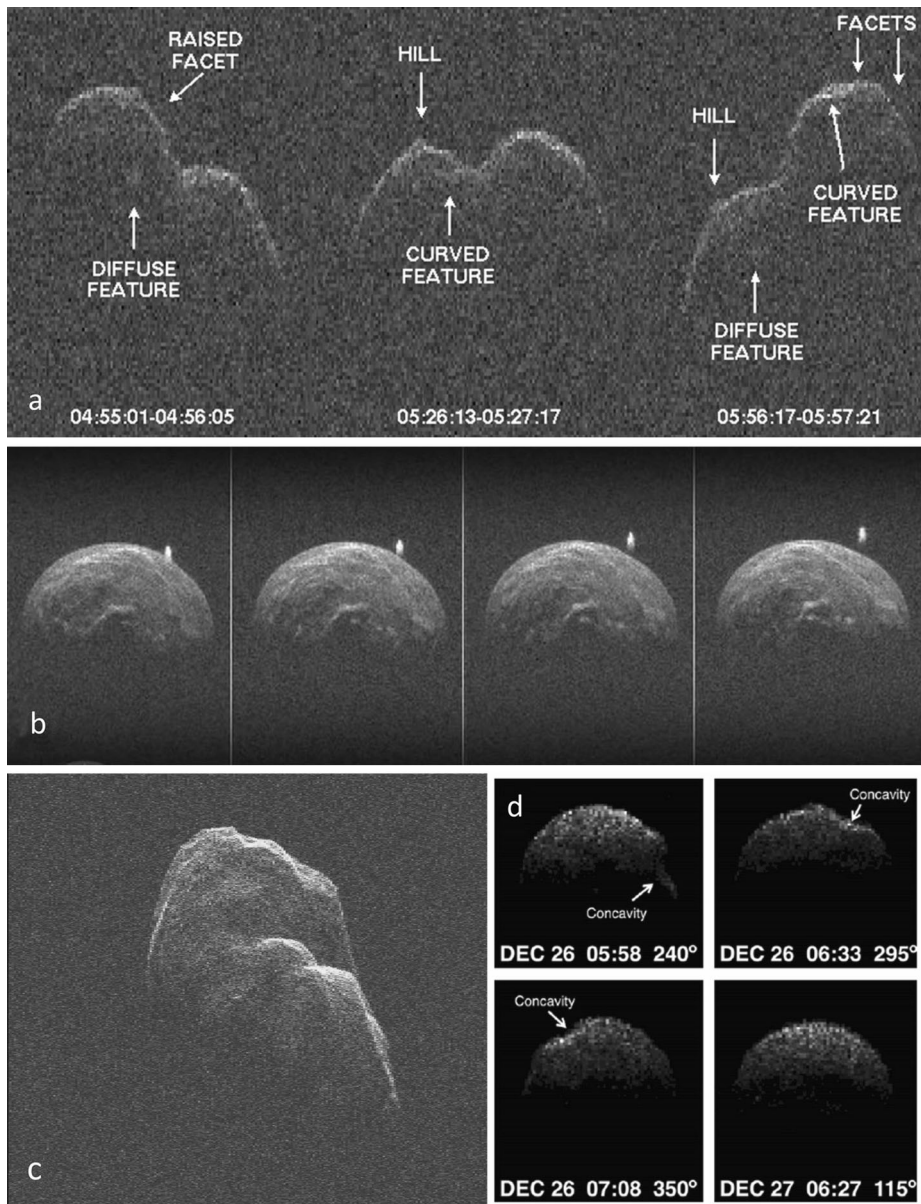
Fig. 32 Radar images of some near-Earth asteroids. (**a**) 2005 CR37 showing a variety of surface structures, facets, hills, curved features and diffuse feature (Benner et al. 2006). (**b**) 2004 BL86 showing a moon (NASA press release Jan 27th 2015). (**c**) Toutatis showing its bifurcated structure (NASA/JPL PIA 16599). (**d**) 2008 EV5 showing a concavity interpreted as a crater (Busch et al. 2011)

gradients. A thick regolith also means a more efficient absorption of energy on impact and a greater amount of glass production and alteration of the target rocks (Hörz and Schaal 1981; Asphaug et al. 2002). The presence of thick dust layer also has major implications for surface operations on an asteroid by explorers and prospectors (Sears et al. 2004).

7.3.2 Rubble Piles and Monoliths

The grooves and ridges observed on asteroids by the missions (see grooves and ridges section above) probably indicate that these asteroids are not rubble piles because these features require asteroid-wide coherence. The grooves on Gaspra (Veverka et al. 1994), the fractures in the Pola Regio region of Ida (Asphaug et al. 1996), that appear to have been opened by the Azzurra crater impact, Rahe Dorsum and many smaller grooves on Eros (Procter et al. 2002), all suggest that these asteroids are not rubble piles. The line of craters (the catena) on Steins has been explained as an asteroid-scaled fracture caused by the impact responsible for the Diamond crater, which also implies a compact body rather than a rubble pile (Keller et al. 2010). Itokawa was described as a rubble pile (Fujiwara et al. 2006), based on its appearance, but this tiny shard may have been produced in the regolith of a larger asteroid and might be better described as a regolith breccia rather than a rubble pile made by disassembly and reaccretion. One of the arguments for a rubble pile is a high calculated porosity and this could, in part, be due to water in the interior of these asteroids Some researchers have suggested that the interior of all asteroids resemble the water-rich CM chondrites (Huang et al. 1996; Akridge and Sears 1998; Sears 2005), while yet others have suggested that the interiors of the of the S asteroids may be differentiated with a core and mantle, but with a chondritic crust (Elkins-Tanton et al. 2011). It has been suggested that most of the S asteroids have surfaces containing melts or partial melts (Sunshine et al. 2004), which would suggest another kind of interior and perhaps metal-rich interiors.

7.3.3 Water, Active Asteroids, and Comets

Dawn's exploration of Vesta taught us that water can appear in unexpected places (Prettyman et al. 2012; Denevi et al. 2012). This distribution of water is not only relevant to astrobiology, but water drives a great many geological and physical processes and is probably the major resource provided by the asteroids to exploration and commercialization efforts. The stability threshold for water in the solar system is referred to as the "snowline" and the asteroid belt straddles this line. Closer to the Sun than the snowline, primary water is absent. Beyond the snowline, primary water is present. The snowline is variously placed at 2.7–3.2 AU (Hayashi 1981; Podolak and Zucker 2004; Martin and Livio 2012). Water currently inside the snowline is assumed to be secondary. Like the Earth's water, it is assumed to have been brought in by interlopers from the outer solar system.

The concept of a snowline arises from the simple thermodynamic calculations (Lewis 1974) and the observation that C asteroids (supposedly water-bearing) dominate in the outer solar system and S asteroids (supposedly dry) dominate in the inner solar system, although there is ample overlap (Chapman 1976). Clearly, distance from the Sun matters. We assume comets are water and other volatile-rich because they formed at very low temperatures far from the Sun (Weidenschilling 1997). The cause of the gradient in the ratio of S to C asteroids is unclear. It may be the result of planetesimals accreting at different temperatures, water-bearing asteroids accreted below the temperatures required for water condensation (Lewis 1974), or it could be the result of the S asteroids being heated by internal radioactivities such as ^{26}Al while the C asteroids escaped this heating (Grimm and McSween 1993). Such would be the case if there the amount of ^{26}Al present decreased with distance from the Sun. This could result if the time of accretion increased with distance from the Sun and by the time the later materials accreted the level of ^{26}Al had decreased.

The question of internal heating is important not only for water retention, but also the nature of the asteroids and their interiors. The discovery of relatively abundant ^{26}Al in the

Ca-Al-rich refractory inclusions in CV chondrites meant that any body larger than 5 km should have melted (Lee et al. 1976). Certainly, there are melted asteroids, Vesta and the V asteroids for instance, but equally clearly many appear totally unmelted, the C, P, D asteroids for instance. It is possible that the refractory inclusions accreted particularly early, which is assumed to be the case, but it is also possible that the distribution of ^{26}Al was heterogeneous.

Complicating any simple picture that links properties such as water content with distance from the Sun is the injection of objects into the inner solar system from the outer solar system. The fraction of the NEAs that are extinct comets is unknown, but many estimates have been made and some are quite high (Weismann et al. 2002). This is important because the interpretation of many properties of NEAs hinges on whether they could contain volatiles.

While Ceres and Vesta are both close to the snowline, Ceres' water is indigenous and throughout the body while Vesta's water is exogenous and surficial. Vesta orbits inside the snowline, Ceres is sometimes inside and sometimes in the outer fringes of the snowline depending on its location along its orbit.

There has been considerable discussion of Ceres and water. Several authors have reported spectral evidence for hydrated minerals on Ceres (Lebofsky et al. 1981; King et al. 1992; Milliken and Rivkin 2009) and models of the density and shape of Ceres have been used to argue for a differentiated interior, silicate core, icy mantle (Thomas et al. 2005; McCord and Sotin 2005; Castillo-Rogez and McCord 2010). An initial observation of water vapor around Ceres (A'Hearn and Feldman 1992) were disputed (Rousselot et al. 2011) but recent remote data have suggested there are local sources of water at mid latitudes (Küppers et al. 2014). As we saw above, recent images of the Ceres from the Dawn spacecraft show bright spots which could be plumes—the plumes of water observed by the Herschel spacecraft (Küppers et al. 2014). Alternatively, they could be ice or evaporite deposits. There are several reports of water-ice on asteroids based on spectroscopic observations (Campins et al. 2010; Rivkin and Emery 2010; Licandro et al. 2010).

Schorghofer (2008) has introduced the concept of a "buried snowline". He shows that moderate levels of burial are sufficient to protect any ice originally present in the asteroid for the age of the solar system. Thus if water-bearing asteroids, or comet nuclei, migrated inside the snowline (Walsh and Morbidelli 2011) subsurface water could be stable for long periods of time. If brought to the surface by some means, for example collision, sublimation of water could be a mechanism for dust activity. Consistent with this idea, there are several "active" asteroids (Jewitt 2012), these are asteroids that eject dust and unexpectedly produce transient, comet-like comae and tails.

There are several main belt asteroids with comet-like tails, presumably caused by the evaporation of water. Probably the most notable is P/2010 A2 which was observed by the Rosetta and Hubble spacecraft to have a complex array of trailing debris (Jewitt et al. 2010; Snodgrass et al. 2010). The tail was apparently produced by the disruption of a 60–100 m asteroid, but it is not clear whether the disruption was caused by the impact of another asteroid or a by an accelerating spin that reached a critical disruption value. Other examples of comets in the main asteroid belt are 133P/Elst-Pizarro, P/2005 U1 (Read), and 118401 (1999 RE70) (Hsieh and Jewitt 2006). The movement of the dust indicates that it was being lifted by the sublimation of water, since impact generated dust would disperse quickly in a ballistic fashion. Laboratory simulations experiments also suggest a drag mechanism for the ejection of cometary dust (Sears et al. 1999). Figure 33 compares the distances of the known active asteroids from the Sun, including those mentioned above, with the nominal snowline at 2.7 to 3.2 AU. Besides the two Centaurs showing evidence for degassing (2060 Charon and 60558 Echeclus), only 176P/LINEAR and 7968 Elst-Pizarro have orbits that

Fig. 33 The orbital range (perihelion to aphelion) of the active asteroids compared with the range of values suggested for the snowline. For clarity, the Centaurs 2060 Charon and 60558 have been left off the diagram
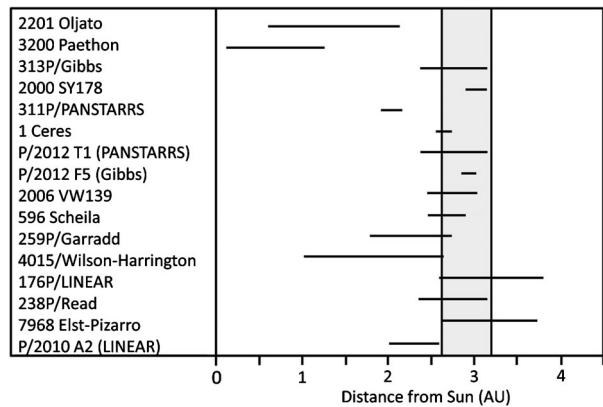

take them outside the snowline, otherwise all these objects orbit inside the snowline. Two active asteroids approach to within 1 AU of the Sun. These objects may be interlopers in the inner solar system, forming in the outer solar system but either way they demonstrate that objects in asteroidal orbits in the inner solar system can be water-bearing. Thus an additional type of process that could explain some of the surface properties of asteroids involves the loss of volatiles, such as formation of the Eros ponds by fluidization of the surface materials (Sears et al. 2015).

The existence of active asteroids and the possibility of structures formed by fluidization processes prompts the question as to whether anything can be learned by comparing comet nuclei with asteroids. Since the early 1980s, Hartmann and his colleagues have argued that there was a continuum between asteroids and comets and they were essentially from the same population, differing systematically in detailed properties depending on their formation location. In particular, they point out the compositional similarity between comets and certain asteroids, namely the P, D, and C type asteroids, and (Cruikshank et al. 1985; Hartmann et al. 1987). Can we learn something about processes on asteroids from cometary surfaces?

Figure 34 shows the images of cometary nuclei obtained by robotic spacecraft to date. The nucleus of Halley's comet (Fig. 34a) was visited by a flotilla of spacecraft in 1986. The images suggest a peanut-shaped nucleus $16 \times 8 \times 8$ km with a ~ 54 h rotation with a density of 0.28 g cm^{-3} (Rickman 1989). The surface features were interpreted to include a "finger", a crater, a chain of hills, a southern jet, a mountain and a central depression (Keller et al. 1988). Fine filaments of dust were pouring out of ~ 0.5 km locations on the surface and reaching over 100 km.

Oberst et al. (2004) also describe Borrelly's (8×4 km) nucleus (Fig. 34b) observed by the Deep Space 1 spacecraft as being peanut shape, with very low albedo (0.008–0.24) and with terrains that are either bright or dark, smooth or mottled. There is high surface roughness in the "neck' of the peanut and near the presumed source of the jets. From non-gravitational motions, Davidsson and Gutiérrez (2004) estimate a density of 0.18–0.30 g cm^{-3}. The $5.5 \times 4.0 \times 3.3$ km nucleus of Comet 81P/Wild (Fig. 34c) contains two kinds of depressions (Brownlee et al. 2006), those with debris rims (which resemble lunar impact pits) and those without, where the latter have steep sides (and resemble impact experiments with porous targets). According to Sekanina et al. (2004) there are about 20 jets, all but two on the sunlit side, ejecting water at $\sim 2 \times 10^{28}$ molecules/s at perihelion. Davidsson and Gutiérrez (2004) suggest that ~ 60 % of the surface is active and from non-gravitational motion of the
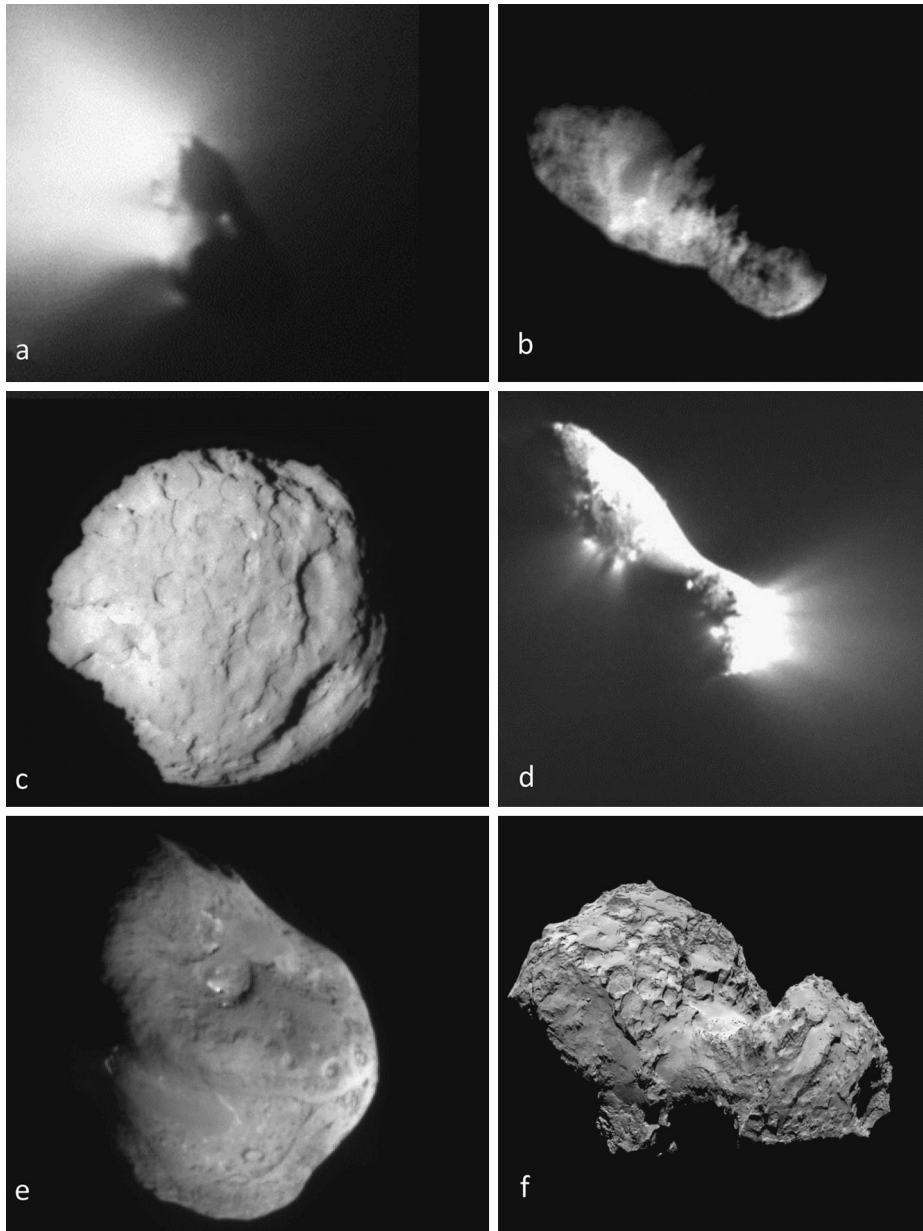
Fig. 34 Images of the nuclei of comets visited by robotic spacecraft. (**a**) The nucleus of Halley's comet (Comet 1P/Halley, 15 × 8 km) imaged by the Giotto spacecraft March 14, 1986 (ESA). (**b**) The nucleus of Comet 19P/Borrelly (8 × 4 km) imaged by the Deep Space 1 spacecraft September 21, 2001 (NASA/JPL). (**c**) The nucleus of Comet 81P/Wild (5.5 × 4.0 × 3.3 km) imaged by the Stardust spacecraft January 2, 2004 (NASA/JPL). (**d**) The nucleus of Comet 103P/Hartley (1.2–1.6 km) imaged by the EPOXI spacecraft November, 2010 (NASA/JPL/UMD). (**e**) The nucleus of Comet 9P/Tempel (7.6 × 4.9 km) imaged by the Deep Impact (July 4, 2005) and Stardust-NEXT spacecraft (February 15, 2011) (NASA/JPL/UMD). (**f**) The nucleus of Comet 67P/Churyumov-Gerasimenko (4.3 × 4.1 km) imaged by the Rosetta spacecraft which went into orbit around the comet on September 10, 2014 (ESA)

nucleus find a density of 0.6–0.8 g cm^{-3}. The nucleus of Comet 103P/Hartley 2 (Fig. 34d) is 1.2–1.6 km, has a density of 0.2–0.4 g cm^{-3}. The nucleus is bifurcated, 2.44 km long, with a smooth variegated waist between the lobes. Its surface is primarily small < 40 m mounds (Thomas et al. 2013). Syal et al. (2013) found that both the narrow-angle and fan-shaped dust jets were emanating from pits, arcuate depressions, scarps, and rimless depressions on the surface of the nucleus, usually the sources were less than 12 m in size.

The 7.6 × 4.9 km nucleus of Comet 9P/Tempel (Fig. 34e) was imaged by both the Deep Impact spacecraft (July 4, 2005) and Stardust-NEXT spacecraft (February 15, 2011). The density is 0.62 +0.47/−0.33 g cm^{-3} and the surface is partially smooth, and partially rough, with the rough terrain consisting of steep-walled pits to albedo and topographic rings, with all ranges of morphological gradation (Thomas et al. 2013). Solid water ice has been detected on its surface (Sunshine et al. 2006). An impact into the nucleus yielded large amounts of microscopic dust particles suggesting a preexisting dust layer tens of meters deep (A'Hearn et al. 2005). Belton and Melosh (2009) have described evidence for fluidization and multiphase transport of particulate material on 9P/Tempel 1. They measured the extent of smooth terrains, slopes of the centerlines and likely source regions and argue that the fluidization is driven by the release of CO and/or CO_2 at ∼ 0.003–0.03 m/s. This is broadly consistent with laboratory measurements (Huang et al. 1996). Particles returned from Tempel 1 are a heterogeneous mixture of nanosized grains of ferromagnesian silicates, Fe, Ni sulfides and metal, reflecting a range of formation conditions including some phases that formed at high temperature (Zolensky et al. 2006). There is no simple linkage with any meteorite class, although a major problem is alteration of the particles by the capture mechanism.

Rosetta is an ESA Cornerstone mission that after three gravity assists from Earth and one from Mars went into orbit around the comet Churyumov-Gerasimenko on 6th August 2014 and put a lander on its surface on 12th November 2014. The orbiter carries 11 science instruments for UV, visible, IR and thermal IR imagery, particle collectors, mass spectrometers, radio sounding and plasma characterization. The ∼ 100 kg lander, Philae, carries 10 science instruments for imaging, collecting samples and analyzing the surface and evolved gases at the molecular, elemental, and isotopic level, and for determining dust and plasma properties. The nucleus of Comet 67P/Churyumov-Gerasimenko (Fig. 34f) (4.3 × 4.1 km, density 0.47 g cm^{-3}) is the best imaged of all the comets and shows a wide variety of structures and textures. It consists of two lobes with a thick dust covered neck from which most of the activity appears to emanate. Airfall, surface dust transport, mass wasting, and insolation weathering, are all important for cometary surface evolution (Thomas et al. 2015). There is also evidence for subsurface fluidization models and mass loss through the ejection of large chunks of material.

As mentioned above, it has long been thought that there was a continuum between asteroids and comets based on overlap of colors (comet nuclei and p, d, c asteroids, Cruikshank et al. 1985). Now we can add in a continuum of densities (comets, TNO, asteroids, Carry 2012), a continuum of albedos, the existence of active asteroids, and similar features in surface morphology (Thomas et al. 2015). It is true that there is considerable range in surface appearance, reflecting maturity of the surface and number of passes in the inner solar system, but mature comets can have thick fine regoliths, mobilization of regolith, ridges, grooves, and craters similar to the asteroids,. Looking for signs of fluidization effects in asteroids, particularly the C asteroids, would be useful and the possibility that the low densities of asteroids are due to subsurface water, rather than porosity, should be kept in mind. At this point is seems relevant to consider what the missions have discovered relevant to another relationship, that between asteroids and meteorites.

7.3.4 The Relationship Between Asteroids and Meteorites

Since the discovery that the reflectivity spectra of Vesta was unusual and matched that of the HED meteorites (McCord et al. 1970; Cochran et al. 2004), there has been little argument over the conclusion that Vesta was the source of these meteorites. Most of the data returned from the Dawn mission confirm this association (McSween et al. 2013), and when spectra from the mission are analyzed in detail, they compare favorably with the same data for the meteorites (De Sanctis et al. 2013). But this merely says that Vesta and the HED meteorites are the same kind of rock, being mixtures of crustal and upper mantle materials. Wasson (2013) has also pointed out that there are a large numbers of iron meteorites that he argues came from around 70 separate differentiated asteroids and that their basaltic asteroid parent should still be around. In other words some of the V asteroids may not be associated with Vesta, contrary to Binzel and Xu (1993). However, the linkage between Vesta and the HEDs is stronger than bulk mineralogy as reflected in the spectra. Vesta was found to contain dark water-rich material on its surface that everyone agrees must be infalling material resembling carbonaceous chondrites (De Sanctis et al. 2012b; McCord et al. 2012). The water is present in sufficient amounts to cause easily visible morphological effects in the form of the "pits" similar to those previously observed on Mars (Denevi et al. 2012; Tornabene et al. 2012). For many decades the HEDs, or more particularly the howardites, breccias of eucrites and diogenites, contained black xenoliths thought to be dehydrated carbonaceous chondrites (Wilkening 1973). Furthermore, there are traces of water in these meteorites (Treiman et al. 2004). Thus two little-known facts about the meteorites, discovered as surprises when the dwarf planet came under close scrutiny, reinforce the linkage.

Some authors have argued that the frequency of impact on Vesta is consistent with the flux of HEDs to Earth, and that the chronology of the HED meteorites is also consistent with the crater density on Vesta (Schenk et al. 2012).

The gamma- and X-ray spectrometer on Eros provided information on bulk composition that was broadly consistent with it being related to the ordinary chondrites, as are the reflectivity spectra. One element that was inconsistent was sulfur, which was severely depleted on the asteroid. Several authors have argued, based on theory and a variety of experiments, that the depletion is related to processes on the surface related to space exposure, say impact-induced volatilization and/or photo- or ion-induced sputtering of sulfur (Nittler et al. 2001; Killen 2003; Kracher and Sears 2005; Loeffler et al. 2008). However, there is no evidence for a similar depletion on Itokawa, the only S asteroid for which we have samples, although this may be because the samples were not representative of the asteroid. A detailed examination of the element ratios also reveals a mismatch between the surface of Eros and the chondrite classes (Fig. 35). This reflects not just an uncertainty over the chondritic affiliation of Eros but that modern meteorite classification requires a level of sophistication in analysis that only sample return can attain.

The mineral chemistry and the oxygen isotope data for tiny grains recovered from Itokawa, described above, point fairly conclusively to a linkage between Itokawa and the LL chondrites. Thus there are two asteroids with firm linkages to specific chondrite classes, both required missions to acquire the necessary data. It is significant that these two NEAs are matches for ordinary chondrites. This linkage has been very controversial, since S asteroids by-and-large do not have spectra that match ordinary chondrites (Britt et al. 1992). It seems to be commonly accepted now that the reason is that space weathering is obscuring the similarity, the formation of nanophase iron particles increases the slope of the continuum, thereby "reddening" the object (Clark et al. 2002b). So why do some match better than
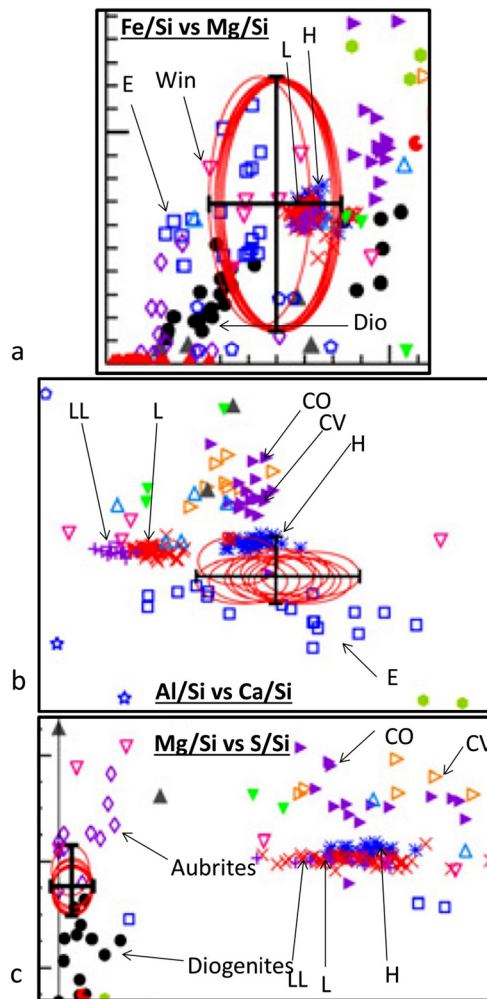
Fig. 35 Details from plots in the Lim and Nittler (2009) paper that compares analytical data from the NEAR-Shoemaker X-ray spectrometer with laboratory analyses for meteorites. (The reader is asked to refer to the original paper for scales; here we are concerned with comparisons within the plots.) (**a**) Fe/Si is plotted against Mg/Si. The analytical ellipse does not center on any particular meteorite class but includes E chondrites, winonaites, diogenites, H and L chondrites. (**b**) Al/Si is plotted against Ca/Si. Again the spacecraft analyses do not uniquely identify any meteorite class but lie between the E chondrites and the H chondrites. (**c**) Mg/Si is plotted against S/Si. In this case the S depletion pulls the spacecraft data away from the chondrites although Mg/Si is lower than the ordinary chondrites (H, L, LL). While the quality of the remote data is impressive, it is not uniquely identifying a meteorite classification for the asteroid. In fact, these data demonstrate the sophistication of analysis required for modern meteorite classification and the need for sample return. Reflectivity spectra eliminate E chondrites as an analog to Eros but cannot distinguish between mineralogically similar meteorites such as ordinary chondrites and winoaites

others? Binzel et al. (2010) have argued that asteroids that come close to Earth experience tidal stresses that refresh the surface and bring less space weathered material to the surface.

It is interesting that Itokawa is LL chondrite material and the LL chondrites appear to be especially common among the NEAs (Vernazza et al. 2008). Rather than reflecting true

abundances, this almost certainly reflects stochastic processes in asteroid collisions. There are peaks in the cosmic ray exposure distribution suggesting a few discrete break-ups (Eugster 2003). The same is true of L chondrites that virtually all came from a major break-up about 500,000 years ago that was conveniently placed for delivery to Earth (Schmitz et al. 1997).

The other S asteroids are a puzzle. Sorted by olivine-pyroxene (and orthopyroxene/clinopyroxene) abundance, as on the BAR plot, relatively few S asteroids are ordinary chondrite-like (Gaffey et al. 1993a, 1993b). Those that could be ordinary chondrite look-a-likes are the so-called S(IV) asteroids. Most of the remaining S classes appear to contain clinopyroxene as their dominant pyroxene and are assumed to be melts or partial melts sincere terrestrially clinopyroxene is associated with igneous rocks (Sunshine et al. 2004). But this conclusion ignores the fact that the most "primitive" (i.e. least metamorphosed) ordinary chondrites also contain clinopyroxene (Van Schmus and Wood 1967). Thus many S asteroids could be ordinary chondrites, but unmetamorphosed, unlike the majority of ordinary chondrites that are highly metamorphosed (Gietzen et al. 2012).

7.4 What Next?

One of the joys of exploration is the unpredictable discoveries. Nevertheless, it is worth pointing out areas of emphasis that can be stressed on the basis of current interpretations. Here are suggestions from the present author.

Samples are essential. The breadth and depth of data that can be obtained and the ability to archive the samples for the future gives returned samples unique scientific value (Sears et al. 2002). They provide ground truth and, in a sense, they unlock the data being obtained from ground-based and spacecraft methods of remote sensing. It is true that remarkable accomplishments are possible using remote methods and that instrument of amazing sophistication are available for placing on robotic spacecraft. But it is very hard indeed to rival the quality of ground-based measurements. The problem with sample return is that it is costly and difficult, but we are now overcoming these barriers and a new age of sample return is unfolding (Kawaguchi et al. 2008; Lauretta et al. 2012). Scientific data that can uniquely be obtained are high quality elemental and isotopic analysis, detailed petrographic analysis to almost the atom level, and chronological investigations by over a dozen complimentary techniques. The mission asteroid experience demonstrates this more powerfully than words. Decades of uncertainty concerning the meteorite links with S asteroids were removed in a few days after samples were returned, at least for Itokawa, even though those samples were grains rather than whole rocks (Nakamura et al. 2014).

Arguably the main uncertainty in asteroid science concerns their interiors (Asphaug et al. 2002; Sanchez and Scheeres 2014). A high priority in the future, after sample return, will be missions to determine the interiors of asteroids (Asphaug et al. 2003). These missions might be orbiters carrying magnetometers or landers carrying seismometers. It seems unlikely that coring devices large enough to penetrate to the asteroid's center will be feasible within the foreseeable future.

Finally, an important question to address in the future is the abundance and role of water in asteroids inside the snow-belt, including NEAs. The detection of subsurface water is a challenge. Impactors might reveal subsurface water, if burial depths are comparable with the depth of a crater that would be formed by impact. Seismometers, subsurface sounding radar (Heggy et al. 2001), gamma spectroscopy and neutron spectroscopy might be able to detect subsurface water if it is shallow and abundant enough. Returned samples might contain water when analyzed by highly sensitive groundbased instruments.

8 Concluding Comments

The explored asteroids have many properties in common, the most notable being their surface features which are the result of long-term exposure to the space environment. All are heavily cratered, the crater densities suggesting lifetimes for the surfaces of a few hundred million to over a billion years. All have regoliths, which are usually thick and sometimes enhanced by ejecta blankets. Often there has been a redistribution of regolith by cratering, seismic shaking, or Yarkovsky forces. Other textural features such as grooves and ridges are commonplace and sometimes seem to be the surface manifestation of global structures.

However, also noteworthy is the diversity of these asteroids. The choice of asteroids for exploration reflects not just our interests and scientific priorities, but also our technical capabilities. Thus they range from two dwarf planets, one with a core, mantle, and basaltic crust, and one with primitive composition but possibly internally zoned by water content, to tiny fragments that appear to be shards, or they are objects that are a little more than rubble and also derived from bigger precursors. In between these extremes are objects much smaller than Vesta but that were also primary planetesimals that formed at the time the solar system formed and have been unaltered except for the surface processes mentioned above. The sizes of the explored asteroids are fairly uniformly spread over the range 550 km to less than 1 km. Nine have fairly similar spin rates (5–15 h) but three are slow rotators (Braile, Mathilde and Toutatis). Most have simple spin with a wide variety of obliquities, but Toutatis is tumbling. The slopes of the phase angle curves varies from $\sim 70 \%$ (Mathilde) to $\sim 40 \%$ (Vesta), suggesting major differences in surface roughness, and surface compositions are highly varied, one asteroid being a member of the C class (Mathilde), seven are various sorts of S asteroid, Vesta is a V asteroid (basaltic) and Lutetia has a featureless spectrum, and variously assigned to the C, D and E class, but probably best thought of as an E asteroid. Over a thousand small grains were returned from Itokawa who properties resemble closely those of the LL chondrite meteorites.

However, we have visited only a small sample of the material available in the form of asteroids. Asteroid spectroscopy has allowed some authors to propose over 25 classes of asteroid with discrete spectra. For the S asteroids alone, our attempts to determine mineralogy has resulted in seven subclasses many of which have no counterpart in the terrestrial or meteorite collections. At the same time, meteorite geochemistry, that is, mineralogical elemental and isotope studies, has produced over 70 discrete types of material most of which has yet to be linked unequivocally with asteroid types. In fact, while we celebrate the successes, the truth is that attempting to link meteorites with asteroids still has a long way to go.

That said, the present author has identified three themes of especial interest, at least to him, that we have discussed above. The number of asteroid-wide geological features, scarps, grooves, fractures etc., suggest that in general, asteroids, except possibly Itokawa, are not rubble piles. This is information about the interior of the asteroids that would not have been possible without the missions. Their low porosity might be due to the presence of considerable amounts of subsurface water rather than high porosities. The presence of water inside the snow-belt is suggested by the growing number of active asteroids most of which spend all of their time, or considerable time, inside the purported snow-line. Several lines of evidence suggest a continuum of objects between comets and asteroids.

So, what the explored asteroids underscore once more is the strong interplay between exploration and science, and that samples in our laboratories are critical to furthering our understanding of the solar system we inhabit. The relationship between science and exploration is one that extends back to the renaissance and whose history is peppered by giants, like James Cook, Lewis and Clark, Alexander Humboldt, and Peter Simon Pallas whose collections became the cornerstones of our national museums.

So what of the future? It is the writer's opinion that three themes of endeavor for future asteroid research are important, the return of samples, investigations of asteroid interiors, and the search for water. Astrobiologists would want to add, search for and identify organics, but since this is extremely difficult to do by remote methods, this too will be an emphasis of studies on returned samples.

References

S. Abe, T. Mukai, N. Hirata, O.S. Barnouin-Jha, A.F. Cheng, H. Demura, R.W. Gaskell, T. Hashimoto, K. Hiraoka, T. Honda, T. Kubota, M. Matsuoka, T. Mizuno, R. Nakamura, D.J. Scheeres, M. Yoshikawa, Mass and local topography measurements of Itokawa by Hayabusa. Science **312**, 1344–1347 (2006a)

M. Abe, Y. Takagi, K. Kitazato, S. Abe, T. Hiroi, F. Vilas, B.E. Clark, P.A. Abell, S.M. Lederer, K.S. Jarvis, T. Nimura, Y. Ueda, A. Fujiwara, Near-infrared spectral results of asteroid Itokawa from the Hayabusa spacecraft. Science **312**, 1334–1338 (2006b)

P.A. Abell, F. Vilas, K.S. Jarvis, M.J. Gaffey, M.S. Kelley, Mineralogical composition of (25143) Itokawa 1998 SF36 from visible and near-infrared reflectance spectroscopy: Evidence for partial melting. Meteorit. Planet. Sci. **42**, 2165–2177 (2007)

M.H. Acuña, B.J. Anderson, C.T. Russell, P. Wasilewski, G. Kletetshka, L. Zanetti, N. Omidi, NEAR magnetic field observations at 433 Eros: First measurements from the surface of an asteroid. Icarus **155**, 220–228 (2002)

M.F. A'Hearn, P.D. Feldman, Water vaporization on Ceres. Icarus **98**, 54–60 (1992)

M.F. A'Hearn, M.J.S. Belton, W.A. Delamere, J. Kissel, K.P. Klaasen, L.A. McFadden, K.J. Meech, H.J. Melosh, P.H. Schultz, J.M. Sunshine, P.C. Thomas, J. Veverka, D.K. Yeomans, M.W. Baca, I. Busko, C.J. Crockett, S.M. Collins, M. Desnoyer, C.A. Eberhardy, C.M. Ernst, T.L. Farnham, L. Feaga, O. Groussin, D. Hampton, S.I. Ipatov, J.-Y. Li, D. Lindler, C.M. Lisse, N. Mastrodemos, W.M. Owen Jr., J.E. Richardson, D.D. Wellnitz, R.L. White, Deep impact: Excavating comet Tempel 1. Science **310**, 258–264 (2005)

D.G. Akridge, D.W. Sears, Regolith and megaregolith formation of H-chondrites: Thermal constraints on the parent body. Icarus **132**, 185–195 (1998)

D.G. Akridge, D.W.G. Sears, The gravitational and aerodynamic sorting of meteoritic chondrules and metal: Experimental results with implications for chondritic meteorites. J. Geophys. Res. **104**, 11,853–11,864 (1999)

E. Ammannito, M.C. De Sanctis, E. Palomba, A. Longobardo, D.W. Mittlefehldt, H.Y. McSween, S. Marchi, M.T. Capria, F. Capaccioni, A. Frigeri, C.M. Pieters, O. Ruesch, F. Tosi, F. Zambon, F. Carraro, S. Fonte, H. Hiesinger, G. Magni, L.A. McFadden, C.A. Raymond, C.T. Russell, J.M. Sunshine, Olivine in an unexpected location on Vesta's surface. Nature **504**, 122–125 (2013a)

E. Ammannito, M.C. De Sanctis, F. Capaccioni, M.T. Capria, F. Carraro, J.-P. Combe, S. Fonte, A. Frigeri, S.P. Joy, A. Longobardo, G. Magni, S. Marchi, T. McCord, L.A. McFadden, H.Y. McSween, E. Palomba, C.M. Pieters, C.A. Polansky, C.A. Raymond, J.M. Sunshine, F. Tosi, F. Zambon, C.T. Russell, Vestan lithologies mapped by the visual and infrared spectrometer on Dawn. Meteorit. Planet. Sci. **48**, 2185–2198 (2013b). doi:10.1111/maps.12192

B. Anderson, M. Acuña, Observations of asteroid-solar wind interactions, in *34th COSPAR Scientific Assembly, the Second World Space Congress*, Houston, TX, USA 10–19 October (2002). Meeting abstract

E. Asphaug, Impact origin of the Vesta family. Meteorit. Planet. Sci. **32**, 965–980 (1997)

E. Asphaug, J.M. Moore, D. Morrison, W. Benz, M.C. Nolan, R.J. Sullivan, Mechanical and geological effects of impact cratering on Ida. Icarus **120**, 158–184 (1996)

E. Asphaug, S.J. Ostro, R.S. Hudson, D.J. Scheeres, W. Benz, Disruption of kilometre-sized asteroids by energetic collisions. Nature **393**, 437–440 (1998)

E. Asphaug, E.V. Ryan, M.T. Zuber, Asteroid interiors, in *Asteroids III*, ed. by W.F. Bottke, A. Cellino, P. Paolicchi, R.P. Binzel (University of Arizona Press, Tucson, 2002), pp. 426–484

E. Asphaug, M.J.S. Belton, A. Cangahuala, L. Keith, K. Klaasen, L. McFadden, G. Neumann, S.J. Ostro, R. Reinert, A. Safaeinili, D.J. Scheeres, D.K. Yeomans, Exploring asteroid interiors: The Deep Interior mission concept, in *Lunar and Planetary Science XXXIV* (2003). Abstract #1906

H.U. Auster, I. Richter, K.H. Glassmeier, G. Berghofer, C.M. Carr, U. Motschmann, Magnetic field investigations during ROSETTA's 2867 Šteins flyby. Planet. Space Sci. **58**, 1124–1128 (2010)

M.A. Barucci, A. Cellino, C. De Sanctis, M. Fulchignoni, K. Lumme, V. Zappala, P. Magnusson, Ground-based Gaspra modelling—comparison with the first Galileo image. Astron. Astrophys. **266**, 385–394 (1992)

M.A. Barucci, M. Fulchignoni, A. Rossei, Rosetta asteroid targets: 2867 Steins and 21 Lutetia. Space Sci. Rev. **128**, 67–78 (2007). doi:10.1007/s11214-006-9029-6

M.A. Barucci, S. Fornasier, E. Dotto, P. Lamy, Asteroids Steins and Lutetia: Surface composition from far infrared observations with the Spitzer space telescope. Astron. Astrophys. **477**, 665–670 (2008)

J.F. Bell III, N.I. Izenberg, P.G. Lucey, B.E. Clark, C. Peterson, M.J. Gaffey, J. Joseph, B. Carcich, A. Harch, M.E. Bell, J. Warren, P.D. Martin, L.A. McFadden, D. Wellnitz, S. Murchie, M. Winter, J. Veverka, P. Thomas, M.S. Robinson, M. Malin, A. Cheng, Near-IR reflectance spectroscopy of 433 Eros from the NIS instrument on the NEAR mission I. Low phase angle observations. Icarus **155**, 119–144 (2002). doi:10.1006/icar.2001.6752

M.J.S. Belton, J. Melosh, Fluidization and multiphase transport of particulate cometary material as an explanation of the smooth terrains and repetitive outbursts on 9P/Tempel 1. Icarus **200**, 280–291 (2009)

M.J.S. Belton, J. Veverka, P. Thomas, P. Helfenstein, D. Simonelli, C. Chapman, M.E. Davies, R. Greeley, R. Greenberg, J. Head, Galileo encounter with 951 Gaspra—first pictures of an asteroid. Science **257**, 1647–1652 (1992)

M.J.S. Belton, C.R. Chapman, K.P. Klaasen, A.P. Harch, P.C. Thomas, J. Veverka, A.S. McEwen, R.T. Pappalardo, Galileo's encounter with 243 Ida: An overview of the imaging experiment. Icarus **120**, 1–19 (1996a)

M.J.S. Belton, B.E.A. Mueller, L.A. D'Amario, D.V. Byrnes, K.P. Klaasen, S. Synnott, H. Breneman, T.V. Johnson, P.C. Thomas, J. Veverka, A.P. Harch, M.E. Davies, W.J. Merline, C.R. Chapman, D. Davis, T. Denk, G. Neukum, J.-M. Petit, R. Greenberg, A. Storrs, B. Zellner, The discovery and orbit of 1993 (243)1 Dactyl. Icarus **120**, 185–199 (1996b)

M.J.S. Belton, T.H. Morgan, N.H. Samarasinha, D.K. Yeomans, *Mitigation of Hazardous Comets and Asteroids* (Cambridge University Press, Cambridge, 2004). ISBN 0-521-82764-7

L.A.M. Benner, M.C. Nolan, S.J. Ostro, J.D. Giorgini, D.P. Pray, A.W. Harris, C. Magri, J.-L. Margo, Near-Earth Asteroid 2005 CR37: Radar images and photometry of a candidate contact binary. Icarus **182**, 474–481 (2006)

S. Besse, P. Lamy, L. Jorda, S. Marchi, C. Barbieri, Identification and physical properties of craters on Asteroid (2867) Steins. Icarus **221**, 1119–1129 (2012)

R.P. Binzel, S. Xu, Chips off asteroid 4 Vesta: Evidence for the parent body of basaltic achondrite meteorites. Science **260**, 186–191 (1993)

R.P. Binzel, S.M. Slivan, P. Magnusson, W.Z. Wisniewski, J. Drummond, K. Lumme, M.A. Barucci, E. Dot, Asteroid 243 Ida: Groundbased photometry and a pre-Galileo physical model. Icarus **105**, 310–325 (1993)

R.P. Binzel, T.H. Burbine, S.J. Bus, Groundbased reconnaissance of Asteroid 253 Mathilde: Visible wavelength spectrum and meteorite comparison. Icarus **119**, 447–449 (1996)

R.P. Binzel, A.W. Harris, S.J. Bus, T.H. Burbine, Spectral properties of near-Earth objects: Palomar and IRTF results for 48 objects including spacecraft targets 9969 Braille and (10302) 1989 ML. Icarus **151**, 139–149 (2001a)

R.P. Binzel, A.S. Rivkin, S. Bus, J. Sunshine, T.S. Burbin, MUSES-C target asteroid (25143) 1998 SF36: A reddened ordinary chondrite. Meteorit. Planet. Sci. **36**, 1167–1172 (2001b)

R.P. Binzel, A. Morbidelli, S. Merouane, F.E. DeMeo, M. Birlan, P. Vernazza, C.A. Thomas, A.S. Rivkin, S.J. Bus, A.T. Tokunaga, Earth encounters as the origin of fresh surfaces on near-Earth asteroids. Nature **463**, 331–334 (2010)

A. Bischoff, A.E. Rubin, K. Keil, D. Stöffler, Lithification of gas-rich chondrite regolith breccias by grain boundary and localized shock melting. Earth Planet. Sci. Lett. **66**, 1–10 (1983)

C. Blanco, S. Catalano, UBV photometry of Vesta. Icarus **40**, 359–363 (1979)

X. Blanco-Cano, N. Omidi, C.T. Russell, Hybrid simulations of solar wind interaction with magnetized asteroids: Comparison with Galileo observations near Gaspra and Ida. J. Geophys. Res. **108**(A5), 1216 (2003), 13 pages. doi:10.1029/2002JA009618

J. Blue, L.R. Gaddis, R. Schulz, K. Aksnes, G. Burba, G. Consolmagno, R. Lopes, P. Masson, M. McGrath, B.A. Smith, G. Valsecchi, G. Williams, C. Wood, Planetary nomenclature: an overview, in *44th Lunar and Planetary Science Conference*, The Woodlands, TX, March 18–22 (2013). LPI Contribution No. 1719, p. 2178

W.F. Bottke Jr., D. Vokrouhlický, D.P. Rubincam, D. Nesvorný, The Yarkovsky and Yorp effects: Implications for asteroid dynamics. Annu. Rev. Earth Planet. Sci. **34**, 157–191 (2006)

E. Bowell, B. Hapke, D. Domingue, K. Lumme, J. Peltoniemi, A.W. Harris, Application of photometric models to asteroids, in *Asteroids II* (University of Arizona Press, Tucson, 1989), pp. 524–556

J.M. Boyce, L. Wilson, P.J. Mouginis-Mark, C.W. Hamilton, L.L. Tornabene, Origin of small pits in martian impact craters. Icarus **221**, 262–275 (2012)

V.J. Bray, P.M. Schenk, Pristine impact crater morphology on Pluto—Expectations for New Horizons. Icarus **246**, 156–164 (2015)

S. Breiter, P. Bartczak, M. Czekaj, B. Oczujda, D. Vokrouhlický, The YORP effect on 25143 Itokawa. Astron. Astrophys. **507**, 1073–1081 (2009). doi:10.1051/0004-6361/200912543

D. Britt, D.J. Tholen, J.F. Bell, C.M. Pieters, Comparison of asteroid and meteorite spectra: Classification by principle component analysis. Icarus **99**, 153–166 (1992)

D.T. Britt, D. Yeomans, K. Housen, G. Consolmagno, Asteroid density, porosity, and structure, in *Asteroids III*, ed. by W.F. Bottke, A. Cellino, P. Paolicchi, R.P. Binzel (University of Arizona Press, Tucson, 2002), pp. 485–500

L.B. Browning, H.Y. McSween, M.E. Zolensky, Correlated alteration effects in CM carbonaceous chondrites. Geochim. Cosmochim. Acta **60**, 2621–2633 (1996)

D.E. Brownlee, P. Tsou, J.D. Anderson, M.S. Hanner, R.L. Newburn, Z. Sekanina, B.C. Clark, F. Hörz, M.E. Zolensky, J. Kissel, J.A.M. McDonnell, S.A. Sandford, A.J. Tuzzolino, Stardust: Comet and interstellar dust sample return mission. J. Geophys. Res. **108**, 8111 (2003), 15 pages. doi:10.1029/2003JE002087

D. Brownlee, P. Tsou, J. Aléon, C.M.O'D. Alexander, T. Araki, S. Bajt, G.A. Baratta, R. Bastien, P. Bland, P. Bleuet, J. Borg, J.P. Bradley, A. Brearley, F. Brenker, S. Brennan, J.C. Bridges, N.D. Browning, J.R. Brucato, E. Bullock, M.J. Burchell, H. Busemann, A. Butterworth, M.J. Chaussidon, A. Cheuvront, M.J. Chi, M.J. Cintala, B.C. Clark, S.J. Clemett, G. Cody, L. Colangeli, G. Cooper, P. Cordier, C. Daghlian, Z. Dai, L. D'Hendecourt, Z. Djouadi, G. Dominguez, T. Duxbury, J.P. Dworkin, D.S. Ebel, T.E. Economou, S. Fakra, S.A.J. Fairey, S. Fallon, G. Ferrini, T. Ferroir, H. Fleckenstein, C. Floss, G. Flynn, I.A. Franchi, M. Fries, Z. Gainsforth, J.-P. Gallien, M. Genge, M.K. Gilles, P. Gillet, J. Gilmour, D.P. Glavin, M. Gounelle, M.M. Grady, G.A. Graham, P.G. Grant, S.F. Green, F. Grossemy, L. Grossman, J.N. Grossman, Y. Guan, K. Hagiya, R. Harvey, P. Heck, G.F. Herzog, P. Hoppe, F. Hörz, J. Huth, I.D. Hutcheon, K. Ignatyev, H. Ishii, M. Ito, D. Jacob, C. Jacobsen, S. Jacobsen, S. Jones, D. Joswiak, A. Jurewicz, A.T. Kearsley, L.P. Keller, H. Khodja, A.L.D. Kilcoyne, J. Kissel, A. Krot, F. Langenhorst, A. Lanzirotti, L. Le, L.A. Leshin, J. Leitner, L. Lemelle, H. Leroux, M.-C. Liu, K. Luening, I. Lyon, G. MacPherson, M.A. Marcus, K. Marhas, B. Marty, G. Matrajt, K. McKeegan, A. Meibom, V. Mennella, K. Messenger, S. Messenger, T. Mikouchi, S. Mostefaoui, T. Nakamura, T. Nakano, M. Newville, L.R. Nittler, I. Ohnishi, K. Ohsumi, K. Okudaira, D.A. Papanastassiou, R. Palma, M.E. Palumbo, R.O. Pepin, D. Perkins, M. Perronnet, P. Pianetta, W. Rao, F.J.M. Rietmeijer, F. Robert, D. Rost, A. Rotundi, R. Ryan, S.A. Sandford, C.S. Schwandt, T.H. See, D. Schlutter, J. Sheffield-Parker, A. Simionovici, S. Simon, I. Sitnitsky, C.J. Snead, M.K. Spencer, F.J. Stadermann, A. Steele, T. Stephan, R. Stroud, J. Susini, S.R. Sutton, Y. Suzuki, M. Taheri, S. Taylor, N.D. Teslich, K. Tomeoka, N. Tomioka, A. Toppani, J.M. Trigo-Rodríguez, D. Troadec, A. Tsuchiyama, A.J. Tuzzolino, T. Tyliszczak, K. Uesugi, M. Velbel, J. Vellenga, E. Vicenzi, L. Vincze, J. Warren, I. Weber, M. Weisberg, A.J. Westphal, S. Wirick, D. Wooden, B. Wopenka, P. Wozniakiewicz, I. Wright, H. Yabuta, H. Yano, E.D. Young, R.N. Zare, T. Zega, K. Ziegler, L. Zimmerman, E. Zinner, Z. Zolensky, Comet 81P/Wild 2 under a microscope. Science **314**, 1711–1716 (2006)

D.L. Buczkowski, D.Y. Wyrick, K.A. Iyer, E.G. Kahn, J.E.C. Scully, A. Nathues, R.W. Gaskell, T. Roatsch, F. Preusker, P.M. Schenk, L. Le Corre, V. Reddy, R.A. Yingst, S. Mest, D.A. Williams, W.B. Garry, O.S. Barnouin, R. Jaumann, C.A. Raymond, C.T. Russell, Large-scale troughs on Vesta: A signature of planetary tectonics. Geophys. Res. Lett. **18**, L18205 (2012)

B.J. Buratti, D.T. Britt, L.A. Soderblom, M.D. Hicks, D.C. Boice, R.H. Brown, R. Meier, R.M. Nelson, J. Oberst, T.C. Owen, A.S. Rivkin, B.R. Sandel, S.A. Stern, N. Thomas, R.V. Yelle, 9969 Braille: Deep Space 1 infrared spectroscopy, geometric albedo, and classification. Icarus **167**, 129–135 (2004)

T.H. Burbine, T.J. McCoy, A. Meibom, B. Gladman, K. Keil, Meteorite parent bodies: Their number and identification, in *Asteroids III*, ed. by W.F. Bottke, A. Cellino, P. Paolicchi, R.P. Binzel (University of Arizona Press, Tucson, 2002), pp. 653–667

S.J. Bus, R.P. Binzel, Phase II of the small main-belt asteroid spectroscopic survey. The Observations. Icarus **158**, 106–145 (2002). doi:10.1006/icar.2002.6857

S.J. Bus, F. Vilas, M.A. Barucci, Visible-wavelength spectroscopy of asteroids, in *Asteroids III*, ed. by W.F. Bottke, A. Cellino, P. Paolicchi, R.P. Binzel (University of Arizona Press, Tucson, 2002), pp. 169–182

M.W. Busch, S.J. Ostro, L.A.M. Benner, M. Brozovic, J.D. Giorgini, J.S. Jao, D.J. Scheeres, C. Magri, M.C. Nolan, E.S. Howell, P.A. Taylor, J.-L. Margot, W. Brisken, Radar observations and the shape of near-Earth asteroid 2008 EV5. Icarus **212**(2), 649–660 (2011)

D.B.J. Bussey, M.S. Robinson, K. Edwards, P.C. Thomas, J. Joseph, S. Murchie, J. Veverka, A.P. Harch, 433 Eros global basemap from NEAR Shoemaker MSI images. Icarus **155**, 38–50 (2002)

W.M. Calvin, T.V.V. King, Spectral characteristics of iron-bearing phyllosilicates: Comparison to Orgueil (CI1), Murchison and Murray (CM2). Meteorit. Planet. Sci. **32**, 693–701 (1997)

H. Campins, K. Hargrove, N. Pinilla-Alonso, E.S. Howell, M.S. Kelley, J. Licandro, T. Mothé-Diniz, Y. Fernández, J. Ziffer, Water ice and organics on the surface of the asteroid 24 Themis. Nature **464**, 1320–1321 (2010)

F. Capaccioni, G. Filacchione, M.C. De Sanctis, F. Tosi, M.T. Capria, E. Ammannito, S. Erard, A. Barucci, G. Arnold, Photometric properties of the asteroid 21 Lutetia from VIRTIS-Rosetta observations, in *44th Lunar and Planetary Science Conference* (2013). Abs. # 2229

M.H. Carr, R.L. Kirk, A. McEwen, J. Veverka, P. Thomas, J.W. Head, S. Murchie, The geology of Gaspra. Icarus **107**, 61–71 (1994)

B. Carry, Density of asteroids. Planet. Space Sci. **73**, 98–118 (2012)

B. Carry, P. Vernazza, C. Dumas, W.J. Merline, O. Mousis, P. Rousselot, E. Jehin, J. Manfroid, M. Fulchignoni, J.-M. Zucconi, The remarkable surface homogeneity of the Dawn mission target (1) Ceres. Icarus **217**, 20–26 (2012)

J.C. Castillo-Rogez, T.B. McCord, Ceres' evolution and present state constrained by shape data. Icarus **205**, 443–459 (2010)

M.A. Chamberlain, M.V. Sykes, G.A. Esquerdo, Ceres lightcurve analysis—period determination. Icarus **188**, 451–456 (2007)

C.R. Chapman, Asteroids as meteorite parent-bodies: The astronomical perspective. Geochim. Cosmochim. Acta **40**, 701–709 (1976)

C.R. Chapman, S-type asteroids, ordinary chondrites, and space weathering: The evidence from Galileo's fly-bys of Gaspra and Ida. Meteorit. Planet. Sci. **31**, 699–725 (1996)

C.R. Chapman, D. Morrison, JHK photometry of 433 Eros and other asteroids. Icarus **28**, 91–94 (1976)

C.R. Chapman, J. Veverka, P.C. Thomas, K. Klaasen, M.J.S. Belton, A. Harch, A. McEwen, T.V. Johnson, P. Helfenstein, M.E. Davies, M.J. Merlin, T. Denk, Discovery and physical properties of Dactyl, a satellite of 243 Ida. Nature **374**, 783–785 (1995)

C.R. Chapman, E.V. Ryan, W.J. Merline, G. Neukum, R. Wagner, P.C. Thomas, J. Veverka, R.A. Sullivan, Cratering on Ida. Icarus **120**, 77–86 (1996a)

C.R. Chapman, J. Veverka, M.J.S. Belton, G. Neukum, D. Morrison, Cratering on Gaspra. Icarus **120**, 231–245 (1996b)

C.R. Chapman, W.J. Merline, P. Thomas, Cratering in Mathilde. Icarus **140**, 28–33 (1999)

C.R. Chapman, W.J. Merline, P.C. Thomas, J. Joseph, A.F. Cheng, N. Izenberg, Impact history of Eros: Craters and boulders. Icarus **155**, 104–118 (2002). doi:10.1006/icar.2001.6744

G.Q. Chen, T.J. Ahrens, R. Hide, Theory of shock magnetization of asteroids Gaspra and Ida, in *AIP Conference Proceedings*, vol. 370 (1996), p. 929. doi:10.1063/1.50597

A.F. Cheng, G. Santo, K.J. Heeres, J.A. Landshof, R.W. Farquhar, R.E. Gold, S.C. Lee, Near-Earth asteroid rendezvous: Mission overview. J. Geophys. Res. **102**, 23,695–23,708 (1997)

A. Cheng, N. Izenberg, C.R. Chapman, M.T. Zuber, Ponded deposits on asteroid 433 Eros. Meteorit. Planet. Sci. **37**, 1095–1105 (2002)

N.S. Chernykh, L.I. Chernykh, History of minor planet observations at the Crimean astrophysical observatory. Mem. Soc. Astron. Ital. **73**, 626 (2002)

M.J. Cintala, K.M. McBride, Block distributions on the lunar surface: A comparison between measurements obtained from surface and orbital photography, in *The Twenty-Fifth Lunar and Planetary Science Conference. Part 1: A-G* (1994), pp. 261–262

M.J. Cintala, J.W. Head, J. Veverka, Characteristics of the cratering process on small satellites and asteroids, in *Proceedings of the 9th Lunar and Planetary Science Conference* (1978), pp. 3803–3830

M.J. Cintala, J.W. Head, L. Wilson, The nature and effects of impact cratering on small bodies, in *Asteroids*, ed. by T. Gehrels, Tucson, AZ (University of Arizona Press, Tuscon, 1979), pp. 579–600. NASA-supported research

B.E. Clark, J. Veverka, P. Helfenstein, P.C. Thomas, J.F. Bell, A. Harch, M.S. Robinson, S.L. Murchie, L.A. McFadden, C.R. Chapman, NEAR photometry of Asteroid 253 Mathilde. Icarus **140**, 53–65 (1999)

B.E. Clark, P. Helfenstein, J.F. Bell III, C. Peterson, J. Veverka, N.I. Izenberg, D. Domingue, D. Wellnitz, L. McFadden, NEAR infrared spectrometer photometry of Asteroid 433 Eros. Icarus **155**, 189–204 (2002a)

B.E. Clark, B. Hapke, C. Pieters, D. Britt, Asteroid space weathering and regolith evolution, in *Asteroids III*, ed. by W.F. Bottke Jr., A. Cellino, P. Paolicchi, R.P. Binzel (University of Arizona Press, Tucson, 2002b), pp. 585–599

A.L. Cochran, F. Vilas, A.S. Jarvis, M.S. Kelley, Investigating the Vesta–vestoid–HED connection. Icarus **167**, 360–368 (2004)

A. Coradini, F. Capaccioni, S. Erard, G. Arnold, M.C. De Sanctis, G. Filacchione, F. Tosi, M.A. Barucci, M.T. Capria, E. Ammannito, D. Grassi, G. Piccioni, S. Giuppi, G. Bellucci, J. Benkhoff, J.P. Bibring, A. Blanco, M. Blecka, D. Bockelee-Morvan, F. Carraro, R. Carlson, U. Carsenty, P. Cerroni, L. Colangeli, M. Combes, M. Combi, J. Crovisier, P. Drossart, E.T. Encrenaz, C. Federico, U. Fink, L. Fonti, L. Giacomini, W.H. Ip, R. Jaumann, E. Kuehrt, Y. Langevin, G. Magni, T. McCord, V. Mennella, S. Mottola, G. Neukum, V. Orofino, P. Palumbo, U. Schade, B. Schmitt, F. Taylor, D. Tiphene, G. Tozzi, The surface composition and temperature of asteroid 21 Lutetia as observed by Rosetta/VIRTIS. Science **334**, 492–494 (2011)

D.P. Cruikshank, W.K. Hartmann, D.J. Tholen, Colour, albedo, and nucleus size of Halley's comet. Nature **315**, 122–124 (1985)

C. Darwin, *The Origin of Species: 150th Anniversary Edition* (Dover, New York, 2006)

B.J.R. Davidsson, P.J. Gutiérrez, Estimating the nucleus density of Comet 19P/Borrelly. Icarus **168**, 392–408 (2004)

M.E. Davies, T.R. Colvin, M.S. Belton, J. Veverka, P.C. Thomas, The direction of the north pole and the control network of Asteroid 243 Ida. Icarus **120**, 33–37 (1996)

J.K. Davies, A.W. Harris, A.S. Rivkin, S.D. Wolters, S.F. Green, N. McBride, R.K. Mann, T.H. Kerr, Near-infrared spectra of 12 near-Earth objects. Icarus **186**, 111–125 (2007)

M.C. De Sanctis, E. Ammannito, M.T. Capria, F. Tosi, F. Capaccioni, F. Zambon, F. Carraro, S. Fonte, A. Frigeri, R. Jaumann, G. Magni, S. Marchi, T.B. McCord, L.A. McFadden, H.Y. McSween, D.W. Mittlefehldt, A. Nathues, E. Palomba, C.M. Pieters, C.A. Raymond, C.T. Russell, M.J. Toplis, D. Turrini, Spectroscopic characterization of mineralogy and its diversity across Vesta. Science **336**, 697–700 (2012a). doi:10.1126/science.1219270

M.C. De Sanctis, J.-P. Combe, E. Ammannito, E. Palomba, A. Longobardo, T.B. McCord, S. Marchi, F. Capaccioni, M.T. Capria, D.W. Mittlefehldt, C.M. Pieters, J. Sunshine, F. Tosi, F. Zambon, F. Carraro, S. Fonte, A. Frigeri, G. Magni, C.A. Raymond, C.T. Russell, D. Turrini, Detection of widespread hydrated materials on Vesta by the VIR-imaging spectrometer on board the Dawn mission. Astrophys. J. Lett. **758**, L36 (2012b) (5 pp). doi:10.1088/2041-8205/758/2/L36

M.C. De Sanctis, E. Ammannito, M.T. Capria, F. Capaccioni, J.-P. Combe, A. Frigeri, A. Longobordo, G. Magni, S. Marchi, T. McCord, E. Palomba, F. Tosi, F. Zambon, F. Carraro, S. Fonte, L.A. McFadden, D.W. Mittlefehdt, C.M. Pieters, R. Jaumann, K. Stephan, C.A. Raymond, C.T. Russell, Vesta's mineralogical composition as revealed by the visible and infrared spectrometer on Dawn. Meteorit. Planet. Sci. **48**, 2166–2184 (2013). doi:10.1111/maps.12138

F.E. DeMeo, R.P. Binzel, S.M. Slivan, S.J. Bus, An extension of the Bus asteroid taxonomy into the near-infrared. Icarus **202**, 160–180 (2009)

H. Demura, S. Kobayashi, E. Nemoto, N. Matsumoto, M. Furuya, A. Yukishita, N. Muranaka, H. Morita, K. Shirakawa, M. Maruya, H. Ohyama, M. Uo, T. Kubota, T. Hashimoto, J. Kawaguchi, A. Fujiwara, J. Saito, S. Sasaki, H. Miyamoto, N. Hirata, Science **312**, 1347–1349 (2006)

B.W. Denevi, D.T. Blewett, D.L. Buczkowski, F. Capaccioni, M.T. Capria, M.C. De Sanctis, W.B. Garry, R.W. Gaskell, L. Le Corre, J.-Y. Li, S. Marchi, T.J. McCoy, A. Nathues, D.P. O'Brien, N.E. Petro, C.M. Pieters, F. Preusker, C.A. Raymond, V. Reddy, C.T. Russell, P. Schenk, J.E.C. Scully, J.M. Sunshine, F. Tosi, D.A. Williams, D. Wyrick, Pitted terrain on Vesta and implications for the presence of volatiles. Science **338**, 246–249 (2012)

B. Dermawan, T. Nakamura, H. Fukushima, H. Sato, F. Yoshida, Y. Sato, CCD photometry of the MUSES-C mission target: Asteroid (25143) 1998 SF36. Publ. Astron. Soc. Jpn. **54**, 635–664 (2002)

A.J. Dombard, O.S. Barnouin, L.M. Prockter, P.C. Thomas, Boulders and ponds on the Asteroid 433 Eros. Icarus **210**, 713–721 (2010)

D.L. Domingue, M. Robinson, B. Carcich, J. Joseph, P. Thomas, B.E. Clark, Disk-integrated photometry of 433 Eros. Icarus **155**, 205–219 (2002)

E. Dotto, M.A. Barucci, M. Fulchignoni, M. di Martino, A. Rotundi, R. Burchi, A. di Paolantonio, M-type asteroids—rotational properties of 16 objects. Astron. Astrophys. Suppl. Ser. **95**, 195–211 (1992)

M.J. Drake, The eucrite/Vesta story. Meteorit. Planet. Sci. **36**, 501–513 (2001)

M.J. Drake, D.S. Lauretta, OSIRIS-Rex asteroid sample return mission, in *Solar System Sample Return Mission* (2011). Abstract #5012

J.D. Drummond, S.J. Weidenschilling, C.R. Chapman, D.R. Davis, Photometric geodesy of main-belt asteroids. II. Analysis of lightcurves for poles, periods, and shapes. Icarus **76**, 19–77 (1988)

J. Drummond, J. Christou, Triaxial ellipsoid dimensions and rotational poles of seven asteroids from Lick Observatory adaptive optics images, and of Ceres. Icarus **197**, 480–496 (2008)

D.D. Durda, C.R. Chapman, W.J. Merline, B.L. Enkse, Detecting crater ejecta-blanket boundaries and constraining source crater regions for boulder tracks and elongated secondary craters on Eros. Meteorit. Planet. Sci. **47**, 1087–1097 (2012). doi:10.1111/j.1945-5100.2012.01380.x

J. Ďurech, D. Vokrouhlický, M. Kaasalainen, P. Weissman, S.C. Lowry, E. Beshore, D. Higgins, Y.N. Krugly, V.G. Shevchenko, N.M. Gaftonyuk, Y.-J. Choi, R.A. Kowalski, S. Larson, B.D. Warner, A.L. Marshalkina, M.A. Ibrahimov, I.E. Molotov, T. Michałowski, K. Kitazato, New photometric observations of asteroids (1862) Apollo and (25143) Itokawa—an analysis of YORP effect. Astron. Astrophys. **488**, 345–350 (2008). doi:10.1051/0004-6361:200809663

T.C. Duxbury, R.L. Newburn, C.H. Acton, E. Carranza, T.P. McElrath, R.E. Ryan, S.P. Synnott, Y.T. Han, D.E. Brownlee, A.R. Cheuvront, W.R. Adams, S.L. Toro-Allen, S. Freund, K.V. Gilliland, K.J. Irish, C.R. Love, J.G. McAllister, S.J. Mumaw, T.H. Oliver, D.E. Perkins, Asteroid 5535 Annefrank size, shape, and orientation: Stardust first results. J. Geophys. Res., Planets **109**, E02002 (2004a)

T.C. Duxbury, R.L. Newburn, D.E. Brownlee, Comet 81P/Wild 2 size, shape, and orientation. J. Geophys. Res. **109**, E12S02 (2004b). doi:10.1029/2004JE002316

M. Ebihara, S. Sekimoto, N. Shirai, Y. Hamajima, M. Yamamoto, K. Kumagai, Y. Oura, T.R. Ireland, F. Kitajima, K. Nagao, T. Nakamura, H. Naraoka, T. Noguchi, R. Okazaki, A. Tsuchiyama, M. Uesugi, H. Yurimoto, M.E. Zolensky, M. Abe, A. Fujimura, T. Mukai, Y. Yada, Neutron activation analysis of a particle returned from asteroid Itokawa. Science **333**, 1119–1121 (2011)

L.T. Elkins-Tanton, B.P. Weiss, M.T. Zuber, Chondrites as samples of differentiated planetesimals. Earth Planet. Sci. Lett. **305**, 1–10 (2011)

S. Erard, O. Forni, M. Ollivier, E. Dotto, T. Roush, F. Poulet, T. Müller, The 2004 opposition of Ceres observed with adaptive optics on the VLT, in *Lunar and Planetary Science XXXVI* (2005), abstract 1388

O. Eugster, Cosmic-ray exposure ages of meteorites and lunar rocks and their significance. Chem. Erde **63**, 3–30 (2003)

F.S. Fanale, J.R. Salval, The water regime on asteroid (1) Ceres. Icarus **82**, 97–110 (1989)

D. Farnocchia, S.R. Chesley, D. Vokrouhlický, A. Milani, F. Spoto, W.F. Bottke, Near Earth asteroids with measurable Yarkovsky effect. Icarus **224**, 1–13 (2013)

S. Fornasier, F. Marzari, E. Dotto, M.A. Barucci, A. Migliorini, Are the E-type Asteroids (2867) Steins, a target of the Rosetta mission, and NEA (3103) Eger remnants of an old asteroid family? Astron. Astrophys. **474**, L29–L32 (2007)

S. Fornasier, A. Migliorini, E. Dotto, M.A. Barucci, Visible and near infrared spectroscopic investigation of E-type asteroids, including 2867 Steins, a target of the Rosetta mission. Icarus **196**, 119–134 (2008)

S. Fornasier, S. Mottola, M.A. Barucci, H. Sierks, S. Hviid, Photometric observations of asteroid 4 Vesta by the OSIRIS cameras onboard the Rosetta spacecraft. Astron. Astrophys. **533**, L9 (2011). doi:10.1051/0004-6361/2011176

G. Forster, A voyage round the world, in His Britannic Majesty's sloop, Resolution, commanded by Capt. James Cook, during the years 1772, 3, 4, and 5. In two volumes. Gale ECCO (2010)

A. Fujiwara, J. Kawaguchi, D.K. Yeomans, M. Abe, T. Mukai, T. Okada, J. Saito, H. Yano, M. Yoshikawa, D.J. Scheeres, O. Barnouin-Jha, A.F. Cheng, H. Demura, R.W. Gaskell, N. Hirata, H. Ikeda, T. Kominato, H. Miyamoto, A.M. Nakamura, R. Nakamura, S. Sasaki, a. Uesugi, The rubble-pile Asteroid Itokawa as observed by Hayabusa. Science **312**, 1330–1334 (2006)

M.J. Gaffey, J.F. Bell, R.H. Brown, T.H. Burbine, J.L. Piatek, K.L. Reed, D.A. Chaky, Mineralogic variations within the S-type asteroid class. Icarus **106**, 573–602 (1993a)

M.J. Gaffey, T.H. Burbine, R.P. Binzel, Asteroid spectroscopy: Progress and perspective. Meteoritics **28**, 161–187 (1993b)

W.B. Garry, M.V. Sykes, D.L. Buczkowski, D.A. Williams, R.A. Yingst, S.C. Mest, R. Jaumann, C.M. Pieters, H. Hiesinger, T. Roatsch, F. Preusker, C.T. Russell, C.A. Raymond, Geologic mapping of Av-10 Oppia quadrangle of asteroid 4 Vesta. Geophys. Res. Abstr. **14**, EGU2012-5711-1 (2012)

T. Gehrels (ed.), *Asteroids* (University of Arizona Press, Tucson, 1979), 1191 pp.

P. Geissler, J.-M. Petit, D.D. Durda, R. Greenberg, W. Bottke, M. Nolan, J. Moore, Erosion and ejecta reaccretion on 243 Ida and its moon. Icarus **120**, 140–157 (1996)

A. Ghosh, S.J. Weidenschilling, H.Y. McSween Jr., A. Rubin, Asteroidal heating and thermal stratification of the Asteroidal Belt, in *Meteorites and the Early Solar System II*, ed. by D.S. Lauretta, H.Y. McSween Jr. (University of Arizona Press, Tucson, 2006), pp. 555–566, 943 pp.

K.M. Gietzen, C.H.S. Lacy, D.R. Ostrowski, D.W.G. Sears, IRTF observations of S complex and other asteroids: Implications for surface compositions, the presence of clinopyroxenes, and their relationship to meteorites. Meteorit. Planet. Sci. **47**, 1789–1808 (2012)

K.-H. Glassmeier, H. Boehnhardt, D. Koschny, E. Kürhrt, I. Richter, Space Sci. Rev. **128**, 1–21 (2007). doi:10.1007/s11214-006-9140-8

J.D. Goldader, D.J. Tholen, D.P. Cruikshank, W.K. Hartmann, Galileo support observations of asteroid Gaspra. Astron. J. **102**, 1503–1509 (1991)

H. Goldschmidt, Discovery of Lutetia Nov. 15. Mon. Not. R. Astron. Soc. **12**, 213 (1852)

R. Greenberg, Eros' Rahe Dorsum: Implications for internal structure. Meteorit. Planet. Sci. **43**, 435–449 (2008)

R. Greenberg, M. Noland, W. Bottke, R. Kolvoord, J. Veverka, Collisional history of Gaspra. Icarus **107**, 84–97 (1994)

R.E. Grimm, H.Y. McSween, Heliocentric zoning of the asteroid belt by aluminum-26 heating. Science **259**, 653–655 (1993)

O. Groussin, P. Lamy, S. Fornasier, L. Jorda, The properties of asteroid (2867) Steins from Spitzer Space Telescope observations and OSIRIS shape reconstruction. Astronomy and Astrophysics **529**(A73), 8 pages (2011)

B. Hapke, Bidirectional reflectance spectroscopy. I—Theory. J. Geophys. Res. **86**, 3039–3054 (1981)

B. Hapke, Bidirectional reflectance spectroscopy. III—Correction for macroscopic roughness. Icarus **59**, 41–59 (1984)

B. Hapke, Bidirectional reflectance spectroscopy. IV—The extinction coefficient and the opposition effect. Icarus **67**, 264–280 (1986)

A.W. Harris, Tumbling asteroids. Icarus **107**, 209–211 (1994)

W.K. Hartmann, *Moons and Planets*, 2nd edn. (Wadsworth, Belmont, 1983)

W.K. Hartmann, D.J. Tholen, D.P. Cruikshank, The relationship of active comets, "extinct" comets, and dark asteroids. Icarus **69**, 33–50 (1987)

S. Hasegawa, K. Murakawa, M. Ishiguro, H. Nonaka, T. Naruhisa, C.J. Davis, M. Ueno, T. Hiroi, Evidence of hydrated and/or hydroxylated minerals on the surface of asteroid 4 Vesta. Geophys. Res. Lett. **30**(21), 2123 (2003). doi:10.1029/2003GL018627

S. Hasegawa, S. Miyasaka, N. Tokimasa, A. Sogame, M.A. Ibrahimov, F. Yoshida, M. Abe, D. Kuroda, BRz' phase function of asteroid 4 Vesta during the 2006 opposition, in *40th Lunar and Planetary Science Conference (Lunar and Planetary Science XL)*, The Woodlands, TX, March 23–27 (2009)

C. Hayashi, Structure of the solar nebula, growth and decay of magnetic fields and effects of magnetic and turbulent viscosities on the nebula. Prog. Theor. Phys. Suppl. **70**, 35–53 (1981)

E. Heggy, P. Paillou, G. Ruffie, J.M. Malezieux, F. Costard, G. Grandjean, On water detection in the Martian subsurface using sounding radar. Icarus **154**, 244–257 (2001)

P. Helfenstein, J. Veverka, Physical characterization of asteroid surfaces from photometric analysis, in *Asteroids II; Proceedings of the Conference*, Tucson, AZ, March 8–11 (University of Arizona Press, Tucson, 1989), pp. 557–593 (A90-27001 10-91)

P. Helfenstein, J. Veverka, P.C. Thomas, D.P. Simonelli, P. Lee, K. Klaasen, T.V. Johnson, H. Breneman, J.W. Head, S. Murchie, Galileo photometry of Asteroid 951 Gaspra. Icarus **107**, 37–60 (1994)

P. Helfenstein, P.J. Veverka, P.C. Thomas, D.P. Simonelli, K. Klaasen, T.V. Johnson, F. Fanale, A.S. Granahan, A.S. McEwen, M. Belton, C. Chapman, Galileo photometry of Asteroid 243 Ida. Icarus **120**, 48–65 (1996)

A.R. Hendrix, F. Vilas, M.C. Festouc, Vesta's UV lightcurve: Hemispheric variation in brightness and spectral reversal. Icarus **162**, 1–9 (2003)

J.K. Hillier, J.M. Bauer, B.J. Buratti, Photometric modeling of Asteroid 5535 Annefrank from Stardust observations. Icarus **211**, 546–552 (2011)

J.L. Hilton, Asteroid masses and densities, in *Asteroids III*, ed. by W.F. Bottke Jr., A. Cellino, P. Paolicchi, R.P. Binzel (University of Arizona Press, Tucson, 2002), pp. 103–112

L.L. Hood, Z. Huang, Formation of magnetic anomalies antipodal to lunar impact basins—two-dimensional model calculations. J. Geophys. Res. **96**, 9837–9846 (1991)

K.C. Horstman, H.J. Melosh, Drainage pits in cohesionless materials: Implications for the surface of Phobos. J. Geophys. Res., Solid Earth **94**, 12433–12441 (1989). doi:10.1029/JB094iB09p12433

M. Horstmann, A. Bischoff, The Almahata Sitta polymict breccia and the late accretion of asteroid 2008 TC3. Chem. Erde **74**, 149–183 (2014)

F. Hörz, R.B. Schaal, Asteroid agglutinate formation and implications for asteroid surfaces. Icarus **46**, 337–353 (1981)

K.R. Housen, L.L. Wilkening, C.R. Chapman, R. Greenberg, Asteroidal regoliths. Icarus **39**, 317–351 (1979)

E.S. Howell, D.T. Britt, J.F. Bell, R.P. Binzel, L.A. Lebofsky, Visible and near-Infrared spectral observations of 4179 Toutatis. Icarus **111**, 468–474 (1994)

H.H. Hsieh, D. Jewitt, A population of comets in the Main Asteroid Belt. Science **312**, 561–563 (2006)

S. Huang, G. Akridge, D.W.G. Sears, Metal-silicate fractionation in the surface dust layers of accreting planetesimals: Implications for the formation of ordinary chondrites and the nature of asteroid surfaces. J. Geophys. Res. **101**, 29373–29385 (1996)

J. Huang, J. Ji, P. Ye, X. Wang, J. Yan, L. Meng, S. Wang, C. Li, Y. Li, D. Qiao, W. Zhao, Y. Zhao, T. Zhang, P. Liu, Y. Jiang, W. Rao, S. Li, C. Huang, W.-H. Ip, S. Hu, M. Zhu, L. Yu, Y. Zou, X. Tang, J. Li, H. Zhao, H. Huang, X. Jiang, J. Bai, The ginger-shaped Asteroid 4179 Toutatis: New observations from a successful flyby of Chang'e-2. Sci. Rep. **3**, 3411 (2013). arXiv:1312.4329 [astro-ph.EP], doi:10.1038/srep03411

R.S. Hudson, S.J. Ostro, Shape and non-principal axis spin state of Asteroid 4179 Toutatis. Science **270**, 84–86 (1995)

R.S. Hudson, S.J. Ostro, Photometric properties of Asteroid 4179 Toutatis from lightcurves and a radar-derived physical model. Icarus **135**, 451–457 (1998)

R. Jaumann, D.A. Williams, D.L. Buczkowski, R.A. Yingst, F. Preusker, H. Hiesinger, N. Schmedemann, T. Kneissl, J.B. Vincent, D.T. Blewett, B.J. Buratti, U. Carsenty, B.W. Denevi, M.C. De Sanctis, W.B. Garry, H.U. Keller, E. Kersten, K. Krohn, J.-Y. Li, S. Marchi, K.D. Matz, T.B. McCord, H.Y. McSween, S.C. Mest, D.W. Mittlefehldt, S. Mottola, A. Nathues, G. Neukum, D.P. O'Brien, C.M. Pieters, T.H. Prettyman, C.A. Raymond, T. Roatsch, C.T. Russell, P. Schenk, B.E. Schmidt, F. Scholten, K. Stephan, M.V. Sykes, P. Tricarico, R. Wagner, M.T. Zuber, H. Sierks, Vesta's shape and morphology. Science **336**, 687–690 (2012)

R. Jaumann, J.-P. Bibring, K.-H. Glassmeier, M. Grott, T.-M. Ho, S. Ulamec, N. Schmitz, H.-U. Auster, J. Biele, H. Kuninaka, T. Okada, M. Yoshikawa, S. Watanabe, M. Fujimoto, T. Spohn, A Mobile Asteroid Surface Scout (MASCOT) for the Hayabusa 2 Mission to 1999 JU3: The scientific approach, in *44th Lunar and Planetary Science Conference*, The Woodlands, TX, March 18–22 (2013), LPI Contribution No. 1719, p. 1500

R. Jaumann, A. Nass, K. Otto, K. Krohn, K. Stephan, T.B. McCord, D.A. Williams, C.A. Raymond, D.T. Blewett, H. Hiesinger, R.A. Yingst, M.C. De Sanctis, E. Palomba, T. Roatsch, K.-D. Matz, F. Preusker, F. Scholten, C.T. Russell, The geological nature of dark material on Vesta and implications for the subsurface structure. Icarus **240**, 3–19 (2014)

P. Jenniskens, M.H. Shaddad, D. Numan, S. Elsir, A.M. Kudoda, M.E. Zolensky, L. Le, G.A. Robinson, J.M. Friedrich, D. Rumble, A. Steele, S.R. Chesley, A. Fitzsimmons, S. Duddy, H.H. Hsieh, G. Ramsay, P.G. Brown, W.N. Edwards, E. Tagliaferri, M.B. Boslough, R.E. Spalding, R. Dantowitz, M. Kozubal, P. Pravec, J. Borovicka, Z. Charvat, J. Vaubaillon, J. Kuiper, J. Albers, J.L. Bishop, R.L. Mancinelli, S.A. Sandford, S.N. Milam, M. Nuevo, S.P. Worden, The impact and recovery of asteroid 2008 TC3. Nature **458**, 485–488 (2009)

D. Jewitt, The active asteroids. Astron. J. **143**, 66 (2012), 14 pages. doi:10.1088/0004-6256/143/3/66

D. Jewitt, H. Weaver, J. Agarwal, M. Mutchler, M. Drahus, A recent disruption of the main-belt asteroid P/2010 A2. Nature **467**, 817–819 (2010)

T.V. Johnson, F.P. Fanale, Optical properties of carbonaceous chondrites and their relationship to asteroids. J. Geophys. Res. **78**, 8507–8518 (1973)

L. Jorda, P.L. Lamy, R.W. Gaskell, M. Kaasalainen, O. Groussin, S. Besse, G. Faury, Asteroid (2867) Steins: Shape, topography and global physical properties from OSIRIS observations. Icarus **221**, 1089–1100 (2012)

M. Jutzi, E. Asphaug, Mega-ejecta on asteroid Vesta. Geophys. Res. Lett. **38**, L01102 (2011). doi:10.1029/2010GL045517

M. Jutzi, N. Thomas, W. Benz, M.R. El Maarry, L. Jorda, E. Kührt, F. Preusker, The influence of recent major crater impacts on the surrounding surfaces of (21) Lutetia. Icarus **226**, 89–100 (2013)

M. Kaasalainen, J. Torppa, Optimization methods for asteroid lightcurve inversion I. Shape determination. Icarus **153**, 24–36 (2001). doi:10.1006/icar.2001.6673

M. Kaasalainen, T. Kwiatkowski, M. Abe, J. Piironen, T. Nakamura, Y. Ohba, B. Dermawan, T. Farnham, F. Colas, S. Lowry, P. Weissman, R.J. Whiteley, D.J. Tholen, S.M. Larson, M. Yoshikawa, I. Toth, F.P. Velichko, CCD photometry and model of MUSES-C target (25143) 1998 SF36. Astron. Astrophys. **405**, L29–L32 (2003)

J. Kawaguchi, A. Fujiwara, T. Uesugi, Hayabusa—its technology and science accomplishment summary and Hayabusa-2. Acta Astronaut. **62**, 639–647 (2008)

K. Keil, Geological history of asteroid 4 Vesta: The "smallest terrestrial planet", in *Asteroids III*, ed. by W. Bottke, A. Cellino, P. Paolicchi, R.P. Binzel (University of Arizona Press, Tucson, 2002), pp. 573–584

H.U. Keller, R. Kramm, N. Thomas, Surface features on the nucleus of Comet Halley. Nature **331**, 227–231 (1988)

H.U. Keller, C. Barbieri, D. Koschny, P. Lamy, H. Rickman, R. Rodrigo, H. Sierks, M.F. A'Hearn, F. Angrilli, M.A. Barucci, J.-L. Bertaux, G. Cremonese, V. Da Deppo, B. Davidsson, M. De Cecco, S. Debei, S. Fornasier, M. Fulle, O. Groussin, P.J. Gutierrez, S.F. Hviid, W.-H. Ip, L. Jorda, J. Knollenberg, J.R. Kramm, E. Kührt, M. Küppers, L.-M. Lara, M. Lazzarin, J. Lopez Moreno, F. Marzari, H. Michalik, G. Naletto, L. Sabau, N. Thomas, K.-P. Wenzel, I. Bertini, S. Besse, F. Ferri, M. Kaasalainen, S. Lowry, S. Marchi, S. Mottola, W. Sabolo, S.E. Schröder, P. Spjuth, P. Vernazza, E-type asteroid (2867) Steins as imaged by OSIRIS on board Rosetta. Science **327**, 190–193 (2010)

R.M. Killen, Depletion of sulfur on the surface of asteroids and the Moon. Meteorit. Planet. Sci. **38**, 383–388 (2003)

T.V.V. King, R.N. Clark, W.M. Calvin, D.M. Sherman, R.H. Brown, Evidence for ammonium-bearing minerals on Ceres. Science **255**, 1551–1553 (1992)

K. Kirsimäe, G.R. Osinsky, Impact-induced hydrothermal activity, in *Impact Cratering, Processes and Products*, ed. by G.R. Osinsky, E. Pierazzo (Wiley-Blackwell, Chichester, 2013), pp. 76–89

KISS Report, *Asteroid retrieval feasibility study* (Keck Institute for Space Studies, Californian Institute of Technology, Pasadena, California, 2012)

M.G. Kivelson, L.F. Bargatze, K.K. Khurana, D.J. Southwood, R.J. Walker, P.J. Coleman Jr., Magnetic field signatures near Galileo's closest approach to Gaspra. Science **261**, 331–334 (1993)

R.L. Klima, C.M. Pieters, M.D. Darby, Spectroscopy of synthetic Mg-Fe pyroxenes I: Spin-allowed and spin-forbidden crystal field bands in the visible and near-infrared. Meteorit. Planet. Sci. **42**, 235–253 (2007)

R.L. Klima, M.D. Dyar, C.M. Pieters, Near-infrared spectra of clinopyroxenes: Effects of calcium content and crystal structure. Meteorit. Planet. Sci. **46**, 379–395 (2011)

T. Kneiss, N. Schmedemann, V. Reddy, D.A. Williams, S.H.G. Walter, A. Neesemann, G.G. Michael, R. Jaumann, K. Krohn, F. Preusker, T. Roatsch, L. Le Corre, A. Nathues, M. Hoffmann, M. Schäfer, D. Buczkowski, W.B. Garry, R.A. Yingst, S.C. Mest, C.T. Russell, C.A. Raymond, Morphology and formation ages of mid-sized post-Rheasilvia craters – Geology of quadrangle Tuccia, Vesta. Icarus **244**, 133–157 (2014)

A.S. Konopliv, S.W. Asmar, B.G. Bills, N. Mastrodemos, R.S. Park, C.A. Raymond, D.E. Smith, M.T. Zuber, The Dawn gravity investigation at Vesta and Ceres. Space Sci. Rev. **163**, 461–486 (2011)

A.S. Konopliv, S.W. Asmar, R.S. Park, B.G. Bills, F. Centinello, A.B. Chamberlin, A. Ermakov, The Vesta gravity field, spin pole and rotation period, landmark positions, and ephemeris from the Dawn tracking and optical data. Icarus **240**, 103–117 (2014)

A. Kracher, D.W.G. Sears, Space weathering and the low sulfur abundance of Eros. Icarus **174**, 36–45 (2005)

N.V. Krivova, E.I. Yagudina, V.A. Shor, The orbit determination of (4179) Toutatis from optical and radar data. Planet. Space Sci. **42**, 741–745 (1994)

K. Krohn, R. Jaumann, K. Otto, T. Hoogenboom, R. Wagnera, D.L. Buczkowski, B. Garry, D.A. Williams, R.A. Yingst, J. Scully, M.C. De Sanctis, T. Kneissl, N. Schmedemann, E. Kersten, K. Stephana, K.-D. Matza, C.M. Pieters, F. Preusker, T. Roatsch, P. Schenk, C.T. Russell, C.A. Raymond, Mass movement on Vesta at steep scarps and crater rims. Icarus **244**, 120–132 (2014)

M. Küppers, L. O'Rourke, D. Bockelé-Morvan, V. Zakharov, S. Lee, P. von Allmen, B. Carry, D. Teyssier, A. Marston, T. Müller, J. Crovisier, M.A. Barucci, R. Moreno, Localized sources of water vapour on the dwarf planet (1) Ceres. Nature **505**, 525–527 (2014)

F. La Forgia, S. Magrin, I. Bertini, M. Lazzarin, M. Pajola, C. Barbieri, Photometric analysis of asteroid (2867) Steins from Rosetta OSIRIS images. Mem. Soc. Astron. Ital. Suppl. **20**, 15–21 (2012)

C.-I. Lagerkvist, A. Erikson, H. Debehogne, L. Festin, P. Magnusson, S. Mottola, T. Oja, G. de Angelis, I.N. Belskaya, M. Dahlgren, M. Gonano-Beurer, J. Lagerros, K. Lumme, S. Pohjolainen, Physical studies of asteroids. XXIX. Photometry and analysis of 27 asteroids. Astron. Astrophys. Suppl. Ser. **113**, 115–129 (1995)

J.S. Lambert, D.J. Tholen, Rotational studies of MUSES-C target asteroid (25143) 1998 SF36. Bull. Am. Astron. Soc. **33**, 1402 (2001). American Astronomical Society, 199th AAS Meeting, #63.03

P.L. Lamy, M. Kaasalainen, S. Lowry, P. Weissman, M.A. Barucci, J. Carvano, Y.-J. Choi, F. Colas, G. Faury, S. Fornasier, O. Groussin, M.D. Hicks, L. Jorda, A. Kryszczynska, S. Larson, I. Toth, B. Warner, Asteroid 2867 Steins II. Multi-telescope visible observations, shape reconstruction, and rotational state. Astron. Astrophys. **487**, 1179–1185 (2008). doi:10.1051/0004-6361:20078995

H.P. Larson, M.A. Feierberg, L.A. Lebofsky, The composition of 2 Pallas and its relation to primitive meteorites. Icarus **56**, 398–408 (1983)

D.S. Lauretta (The OSIRIS-REx Team), An overview of the OSIRIS_REX asteroid sample return mission, in *43rd Lunar and Planetary Science Conference* (2012). Abstract #2491

M. Lazzarin, S. Fornasier, M.A. Barucci, M. Birlan, Groundbased investigation of Asteroid 9969 Braille, target of the spacecraft mission Deep Space 1. Astron. Astrophys. **375**, 281–284 (2001)

M. Lazzarin, S. Marchi, S. Magrin, C. Barbieri, Visible spectral properties of asteroid 21 Lutetia, target of Rosetta Mission. Astron. Astrophys. **425**, L25–L28 (2004). doi:10.1051/0004-6361:200400054

L. Le Corre, V. Reddy, N. Schmedemann, K.J. Becker, D.P. O'Brien, N. Yamashita, P.N. Peplowski, T.H. Prettyman, J.-Y. Li, E.A. Cloutis, B.W. Denevi, T. Kneissl, E. Palmer, R.W. Gaskell, A. Nathues, M.J. Gaffey, D.W. Mittlefehldt, W.B. Garry, H. Sierks, C.T. Russell, C.A. Raymond, M.C. De Sanctis, E. Ammanito, Olivine or impact melt: Nature of the "Orange" material on Vesta from Dawn. Icarus **226**, 1568–1594 (2013)

L.A. Lebofsky, M.A. Feierberg, H.P. Larson, A.T. Tokunaga, The 1.7- to 4.2-micron spectrum of Asteroid 1 Ceres—Evidence for structural water in clay minerals. Icarus **48**, 453–459 (1981)

S.M. Lederer, D.L. Domingue, F. Vilas, M. Abe, T.L. Farnham, K.S. Jarvis, S.C. Lowry, Y. Ohba, P.R. Weissman, L.M. French, H. Fukai, S. Hasegawa, M. Ishiguro, S.M. Larson, Y. Takagi, Physical characteristics of Hayabusa target Asteroid 25143 Itokawa. Icarus **173**, 153–165 (2005)

T. Lee, D.A. Papanastassiou, G.J. Wasserburg, Demonstration of ^{26}Mg excess in Allende and evidence for ^{26}Al. Geophys. Res. Lett. **3**, 41–44 (1976)

P. Lee, J. Veverka, P.C. Thomas, P. Helfenstein, M.J.S. Belton, C.R. Chapman, R. Greeley, R.T. Pappalardo, R. Sullivan, J.W. Head, Ejecta blocks on 243 Ida and on other asteroids. Icarus **120**, 87–105 (1996)

J.S. Lewis, The temperature gradient in the solar nebula. Science **186**, 440–443 (1974)

J.S. Lewis, *Mining the Sky* (Addison-Wesley, Reading, 1996), 274 pp.

M. Lewis, W. Clark, *The Journals of Lewis and Clark* (Kessinger Publishing, Whitefish, 2004), p. 312

J.-Y. Li, R.P. Binzel, S.M. Slivan, P. Magnusson, W.Z. Wisniewski, J. Drummond, K. Lumme, M.A. Barucci, E. Dotto, C. Angeli, D. Lazzaro, S. Mottola, M. Gonano-Beurer, T. Michałowski, G. De Angelis, D.J. Tholen, M. Di Martino, M. Hoffmann, E.H. Geyer, F. Velichko, Asteroid 243 Ida: Groundbased photometry and a pre-Galileo physical model. Icarus **105**, 310–325 (1993)

J.-Y. Li, L.A. McFadden, J.W. Parker, E.F. Young, A.S. Stern, P.C. Thomas, C.T. Russell, M.V. Sykes, Photometric analysis of 1 Ceres and surface mapping from HST observations. Icarus **182**, 143–160 (2006)

Y. Li, Z.Z. Wang, J.S. Jiang, Simulations on the influence of lunar surface brightness temperature profiles on CE-1 lunar microwave sounder brightness temperature. Sci. China Earth Sci. **53**, 1379–1391 (2010)

J.-Y. Li, P.C. Thomas, B. Carcich, M.J. Mutchler, L.A. McFadden, C.T. Russell, S.S. Weinstein-Weiss, M.D. Rayman, C.A. Raymond, Improved measurement of Asteroid (4) Vesta's rotational axis orientation. Icarus **211**, 528–534 (2011)

J.-Y. Li, L. Le Corre, S.E. Schröder, V. Reddy, B.W. Denevi, B.J. Buratti, S. Mottola, M. Hoffmann, P. Gutierrez-Marques, A. Nathues, C.T. Russell, C.A. Raymond, Global photometric properties of Asteroid (4) Vesta observed with Dawn Framing Camera. Icarus **226**, 1252–1274 (2013)

J.-Y. Li, B.J. Buratti, C.M. De Sanctis, B.W. Denevi, M. Hoffmann, A. Longobardo, S. Mottola, A. Nathues, V. Reddy, C.T. Russell, S.E. Schröder, The photometric properties of Vesta and the implications, in *Workshop on Vesta in the Light of Dawn: First Exploration of a Protoplanet in the Asteroid Belt* (2014). Abstract # 2032

J. Licandro, H. Campins, M. Kelley, K. Hargrove, N. Pinilla-Alonso, D. Cruikshank, A.S. Rivkin, J. Emery, (65) Cybele: detection of small silicate grains, water-ice, and organics. Astron. Astrophys. **525**, A34 (2010) (7 pages)

L.F. Lim, L.R. Nittler, Elemental composition of 433 Eros: New calibration of the NEAR-Shoemaker XRS data. Icarus **200**, 129–146 (2009)

M.J. Loeffler, C.A. Dukes, W.Y. Chang, L.A. McFadden, R.A. Baragiola, Laboratory simulations of sulfur depletion at Eros. Icarus **195**, 622–629 (2008)

A. Longobardo, F. Capaccioni, E. Palomba, M.C. De Sanctis, F. Tosi, S.E. Schroeder, J.-Y. Li, M.T. Capria, E. Ammannito, C.A. Raymond, C.T. Russell, Retrieval of disk-resolved phase functions of Vesta and comparison with other asteroids, in *Workshop on Vesta in the Light of Dawn: First Exploration of a Protoplanet in the Asteroid Belt* (2014). Abstract # 2028

S.G. Love, T.J. Ahrens, Catastrophic impacts on gravity dominated asteroids. Icarus **124**, 141–155 (1996)

S.C. Lowry, P.R. Weissman, M.D. Hicks, CCD observations of Asteroid 1998 SF36 (25143). Bull. Am. Astron. Soc. **33**, 1150 (2001). American Astronomical Society, DPS Meeting #33, #59.09

S.C. Lowry, P.R. Weissman, M.D. Hicks, R.J. Whiteley, S. Larson, Physical properties of Asteroid (25143) Itokawa—target of the Hayabusa sample return mission. Icarus **176**, 408–417 (2005)

S.C. Lowry, P.R. Weissman, S.R. Duddy, B. Rozitis, A. Fitzsimmons, S.F. Green, M.D. Hicks, C. Snodgrass, S.D. Wolters, S.R. Chesley, J. Pittichová, P. van Oers, The internal structure of asteroid (25143) Itokawa as revealed by detection of YORP spin-up. Astron. Astrophys. **562**, A48 (2014), 9 pages

K. Lumme, E. Bowell, Radiative transfer in the surfaces of atmosphereless bodies. I—Theory. Astron. J. **86**, 1694–1704 (1981a)

K. Lumme, E. Bowell, Radiative transfer in the surfaces of atmosphereless bodies. I—Theory. II—Interpretation of phase curves. Astron. J. **86**, 1705–1721 (1981b)

D.F. Lupishko, S.V. Vasilyev, S. Efimov Ju, N.M. Shakhovskoj, UBVRI-polarimetry of asteroid 4179 Toutatis. Icarus **113**, 200–205 (1995)

W.T. Lynn, The discovery of Vesta. Observatory **30**, 103–105 (1907)

P. Magnusson, M.A. Barucci, R.P. Binzel, C. Blanco, M. Di Martino, J.D. Goldader, M. Gonano-Beurer, A.W. Harris, T. Micha-Lowski, S. Mottola, D.J. Tholen, W.Z. Wisniewski, Asteroid 951 Gaspra: Pre-Galileo physical model. Icarus **97**, 124–129 (1992)

C. Magri, S.J. Ostro, K.D. Rosema, M.L. Thomas, D.L. Mitchell, D.B. Campbell, J.F. Chandler, I.I. Shapiro, J.D. Giorgini, D.J. Yeomans, Mainbelt asteroids: Results of Arecibo and Goldstone Radar observations of 37 objects during 1980–1995. Icarus **140**, 379–407 (1999)

S. Marchi, C. Barbieri, M. Küppers, F. Marzari, B. Davidsson, H.U. Keller, S. Besse, P. Lamy, S. Mottola, M. Massironi, G. Cremonese, The cratering history of asteroid (2867) Steins. Planet. Space Sci. **58**, 1116–1123 (2010)

S. Marchi, H.Y. McSween, D.P. O'Brien, P. Schenk, M.C. De Sanctis, R. Gaskell, R. Jaumann, S. Mottola, F. Preusker, C.A. Raymond, T. Roatsch, C.T. Russell, The violent collisional history of Asteroid 4 Vesta. Science **336**, 690–694 (2012)

R.G. Martin, M. Livio, On the evolution of the snow line in protoplanetary discs. Mon. Not. R. Astron. Soc. **425**, L6–L9 (2012)

F. Marzari, D. Davis, V. Vanzani, Collisional evolution of asteroid families. Icarus **113**, 168–187 (1995)

T.B. McCord, M.J. Gaffey, Asteroids—surface composition from reflection spectroscopy. Science **186**, 352–355 (1974)

T.B. McCord, C. Sotin, Ceres: Evolution and current state. J. Geophys. Res. **110**, E05009 (2005). doi:10.1029/2004JE002244

T.B. McCord, J.B. Adams, T.V. Johnson, Asteroid Vesta: Spectral reflectivity and compositional implications. Science **168**, 1445–1447 (1970)

T.B. McCord, J.-Y. Li, J.-P. Combe, H.Y. McSween, R. Jaumann, V. Reddy, F. Tosi, D.A. Williams, D.T. Blewett, D. Turrini, E. Palomba, C.M. Pieters, M.C. De Sanctis, E. Ammannito, M.T. Capria, L. Le Corre, A. Longobardo, A. Nathues, D.W. Mittlefehldt, S.E. Schröder, H. Hiesinger, A.W. Beck, F. Capaccioni, U. Carsenty, H.U. Keller, B.W. Denevi, J.M. Sunshine, C.A. Raymond, C.T. Russell, Dark material on Vesta from the infall of carbonaceous volatile-rich material. Nature **491**, 83–86 (2012)

D.S. McKay, T.D. Swindle, R. Greenberg, Asteroidal regoliths—what we do not know, in *Asteroids II*, ed. by R.P. Binzel, T. Gehrels, M.S. Matthews (University of Arizona Press, Tucson, 1989), pp. 921–945

H.Y. McSween Jr., Are carbonaceous chondrites primitive or processed? A review. J. Geophys. Space Phys. **17**, 1059–1078 (1979)

H.Y. McSween, R.P. Binzel, M.C. De Sanctis, E. Ammannito, T.H. Prettyman, A.W. Beck, V. Reddy, L. Le Corre, M.J. Gaffey, T.B. McCord, C.A. Raymond, C.T. Russell (The Dawn Science Team), Dawn: The Vesta–HED connection and the geologic context for eucrites, diogenites, and howardites. Meteorit. Planet. Sci. **48**, 2090–2104 (2013)

A.J. Meadows, Remanent magnetization in meteorites. Nature **237**, 274 (1972). doi:10.1038/237274a0

H.J. Melosh, *Impact Cratering: A Geologic Process* (Oxford University Press, London, 1989)

G.G. Michael, Planetary surface dating from crater size-frequency distribution measurements: Multiple resurfacing episodes and differential isochron fitting. Icarus **226**, 885–890 (2013)

J.K. Miller, A.S. Konopliv, P.G. Antreasian, J.J. Bordi, S. Chesley, C.E. Helfrich, W.M. Owen, T.C. Wang, B.G. Williams, D.K. Yeomans, D.J. Scheeres, Determination of shape, gravity, and rotational state of Asteroid 433 Eros. Icarus **155**, 3–17 (2002)

R.E. Milliken, A.S. Rivkin, Brucite and carbonate assemblages from altered olivine-rich materials on Ceres. Nat. Geosci. **2**, 258–261 (2009)

R.L. Millis, L.H. Wasserman, O.G. Franz, R.A. Nye, R.C. Oliver, T.J. Kreid, S.E. Jones, W. Hubbard, L. Lebofsky, R. Goff, R. Marcialis, M. Sykes, J. Frecker, D. Hunten, B. Zellner, H. Reitsema, G. Schneider, E. Dunham, J. Klavetter, K. Meech, T. Oswalt, J. Rafert, E. Strother, J. Smith, H. Povenmire, B. Jones, D. Kornbluh, L. Reed, K. Izor, M.F. A'Hearn, R. Schnurr, W. Osborn, D. Parker, W.T. Douglas, J.D. Beish, A.R. Klemola, M. Rios, A. Sanchez, J. Piironen, M. Mooney, R.S. Ireland, D. Leibow, The size, shape, density, and albedo of Ceres from its occultation of BD+8 deg 471. Icarus **72**, 507–518 (1987)

H. Miyamoto, H. Yano, D.J. Scheeres, S. Abe, O. Barnouin-Jha, A.F. Cheng, H. Demura, R.W. Gaskell, N. Hirata, M. Ishiguro, T. Michikami, A.M. Nakamura, R. Nakamura, J. Saito, S. Sasaki, Regolith migration and sorting on asteroid Itokawa. Science **316**, 1011–1014 (2007)

A. Morbidelli, W.F. Bottke Jr., Ch. Froeschlé, P. Michel, Origin and evolution of near-Earth objects, in *Asteroids III*, ed. by W.F. Bottke Jr., A. Cellino, P. Paolicchi, R.P. Binzel (University of Arizona Press, Tucson, 2002), pp. 409–422

J. Morden, D.W. Collison, The implications of the magnetism of ordinary chondrite meteorites. Earth Planet. Sci. Lett. **109**, 185–204 (1992)

S. Mottola, M. Di Martino, M. Gonano-Beurer, H. Hoffmann, G. Neukum, Ground-based observations of 951 Gaspra: CCD lightcurves and spectrophotometry with the Galileo filters, in *Asteroids, Comets and Meteors 1991* (Lunar and Planetary Institute, Houston, 1993), pp. 421–424

S. Mottola, W.D. Sears, A. Erikson, A.W. Harris, J.W. Young, G. Hahn, M. Dahlgren, B.E.A. Mueller, W. Owen, G.-H. Ricardo, J. Licandro, M.A. Barucci, C. Angeli, G. Neukum, C.-I. Lagerkvist, L.J. Felix, The slow rotation of 253 Mathilde. Planet. Space Sci. **43**, 1609–1613 (1995)

M. Mueller, A.W. Harris, S.J. Bus, J.L. Hora, M. Kassis, J.D. Adams, The size and albedo of Rosetta fly-by target 21 Lutetia from new IRTF measurements and thermal modeling. Astron. Astrophys. **447**, 1153–1158 (2006). doi:10.1051/0004-6361:20053742

S.L. Murchie, C.M. Pieters, Spectral properties and rotational spectral heterogeneity of 433 Eros. J. Geophys. Res. **101**, 2201–2214 (1996)

S. Murchie, M. Robinson, B. Clark, P. Thomas, J. Joseph, B. Bussey, D. Domingue, J. Veverka, N. Izenberg, C. Chapman, Color variations on Eros from NEAR multispectral imaging. Icarus **155**, 145–168 (2002)

K. Nagao, R. Okazaki, T. Nakamura, Y.N. Miura, T. Osawa, K. Bajo, S. Matsuda, M. Ebihara, T.R. Ireland, F. Kitajima, H. Naraoka, T. Noguchi, A. Tsuchiyama, H. Yurimoto, M.E. Zolensky, M. Uesugi, K. Shirai, M. Abe, T. Yada, Y. Ishibashi, A. Fujimura, T. Mukai, M. Ueno, T. Okada, M. Yoshikawa, J. Kawaguchi, Irradiation history of Itokawa regolith material deduced from noble gases in the Hayabusa samples. Science **333**, 1128–1131 (2011)

T. Nakamura, T. Noguchi, M. Tanaka, M.E. Zolensky, M. Kimura, A. Tsuchiyama, A. Nakato, T. Ogami, H. Ishida, M. Uesugi, T. Yada, K. Shirai, A. Fujimura, R. Okazaki, S.A. Sandford, Y. Ishibashi, M. Abe, T. Okada, M. Ueno, T. Mukai, M. Yoshikawa, J. Kawaguchi, Itokawa dust particles: A direct link between S-type asteroids and ordinary chondrites. Science **333**, 1113–1116 (2011)

T. Nakamura, A. Nakato, H. Ishida, S. Wakita, T. Noguchi, M.E. Zolensky, M. Tanaka, M. Kimura, A. Tshuchakahitoiyama, T. Ogami, T. Hashimoto, M. Konno, M. Uesugi, T. Yada, K. Shirai, A. Fujimura, R. Okazaki, S.A. Sandford, Y. Ishibashi, M. Abe, T. Okada, M. Ueno, J. Kawaguchi, Mineral chemistry of MUSES-C Regio inferred from analysis of dust particles collected from the first- and second-touchdown sites on asteroid Itokawa. Meteorit. Planet. Sci. **49**, 215–227 (2014)

A. Nathues, M.V. Sykes, I. Büttner, D.L. Buczkowski, U. Carsenty, J. Castillo-Rogez, U. Christensen, P. Gutierrez-Marques, I. Hall, M. Hoffmann, R. Jaumann, S. Joy, H.U. Keller, E. Kersten, K. Krohn, J.-Y. Li, S. Marchi, K.-D. Matz, T.B. McCord, L.A. McFadden, K. Mengel, V. Mertens, S. Mottola, W. Neumann, N. Mastrodemos, D.P. O'Brien, K. Otto, C. Pieters, S. Pieth, C. Polanskey, F. Preusker, M.D. Rayman, C. Raymond, V. Reddy, J. Ripken, C. Roatsch, T. Russel, M. Schäfer, T. Schäfer, P. Schenk, N. Schmedemann, F.T. Scholten, S.E. Schröder, F. Schulzeck, H. Sierks, D. Smith, K. Stephan, G. Thangjam, M. Weiland, D. Williams, M. Zuber, Dawn framing camera clear filter imaging on Ceres approach, in *46th Lunar and Planetary Science Conference*, The Woodlands, TX, 16–20 March (2015), pp. 16–20. Abstract #2069

D. Nesvorný, A. Morbidelli, D. Vokrouhlický, W.F. Bottke, M. Brož, The Flora family: A case of the dynamically dispersed collisional swarm? Icarus **157**, 155–172 (2002)

R.L. Newburn, T.C. Duxbury, M. Hanner, B.V. Semenov, E.E. Hirst, R.S. Bhat, S. Bhaskaran, T.-C.M. Wang, P. Tsou, D.E. Brownlee, A.R. Cheuvront, D.E. Gingerich, G.R. Bollendonk, J.M. Vellinga, K.A. Parham, S.J. Mumaw, Phase curve and albedo of asteroid 5535 Annefrank. J. Geophys. Res. **108** (3–1) 5117 (2003). doi:10.1029/2003JE002106

M.M. Nieto, *Titius-Bode Law of Planetary Distances: Its History and Theory*. Monographs in Natural Philosophy (Pergamon, Elmsford, 1972), 168 pp.

S. Nishihara, M. Abe, S. Hasegawa, M. Ishiguro, K. Kitazato, N. Miura, H. Nonaka, Y. Ohba, M. Okyudo, T. Ozawa, Y. Sarugaku, M. Ueno, Ground-based lightcurve of (25143) Itokawa, 2001–2004, in *Lunar and Planetary Science XXXVI* (2005). Abstract # 1833

L.R. Nittler, R.D. Starr, L. Lim, T.J. McCoy, T.H. Burbine, R.C. Reedy, J.I. Trombka, P. Gorenstein, S.W. Squyres, W.V. Boynton, T.P. McClanahan, J.S. Bhangoo, P.E. Clark, M.E. Murphy, R. Killen, X-ray fluorescence measurements of the surface elemental composition of asteroid 433 Eros. Meteorit. Planet. Sci. **36**, 1673–1695 (2001)

T. Noguchi, T. Nakamura, M. Kimura, M.E. Zolensky, M. Tanaka, T. Hashimoto, M. Konno, A. Nakato, T. Ogami, A. Fujimura, M. Abe, T. Yada, T. Mukai, M. Ueno, T. Okada, K. Shirai, Y. Ishibashi, R. Okazaki, Incipient space weathering observed on the surface of Itokawa dust particles. Science **333**, 1121–1125 (2011)

T. Noguchi, M. Kimura, T. Hashimoto, M. Konno, T. Nakamura, M.E. Zolensky, R. Okazaki, M. Tanaka, A. Tsuchiyama, A. Nakato, T. Ogami, H. Ishida, R. Sagae, S. Tsujimoto, T. Matsumoto, J. Matsuno, A. Fujimura, M. Abe, T. Yada, T. Mukai, M. Ueno, T. Okada, K. Shirai, Y. Ishibashi, Space weathered rims found on the surfaces of the Itokawa dust particles. Meteorit. Planet. Sci. **49**, 188–214 (2014)

J. Oberst, S. Mottola, M. Di Martino, M. Hicks, B. Buratti, L. Soderblom, N. Thomas, A model for rotation and shape of Asteroid 9969 Braille from ground-based observations and images obtained during the Deep Space 1 (DS1) flyby. Icarus **153**, 16–23 (2001)

J. Oberst, B. Giese, E. Howington-Kraus, R. Kirk, L. Soderblom, B. Buratti, M. Hicks, R. Nelson, D. Britt, The nucleus of Comet Borrelly: A study of morphology and surface brightness. Icarus **167**, 70–79 (2004)

D.P. O'Brien, The Yarkovsky effect is not responsible for small crater depletion on Eros and Itokawa. Icarus **203**, 112–118 (2009). 2009

Y. Ohba, M. Abe, S. Hasegawa, M. Ishiguro, T. Kwiatkowski, F. Colas, B. Dermawan, A. Fujiwara, Pole orientation and triaxial ellipsoid shape of (25143) 1998 SF36, a target asteroid of the MUSES-C∗ mission. Earth Planets Space **55**, 341–347 (2003)

T. Okamoto, A.M. Nakamura, S. Hasegawa, K. Kurosawa, K. Ikezaki, A. Tsuchiyama, Impact experiments of exotic dust grain capture by highly porous primitive bodies. Icarus **224**, 209–217 (2013)

W.H. Olbers, Wiederum ein neuer Planet. Ann. Phys. **25**, 344 (1807)

G.R. Osinsky, E. Pierazzo, *Impact Cratering: Processes and Products* (Wiley-Blackwell, Chichester, 2013), 316 pages. ISBN 978-1-4051-9829-5

S.J. Ostro, K.D. Rosema, R.F. Jurgens, The shape of Eros. Icarus **84**, 334–351 (1990). 1990

S.J. Ostro, R.S. Hudson, R.F. Jurgens, K.D. Rosema, D.B. Campbell, D.K. Yeomans, J.F. Chandler, J.D. Giorgini, R. Winkler, R. Rose, S.D. Howard, M.A. Slade, P. Perillat, I.I. Shapiro, Radar images of Asteroid 4179 Toutatis. Science **270**, 80–83 (1995)

S. Ostro, J.-L. Margot, L.A.M. Benner, J.D. Giorgini, D.J. Scheeres, E.G. Fahnestock, S.B. Broschart, J. Bellerose, M.C. Nolan, C. Magri, P. Pravec, P. Scheirich, R. Rose, R.F. Jurgens, E.M. De Jong, S. Suzuki, Radar imaging of binary near-Earth Asteroid (66391) 1999 KW4. Science **314**, 1276–1280 (2006)

P.S. Pallas, Reisen durch verschiedene Provinze des Russichen, volume III. St. Petersburg (1776)

J.W. Parker, S.A. Stern, P.C. Thomas, M.C. Festou, J.W. Merline, E.F. Young, R.P. Binzel, L.A. Lebofsky, Analysis of the first disk-resolved images of Ceres from ultraviolet observations with the Hubble Space Telescope. Astron. J. **123**, 549–557 (2002)

M. Pätzold, T.P. Andert, S.W. Asmar, J.D. Anderson, J.-P. Barriot, M.K. Bird, B. Häusler, M. Hahn, S. Tellmann, H. Sierks, P. Lamy, B.P. Weiss, Asteroid 21 Lutetia: Low mass, high density. Science **334**, 491–492 (2011)

P.N. Peplowski, D. Bazell, L.G. Evans, J.O. Goldstein, D.J. Lawrence, L.R. Nittler, Hydrogen and major element concentrations on 433 Eros: Evidence for an L- or LL-chondrite-like surface composition. Meteorit. Planet. Sci. **50**, 353–367 (2015)

D. Perna, E. Dotto, M. Lazzarin, S. Magrin, M. Fulchignoni, M.A. Barucci, S. Fornasier, S. Marchi, C. Barbieri, Inhomogeneities on the surface of 21 Lutetia, the asteroid target of the Rosetta mission. Ground-based results before the Rosetta fly-by. Astron. Astrophys. **513**, L4 (2010). doi:10.1051/0004-6361/201014051

L. Pesonen, M. Terho, I.T. Kukkonen, Physical properties of 368 meteorites: Implications for meteorite magnetism and planetary geophysics, in *Proceedings of the NIPR Symposium of Antarctic Meteorites*, vol. 6 (1993), pp. 401–416

C.M. Pieters, E. Ammannito, D.T. Blewett, B.W. Denevi, M.C. De Sanctis, M.J. Gaffey, L. Le Corre, J.-Y. Li, S. Marchi, T.B. McCord, L.A. McFadden, D.W. Mittlefehldt, A. Nathues, E. Palmer, V. Reddy, C.A. Raymond, C.T. Russell, Distinctive space weathering on Vesta from regolith mixing processes. Nature **491**, 79–82 (2012)

M. Podolak, S. Zucker, A note on the snow line in protostellar accretion disks. Meteorit. Planet. Sci. **39**, 1859–1868 (2004)

P. Pravec, A.W. Harris, Fast and slow rotation of asteroids. Icarus **148**, 12–20 (2000). doi:10.1006/icar. 2000.6482

P. Pravec, A.W. Harris, P. Scheirich, P. Kušniráka, L. Šarounová, C.W. Hergenrother, S. Mottola, M.D. Hicks, G. Masi, Y.N. Krugly, V.G. Shevchenko, M.C. Nolan, E.S. Howell, M. Kaasalainen, A. Galád, P. Brown, D.R. DeGraff, J.V. Lambert, W.R. Cooney Jr., S. Foglia, Tumbling asteroids. Icarus **173**, 108–131 (2005)

T.H. Prettyman, D.W. Mittlefehldt, N. Yamashita, D.J. Lawrence, A.W. Beck, W.C. Feldman, T.J. McCoy, H.Y. McSween, M.J. Toplis, T.N. Titus, P. Tricarico, R.C. Reedy, J.S. Hendricks, O. Forni, L. Le Corre, J.-Y. Li, H. Mizzon, R. Vishnu, C.A. Raymond, C.T. Russell, Elemental mapping by Dawn reveals exogenic H in Vesta's regolith. Science **338**, 242–246 (2012)

T.H. Prettyman, D.W. Mittlefehldt, N.Y. Yamashita, A.W. Beck, W.C. Feldman, J.S. Hendricks, D.J. Lawrence, T.J. McCoy, H.Y. McSween, P.N. Peplowski, R.C. Reedy, M.J. Toplis, L. Le Corre, H. Mizzon, V. Reddy, T.N. Titus, C.A. Raymond, C.T. Russell, Neutron absorption constraints on the composition of 4 Vesta. Meteorit. Planet. Sci. **48**, 2211–2236 (2013)

D. Preusker, F. Scholten, R. Jaumann, C.A. Raymond, C.T. Russell, High resolution Vesta High Altitude Mapping Orbit (HAMO) Atlas derived from Dawn framing camera images. Planet. Space Sci. **73**, 283–286 (2012)

L. Procter, P. Thomas, M. Robinson, J. Joseph, A. Milne, B. Bussey, J. Veverka, A. Cheng, Surface expressions of structural features on Eros. Icarus **155**, 75–93 (2002). 2002

H. Raab, Johann Palisa, the most successful visual discoverer of asteroids (2002). As of April 2014 available at http://www.astrometrica.at/Papers/Palisa.pdf

M.D. Rayman, P.A. Chadbourne, J.S. Culwell, S.N. Williams, Mission design for Deep Space 1: A low-thrust technology validation mission. Acta Astronaut. **45**, 381–388 (1999)

M.D. Rayman, T.C. Fraschetti, C.A. Raymond, C.T. Russell, Dawn: A mission in development for exploration of main belt asteroids Vesta and Ceres. Acta Astronaut. **58**, 605–616 (2006)

C.A. Raymond, R.S. Park, S.W. Asmar, A.S. Konopliv, D.L. Buczkowski, M.C. De Sanctis, H.Y. McSween, C.T. Russell, R. Jaumann, F. Preusker, V. Terra, An ancient mascon in the southern hemisphere of Vesta, in *44th Lunar and Planetary Science Conference*, The Woodlands, TX, March 18–22 (2013), LPI Contribution No. 1719, p. 2882

C.A. Raymond, R. Park, S.W. Asmar, A.S. Konopliv, M.C. De Sanctis, R. Jaumann, H.Y. McSween, C.T. Russell, D.E. Smith, M. Toplis, M.T. Zuber, Constraints on Vesta's interior evolution from Dawn geophysical data, in *Workshop on "Vesta in the Light of Dawn: First Exploration of a Protoplanet in the Asteroid Belt"* (2014). Abstract # 2051

V. Reddy, J.A. Sanchez, M.J. Gaffey, P.A. Abell, L. Le Corre, P.S. Hardersen, Composition of near-Earth Asteroid (4179) Toutatis. Icarus **221**, 1177–1179 (2012)

V. Reddy, J.-Y. Lia, L. Le Correa, J.E.C. Scully, R. Gaskell, C.T. Russell, R.S. Park, A. Nathues, C. Raymond, M.J. Gaffey, H. Sierks, K.J. Becker, L.A. McFadden, Comparing Dawn, Hubble Space Telescope, and ground-based interpretations of (4) Vesta. Icarus **226**, 1103–1114 (2013)

D.C. Richardson, W.F. Bottke, G. Love Stanley, Tidal distortion and disruption of Earth-crossing asteroids. Icarus **134**(1), 47–76 (1998)

I. Richter, D.E. Brinza, M. Cassel, K.-H. Glassmeier, F. Kuhnke, G. Musmann, C. Othmer, K. Schwingenschuh, B.T. Tsurutani, First direct magnetic field measurements of an asteroidal magnetic field: DS1 at Braille. Geophys. Res. Lett. **28**, 1913–1916 (2001)

H. Richter, U. Auster, K.H. Glassmeier, C. Koenders, C.M. Carr, U. Motschmann, J. Müller, S. McKenna-Lawlor, Magnetic field measurements during the ROSETTA flyby at asteroid (21) Lutetia. Planet. Space Sci. **66**, 155–164 (2012)

H. Rickman, The nucleus of comet Halley: Surface structure, mean density, gas and dust production. Adv. Space Res. **9**, 59–71 (1989)

A.S. Rivkin, J.P. Emery, Detection of ice and organics on an asteroidal surface. Nature **464**, 1322–1323 (2010)

A.S. Rivkin, E.L. Volquardsen, Rotationally-resolved spectra of Ceres in the 3-µm region. Icarus **206**, 327–333 (2010)

A.S. Rivkin, E.S. Howell, F. Vilas, L.A. Lebofsky, Hydrated minerals on asteroids: The astronomical record, in *Asteroids III*, ed. by W.F. Bottke Jr., A. Cellino, P. Paolicchi, R.P. Binzel (University of Arizona Press, Tucson, 2002), pp. 235–253

A.S. Rivkin, J.K. Davies, J.R. Johnson, S.L. Ellison, D.E. Trilling, R.H. Brown, L.A. Lebofsky, Hydrogen concentrations on C-class asteroids derived from remote sensing. Meteorit. Planet. Sci. **38**, 1383–1398 (2003)

A.S. Rivkin, E.L. Volquardsen, B.E. Clark, The surface composition of Ceres: Discovery of carbonates and iron-rich clays. Icarus **185**, 563–567 (2006)

A.S. Rivkin, B.E. Clark, M. Ockert-Bell, E. Volquardsen, E.S. Howell, S.J. Bus, C.A. Thomas, M. Shepard, Asteroid 21 Lutetia at 3 µm: Observations with IRTF SpeX. Icarus **216**, 62–68 (2011a)

A.S. Rivkin, C.A. Thomas, D.E. Trilling, M.-T. Enga, J.A. Grier, Ordinary chondrite-like colors in small Koronis family members. Icarus **211**, 1294–1297 (2011b)

F.E. Roach, A composite light curve for Eros. Astrophys. J. **95**, 310–313 (1942)

Th. Roatsch, E. Kersten, K.-D. Matz, F. Preusker, F. Scholten, R. Jaumann, C.A. Raymond, C.T. Russell, High resolution Vesta High Altitude Mapping Orbit (HAMO) Atlas derived from Dawn framing camera images. Planet. Space Sci. **73**, 283–286 (2012)

J.H. Roberts, E.G. Kahn, O.S. Barnouin, C.M. Ernst, L.M. Prockter, R.W. Gaskell, Origin and flatness of ponds on asteroid 433 Eros. Meteorit. Planet. Sci. **49**, 1735–1748 (2014a)

J.H. Roberts, O.S. Barnouin, E.G. Kahn, L.M. Prockter, Observational bias and the apparent distribution of ponds on Eros. Icarus **241**, 160–164 (2014b)

M.S. Robinson, P.C. Thomas, J. Veverka, S. Murchie, B. Carcich, The nature of ponded deposits on Eros. Nature **413**, 396–400 (2001)

M.S. Robinson, P.C. Thomas, J. Veverka, S.L. Murchie, B.B. Wilcox, The geology of 433 Eros. Meteorit. Planet. Sci. **37**, 1651–1684 (2002)

P. Rousselot, E. Jehin, J. Manfroid, O. Mousis, C. Dumas, B. Carry, U. Marboeuf, J.-M. Zucconi, A search for water vaporization on Ceres. Astron. J. **142**, 125 (2011) (6 pp.)

A.E. Rubin, J.M. Trigo-Rodríguez, H. Heinz, J.T. Wasson, Progressive aqueous alteration of CM carbonaceous chondrites. Geochim. Cosmochim. Acta **71**, 2361–2382 (2007)

D.P. Rubincam, Radiative spin-up and spin-down of small asteroids. Icarus **148**, 2–11 (2000)

C.T. Russell, C.A. Raymond, The Dawn mission to Vesta and Ceres. Space Sci. Rev. **163**, 3–23 (2011)

C.T. Russell, C.A. Raymond, A. Coradini, H.Y. McSween, M.T. Zuber, A. Nathues, M.C. De Sanctis, R. Jaumann, A.S. Konopliv, F. Preusker, S.W. Asmar, R.S. Park, R. Gaskell, H.U. Keller, S. Mottola, T. Roatsch, J.E.C. Scully, D.E. Smith, P. Tricarico, M.J. Toplis, U.R. Christensen, W.C. Feldman, D.J. Lawrence, T.J. McCoy, T.H. Prettyman, R.C. Reedy, M.E. Sykes, T.N. Titus, Dawn at Vesta: Testing the protoplanetary paradigm. Science **336**, 684–686 (2012)

C.T. Russell, C.A. Raymond, R. Jaumann, H.Y. McSween, M.C. De Sanctis, A. Nathues, T.H. Prettyman, E. Ammannito, V. Reddy, F. Preusker, D.P. O'Brien, S. Marchi, B.W. Denevi, D.L. Buczkowski, C.M. Pieters, T.B. McCord, J.-Y. Li, D.W. Mittlefehldt, J.-P. Combe, D.A. Williams, H. Hiesinger, R.A. Yingst, C.A. Polanskey, S.P. Joy, Dawn completes its mission at 4 Vesta. Meteorit. Planet. Sci. **48**, 2076–2089 (2013). doi:10.1111/maps.12091

C.T. Russell, C.A. Raymond, A. Nathues, P. Gutierrez-Marquez, M.C. De Sanctis, C.T.E. Ammannito, T.H. Prettyman, A. Konopliv, R. Park, H.Y. McSween, R. Jaumann, S. Joy, C.A. Polanskey, M. Rayman (Dawn Science Team), Dawn arrives at Ceres: Better than Hubble resolution. Presented at the 46th Lunar and Planetary Science Conference, The Woodlands, TX, March 16–20 (2015). Abstract #1131

O. Saint-Pé, M. Combes, F. Rigaut, Ceres surface properties by high-resolution imaging from earth. Icarus **105**, 271–281 (1993)

J. Saito, H. Miyamoto, R. Nakamura, M. Ishiguro, T. Michikami, A.M. Nakamura, H. Demura, S. Sasaki, N. Hirata, C. Honda, A. Yamamoto, Y. Yokota, T. Fuse, F. Yoshida, D.J. Tholen, R.W. Gaskell, T. Hashimoto, T. Kubota, Y. Higuchi, T. Nakamura, P. Smith, K. Hiraoka, T. Honda, S. Kobayashi, M. Furuya, N. Matsumoto, E. Nemoto, A. Yukishita, K. Kitazato, B. Dermawan, A. Sogame, J. Terazono, C. Shinohara, H. Akiyama, Detailed images of Asteroid 25143 Itokawa from Hayabusa. Science **312**, 1341–1344 (2006)

P.S. Sanchez, D.J. Scheeres, The strength of regolith and rubble pile asteroids. Meteorit. Planet. Sci. **49**, 788–811 (2014). doi:10.1111/maps.12293

D.J. Scheeres, R.W. Gaskell, Effect of density inhomogeneity on YORP: The case of Itokawa. Icarus **198**, 125–129 (2008)

D.J. Scheeres, S.J. Ostro, R.S. Hudson, E.M. DeJong, S. Suzuki, Dynamics of orbits close to Asteroid 4179 Toutatis. Icarus **132**, 53–79 (1998)

D.J. Scheeres, S.J. Ostro, R.A. Werner, E. Asphaug, R.S. Hudson, Effects of gravitational interactions on asteroid spin states. Icarus **147**, 106–118 (2000)

D.J. Scheeres, E.G. Fahnestock, S.J. Ostro, J.-L. Margot, L.A.M. Benner, S.B. Broschart, J. Bellerose, J.D. Giorgini, M.C. Nolan, C. Magri, P. Pravec, P. Scheirich, R. Rose, R.F. Jurgens, E.M. De Jong, S. Suzuki, Dynamical configuration of binary near-Earth Asteroid (66391) 1999 KW4. Science **314**, 1280–1283 (2006)

D.J. Scheeres, M. Abe, M. Yoshikawa, R. Nakamura, R.W. Gaskell, P.A. Abell, The effect of YORP on Itokawa. Icarus **188**, 425–429 (2007)

P. Schenk, D.P. O'Brien, S. Marchi, R. Gaskell, F. Preusker, T. Roatsch, R. Jaumann, D. Buczkowski, T. McCord, H.Y. McSween, D. Williams, A. Yingst, C. Raymond, C. Russell, The geologically recent giant impact basins at Vesta's south pole. Science **336**, 694–697 (2012)

B.E. Schmidt, J. Bauer, B.J. Buratti, C.T. Russell, Rotational light curve and rotation period of 5535 Annefrank, in *Lunar and Planetary Science XXXVIII* (2007). Abstract #1859

B. Schmitz, B. Peucker-Ehrenbrink, M. Lindström, M. Tassinari, Accretion rates of meteorites and cosmic dust in the early Ordovician. Science **278**, 88–90 (1997)

N. Schorghofer, The lifetime of ice on main belt asteroids. Astrophys. J. **682**, 697–705 (2008)

J. Schubart, D.L. Matson, Masses and densities of asteroids, in *Asteroids*, ed. by T. Gehrels (University of Arizona Press, Tucson, 1979), pp. 84–97

P.H. Schultz, D.E. Gault, Seismic effects from major basin formations on the Moon and Mercury. Moon **12**, 159–177 (1975)

J.E.C. Scully, A. Yin, C.T. Russell, B.W. Denevi, V. Reddy, Potential transient liquid water flow features in fresh craters on Vesta, in *Fall AGU Meeting*, December 3–7 (2012)

J.E.C. Scully, C.T. Russell, A. Yin, R. Jaumann, H.Y. McSween, C.A. Raymond, V. Reddy, L. Le Corre, Gullies on Vesta, related geological features and possible formation mechanisms, in *44th Lunar and Planetary Science Conference*, The Woodlands, TX, 18–22 March (2013), pp. 18–22. LPI Contribution No. 1578, abstract #1796

J.E.C. Scully, C.T. Russell, A. Yin, R. Jaumann, E. Carey, H.Y. McSween, J. Castillo-Rogez, C.A. Raymond, V. Reddy, L. Le Corre, Sub-curvilinear gullies interpreted as evidence for transient water flow on Vesta, in *45th Lunar and Planetary Science Conference*, The Woodlands, TX, 17–21 March (2014), pp. 17–21. LPI Contribution No. 1777, abstract #1796

D.W. Sears, *The Nature and Origin of Meteorites* (Oxford University Press, London, 1978)

D.W.G. Sears, *The Origin of Chondrules and Chondrites* (Cambridge University Press, Cambridge, 2005)

D.W.G. Sears, H. Kochan, W.F. Huebner, Simulation experiments and surface processes on comets. Meteorit. Planet. Sci. **34**, 497–525 (1999)

D.W.G. Sears, C.C. Allen, D.T. Britt, D.E. Brownlee, A.F. Cheng, C.R. Chapman, B.C. Clark, B.G. Drake, R.A. Fevig, I.A. Franchi, A. Fujiwara, S.P. Gorevan, H. Kochan, J.S. Lewis, M.M. Lindstrom, K. Nishiizumi, M.S. Race, D.J. Scheeres, E.R.D. Scott, G.J. Taylor, H. Yano, Near-Earth Asteroid Sample Return, in *The Future of Solar System Exploration (2003–2013)—Community Contributions to the NRC*

Solar System Exploration Decadal Survey, ed. by M.V. Sykes. ASP Conference Proceedings, vol. 272 (Astronomical Society of the Pacific, San Francisco, 2002), pp. 111–140. 2002

D. Sears, M. Franzen, S. Moore, S. Nichols, M. Kareev, P. Benoit, Mission operations in low-gravity regolith and dust, in *Mitigation of Hazardous Comets and Asteroids*, ed. by M. Belton, T.H. Morgan, N. Samarasinha, D.K. Yeomans (Cambridge University Press, Cambridge, 2004), pp. 337–352. 2004. ISBN 0-521-82764-7

D.W.G. Sears, L.L. Tornabene, G.R. Osinsky, S.S. Hughes, J.L. Heldmann, Formation of the "ponds" on asteroid (433) Eros by fluidization. Planet. Space Sci. (2015 in press)

Z. Sekanina, D.E. Brownlee, T.E. Economou, A.J. Tuzzolino, S.F. Green, Modeling the nucleus and jets of comet 81P/Wild 2 based on the Stardust encounter data. Science **304**, 1769–1774 (2004)

M.K. Shepard, P. Helfenstein, A test of the Hapke photometric model. J. Geophys. Res. **112**(E3), E03001 (2007)

E.M. Shoemaker, R.M. Batson, H.E. Holt, E.C. Morris, J.J. Rennilson, E.A. Whitaker, Television observations from Surveyor 3. J. Geophys. Res. **73**, 3989–4043 (1968). doi:10.1029/JB073i012p03989

H. Sierks, P. Lamy, C. Barbieri, D. Koschny, H. Rickman, R. Rodrigo, M.F. A'Hearn, F. Angrilli, M.A. Barucci, J.-L. Bertaux, I. Bertini, S. Besse, B. Carry, G. Cremonese, V. Da Deppo, B. Davidsson, S. Debei, M. De Cecco, J. De Leon, F. Ferri, S. Fornasier, M. Fulle, S.F. Hviid, R.W. Gaskell, O. Groussin, P. Gutierrez, W. Ip, L. Jorda, M. Kaasalainen, H.U. Keller, J. Knollenberg, R. Kramm, E. Kührt, M. Küppers, L. Lara, M. Lazzarin, C. Leyrat, J.J. Moreno, M.S. Lopez, S. Marchi, F. Marzari, M. Massironi, H. Michalik, R. Moissl, G. Naletto, F. Preusker, L. Sabau, W. Sabolo, F. Scholten, C. Snodgrass, N. Thomas, C. Tubiana, P. Vernazza, J.-B. Vincent, K.-P. Wenzel, T. Andert, M. Pätzold, B.P. Weiss, Images of Asteroid 21 Lutetia: A remnant planetesimal from the early solar system. Science **334**, 487–490 (2011)

D.P. Simonelli, J. Veverka, P.C. Thomas, P. Helfenstein, B.T. Carcich, M.J.S. Belton, Ida lightcurves: Consistency with Galileo shape and photometric models. Icarus **120**, 38–47 (1996)

S. Siregar, E. Soegiartini, Orbital evolution of 4179 Toutatis, in *Proceedings of the 4th Southeast Astronomy Network Meeting*, Bandung, 10–11 October, 2010 (2012)

C. Snodgrass, C. Tubiana, J.-V. Vincent, H. Sierks, S. Hviid, R. Moiss, H. Boehnhardt, C. Barbieri, D. Koschny, P. Lamy, H. Rickman, R. Rodrigo, B. Carry, S.C. Lowry, R.J.M. Laird, P.R. Weissman, A. Fitzsimmons, S. Marchi (the OSIRIS team), A collision in 2009 as the origin of the debris trail of asteroid P/2010 A2. Nature **467**, 814–816 (2010)

J. Souchay, H. Kinoshita, H. Nakai, S. Roux, A precise modeling of Eros 433 rotation. Icarus **166**, 285–296 (2003)

J.R. Spencer, L.A. Akimov, C. Angeli, P. Angelini, M.A. Barucci, P. Birch, C. Blanco, M.W. Buie, A. Caruso, V.G. Chiornij, F. Colas, P. Dentchev, N.I. Dorokhov, M.C. De Sanctis, E. Dotto, O.B. Ezhkova, M. Fulchignoni, S. Green, A.W. Harris, E.S. Howell, T. Hudecek, A.V. Kalashnikov, V.V. Kobelev, Z.B. Korobova, N.I. Koshkin, V.P. Kozhevnikov, Y.N. Krugly, D. Lazzaro, J. Lecacheux, J. MacConnell, S.Y. Mel'nikov, T. Michalowski, B.E.A. Mueller, T. Nakamura, C. Neese, M.C. Nolan, W. Osborn, P. Pravec, D. Riccioli, V.S. Shevchenko, V.G. Shevchenko, D.J. Tholen, F.P. Velichko, C. Venditti, R. Venditti, W. Wisniewski, J. Young, B. Zellner, The lightcurve of 4179 Toutatis: Evidence for complex rotation. Icarus **117**, 71–89 (1995)

C.B. Stephenson, The light-curve and the color of Vesta. Astrophys. J. **114**, 500–504 (1951)

D. Stöffler, N.A. Artemieva, K. Wünnemann, W.U. Reimold, J. Jacob, B.K. Hansen, I.A.T. Summerson, Ries crater and suevite revisited—observations and modeling. Part I: Observations. Meteorit. Planet. Sci. **48**, 515–589 (2013). doi:10.1111/maps.12086

G.H. Stokes, J.B. Evans, S.M. Larson, Near-Earth asteroid search programs, in *Asteroids III*, ed. by W.F. Bottke Jr., A. Cellino, P. Paolicchi, R.P. Binzel (University of Arizona Press, Tucson, 2002), pp. 45–54

R. Sullivan, R. Greeley, P. Pappalardo, E. Asphaug, J.M. Moore, D. Morrison, M.J.S. Belton, M. Carr, C.R. Chapman, P. Geissler, R. Greenberg, Geology of 243 Ida. Icarus **120**, 119–139 (1996)

J.M. Sunshine, J. Bus Schelte, T.J. McCoy, T.H. Burbine, C.M. Corrigan, R.P. Binzel, High-calcium pyroxene as an indicator of igneous differentiation in asteroids and meteorites. Meteorit. Planet. Sci. **39**, 1343–1357 (2004)

J.M. Sunshine, M.F. A'Hearn, O. Groussin, J.-Y. Li, M.J.S. Belton, W.A. Delamere, J. Kissel, K.P. Klaasen, L.A. McFadden, K.J. Meech, H.J. Melosh, P.H. Schultz, P.C. Thomas, J. Veverka, D.K. Yeomans, I.C. Busko, M. Desnoyer, T.L. Farnham, L.M. Feaga, D.L. Hampton, D.J. Lindler, C.M. Lisse, D.D. Wellnitz, Exposed water ice deposits on the surface of Comet 9P/Tempel. Science **311**, 1453–1455 (2006)

M.S. Syal, P.H. Schultz, J.M. Sunshine, M.F. A'Hearn, T.L. Farnham, D.S.P. Dearborn, Geologic control of jet formation on Comet 103P/Hartley 2. Icarus **222**, 610–624 (2013)

M. Tanaka, T. Nakamura, T. Noguchi, A. Nalakto, H. Ishida, T. Yada, K. Shirai, A. Fujimura, Y. Ishibashi, M. Abe, T. Okada, T. Mukai, Crystallization temperature determination of Itokawa particles by plagioclase thermometry with X-ray diffraction data obtained by a high-resolution synchrotron Gandolfi camera. Meteorit. Planet. Sci. **49**(2), 237–244 (2014)

G.J. Taylor, P. Maggiore, E.R.D. Scott, A.E. Rubin, K. Keil, Original structures, and fragmentation and re-assembly histories of asteroids: Evidence from meteorites. Icarus **69**, 1–13 (1987)

E.F. Tedesco, P.V. Noah, M. Noah, S.D. Price, IRAS Minor Planet Survey. IRAS-A-FPA-3-RDR-IMPS-V6.0. NASA Planetary Data System (2004)

D.J. Tholen, Asteroid taxonomic classifications, in *Asteroids II* (University of Arizona Press, Tucson, 1989), pp. 1139–1150

P.C. Thomas, J. Veverka, D. Simonelli, P. Helfenstein, B. Carcich, M.J.S. Belton, M.E. Davies, C. Chapman, The shape of Gaspra. Icarus **107**, 23–36 (1994)

P.C. Thomas, M.J.S. Belton, B. Carcich, C.R. Chapman, M.E. Davies, R. Sullivan, J. Veverka, The shape of Ida. Icarus **120**, 20–32 (1996)

P.C. Thomas, R.P. Binzel, M.J. Gaffey, B.H. Zellner, A.D. Storrs, E. Wells, Vesta: Spin pole, size, and shape from HST images. Icarus **128**, 88–94 (1997)

P.C. Thomas, J. Veverka, J.F. Bell III, B.E. Clark, B. Carcich, J. Joseph, M. Robinson, L.A. McFadden, M.C. Malin, C.R. Chapman, W. Merline, S. Murchie, Mathilde: Size, shape, and geology. Icarus **140**, 17–27 (1999)

P.C. Thomas, J. Veverka, M.S. Robinson, S. Murchie, Shoemaker crater as the source of most ejecta blocks on the asteroid 433 Eros. Nature **413**, 394–396 (2001)

P.C. Thomas, L. Prockter, M. Robinson, J. Joseph, J. Veverka, Global structure of asteroid 433 Eros. Geophys. Res. Lett. **29**, 46-1 (2002a). doi:10.1029/2001GL014599

P.C. Thomas, J. Joseph, B. Carcich, J. Veverka, B.E. Clark, J.F. Bell III, A.W. Byrd, R. Chomko, M. Robinson, S. Murchie, L. Prockter, A. Cheng, N. Izenberg, M. Malin, C. Chapman, L.A. McFadden, R. Kirk, M. Gaffey, P.G. Lucey, Eros: Shape, topography, and slope processes. Icarus **155**, 18–37 (2002b)

P.C. Thomas, J.W. Parker, L.A. McFadden, C.T. Russell, S.S. Stern, M.V. Sykes, E.F. Young, Differentiation of the asteroid Ceres as revealed by its shape. Nature **437**, 224–226 (2005). doi:10.1038/nature03938

P.C. Thomas, M.F. A'Hearn, J. Veverka, M.J.S. Belton, J. Kissel, K.P. Klaasen, L.A. McFadden, H.J. Melosh, P.H. Schultz, S. Besse, B.T. Carcich, T.L. Farnham, O. Groussin, B. Hermalyn, Y.-J. Li, D.J. Lindler, C.M. Lisse, K. Meech, J.E. Richardson, Shape, density, and geology of the nucleus of Comet 103P/Hartley 2. Icarus **222**, 550–558 (2013)

N. Thomas, H. Sierks, C. Barbieri, P.L. Lamy, R. Rodrigo, H. Rickman, D. Koschny, U.W. Keller, J. Agarwal, M.F. A'Hearn, F. Angrilli, A.-T. Auger, M.A. Barucci, J.-L. Bertaux, I. Bertini, S. Besse, D. Bodewits, G. Cremonese, V. Da Deppo, B. Davidsson, M. De Cecco, S. Debei, M.R. El-Maarry, F. Ferri, S. Fornasier, M. Fulle, L. Giacomini, O. Groussin, P.J. Gutierrez, C. Güttler, S.F. Hviid, W.-H. Ip, L. Jorda, J. Knollenberg, J.-R. Kramm, E. Kührt, M. Küppers, F. La Forgia, L.M. Lara, M. Lazzarin, J.J.L. Moreno, S. Magrin, S. Marchi, F. Marzari, M. Massironi, H. Michalik, R. Moissl, S. Mottola, G. Naletto, N. Oklay, A. Pommerol, F. Preusker, L. Sabau, F. Scholten, C. Snodgrass, C. Tubiana, J.-B. Vincent, K.-P. Wenzel, The morphological diversity of comet 67P/Churyumov-Gerasimenko. Science **347**, 6220 (2015). doi:10.1126/science.aaa0440

C.W. Thomson, Report on the scientific results of the voyage of H.M.S. Challenger during the years 1873–76: Under the command of Captain George S. Nares, R.N., F.R.S. and Captain Frank Turle Thomson, R.N. Her Majesty's Stationary Office, London (1880)

L.L. Tornabene, G.R. Osinski, A.S. McEwen, J.M. Boyce, V.J. Bray, C.M. Caudill, J.A. Grant, C.W. Hamilton, S. Mattson, P.J. Mouginis-Mark, Widespread crater-related pitted materials on Mars: Further evidence for the role of target volatiles during the impact process. Icarus **220**, 348–368 (2012)

J. Torppa, M. Kaasalainen, T. Michałowski, T. Kwiatkowski, A. Kryszczyńska, P. Denchev, R. Kowalski, Shapes and rotational properties of thirty asteroids from photometric data. Icarus **164**, 346–383 (2003)

A.H. Treiman, A. Lanzirotti, D. Xirouchakis, Ancient water on asteroid 4 Vesta: Evidence from a quartz veinlet in the Serra de Mage eucrite meteorite. Earth Planet. Sci. Lett. **219**, 189–199 (2004)

J.I. Trombka, S.W. Squyres, P.C. Thomas, R.P. Binzel, M.J. Gaffey, B.H. Zellner, A.D. Storrs, E. Wells, Vesta: Spin pole, size, and shape from HST images. Icarus **128**, 88–94 (1997)

J.I. Trombka, S.W. Squyres, J. Brückner, W.V. Boynton, R.C. Reedy, T.J. McCoy, P. Gorenstein, L.G. Evans, J.R. Arnold, R.D. Starr, L.R. Nittler, M.E. Murphy, I. Mikheeva, R.L. McNutt Jr., T.P. McClanahan, E. McCartney, J.O. Goldsten, R.E. Gold, S.R. Floyd, P.E. Clark, T.H. Burbine, J.S. Bhangoo, S.H. Bailey, M. Petaev, The elemental composition of Asteroid 433 Eros: Results of the NEAR-Shoemaker X-ray spectrometer. Science **289**, 2102–2105 (2000)

W.R. Van Schmus, J.A. Wood, A chemical-petrologic classification for the chondritic meteorites. Geochim. Cosmochim. Acta **31**, 747–765 (1967)

P. Vernazza, T. Mothé-Diniz, M.A. Barucci, M. Birlan, J.M. Carvano, G. Strazzulla, M. Fulchignoni, A. Migliorini, Analysis of near-IR spectra of 1 Ceres and 4 Vesta, targets of the Dawn mission. Astron. Astrophys. **436**, 1113–1121 (2005)

P. Vernazza, R.P. Binzel, C.A. Thomas, F.E. DeMeo, S.J. Bus, A.S. Rivkin, A.T. Tokunaga, Compositional differences between meteorites and near-Earth asteroids. Nature **454**, 858–860 (2008). doi:10.1038/nature07154

P. Vernazza, R. Brunetto, R.P. Binzel, C. Perrond, D. Fulvio, G. Strazzulla, M. Fulchignoni, Plausible parent bodies for enstatite chondrites and mesosiderites: Implications for Lutetia's fly-by. Icarus **202**, 477–486 (2009)

P. Vernazza, P. Lamy, O. Groussin, T. Hiroi, L. Jorda, P.L. King, M.R.M. Izawa, F. Marchis, M. Birlan, R. Brunetto, Asteroid (21) Lutetia as a remnant of Earth's precursor planetesimals. Icarus **216**, 650–659 (2011)

J. Veverka, P. Helfenstein, P. Lee, P. Thomas, A. McEwen, M. Belton, K. Klaasen, T.V. Johnson, J. Granahan, F. Fanale, P. Geissler, J.W. Head III, Ida and Dactyl: Spectral reflectance and color variations. Icarus **120**, 66–76 (1996)

J. Veverka, M. Belton, K. Klaasen, C. Chapman, Galileo's encounter with 951 Gaspra: Overview. Icarus **107**, 2–17 (1994)

J. Veverka, P. Thomas, A. Harch, B. Clark, J.F. Bell III, B. Carcich, J. Joseph, S. Murchie, N. Izenberg, C. Chapman, W. Merline, L. McFadden, M. Robinson, NEAR encounter with Asteroid 253 Mathilde: Overview. Icarus **140**, 3–16 (1999a)

J. Veverka, P.C. Thomas, J.F. Bell, M. Bell III, B. Carcich, B. Clark, A. Harch, J. Joseph, P. Martin, M. Robinson, S. Murchie, N. Izenberg, E. Hawkins, J. Warren, R. Farquhar, A. Cheng, D. Dunham, C. Chapman, W.J. Merline, L. McFadden, D. Wellnitz, M. Malin, W.M. Owen Jr., J.K. Miller, B.G. Williams, D.K. Yeomans, Imaging of asteroid 433 Eros during NEAR's flyby reconnaissance. Science **285**, 562–564 (1999b)

J. Veverka, M. Robinson, P. Thomas, S. Murchie, J.F. Bell III, N. Izenberg, C. Chapman, A. Harch, M. Bell, B. Carcich, A. Cheng, B. Clark, D. Domingue, D. Dunham, R. Farquhar, M.J. Gaffey, E. Hawkins, J. Joseph, R. Kirk, H. Li, P. Lucey, M. Malin, P. Martin, L. McFadden, W.J. Merline, J.K. Miller, W.M. Owen Jr., C. Peterson, L. Prockter, J. Warren, D. Wellnitz, B.G. Williams, D.K. Yeomans, NEAR at Eros: Imaging and spectral results. Science **289**, 2088–2097 (2000)

J. Veverka, B. Farquhar, M. Robinson, P. Thomas, S. Murchie, A. Harch, P.G. Antreasian, S.R. Chesley, J.K. Miller, W.M. Owen, B.G. Williams, D. Yeomans, D. Dunham, G. Heyler, M. Holdridge, R.L. Nelson, K.E. Whittenburg, J.C. Ray, B. Carcich, A. Cheng, C. Chapman, J.F. Bell, M. Bell, B. Bussey, B. Clark, D. Domingue, M.J. Gaffey, E. Hawkins, N. Izenberg, J. Joseph, R. Kirk, P. Lucey, M. Malin, L. McFadden, W.J. Merline, C. Peterson, L. Prockter, J. Warren, D. Wellnitz, The landing of the NEAR-Shoemaker spacecraft on asteroid 433 Eros. Nature **413**, 390–393 (2001)

B. Viateau, M. Rapaport, Mass and density of asteroids (4) Vesta and (11) Parthenope. Astron. Astrophys. **370**, 602–609 (2001)

F. Vilas, A cheaper, faster, better way to detect water of hydration on Solar System bodies. Icarus **111**, 456–467 (1994)

F. Vilas, M.J. Gaffey, Phyllosilicate absorption features in main-belt and outer-belt asteroid reflectance spectra. Science **246**, 790–792 (1989)

F. Vilas, L.A. McFadden, CCD reflectance spectra of selected asteroids. I. Presentation and data analysis considerations. Icarus **100**, 85–94 (1992)

J.-B. Vincent, S. Besse, S. Marchi, H. Sierks, M. Massironi, Physical properties of craters on asteroid (21) Lutetia. Planet. Space Sci. **66**, 79–86 (2012)

A. Von Humboldt, *Personal Narrative of a Journey to the Equinoctial Regions of the New Continent*. Penguin Classics (Penguin, Baltimore, 1996). Abridged edition

S. Wakita, T. Nakamura, T. Ikeda, H. Yurimoto, Thermal modeling for a parent body of Itokawa. Meteorit. Planet. Sci. **49**, 228–236 (2013)

K.J. Walsh, A. Morbidelli, The effect of an early planetesimal-driven migration of the giant planets on terrestrial planet formation. Astron. Astrophys. **526**, A126 (2011) (8 pages)

Z.Z. Wang, Y. Li, X.H. Zhang, J.S. Jiang, C.D. Xu, D.H. Zhang, W.G. Zhang, Calibration and brightness temperature algorithm of CE-1 Lunar Microwave Sounder. Sci. China Earth Sci. **53**, 1392–1406 (2010)

J.T. Wasson, Vesta and extensively melted asteroids: Why HED meteorites are probably not from Vesta. Earth Planet. Sci. Lett. **381**, 138–146 (2013)

S.J. Weidenschilling, The origin of comets in the solar nebula: A unified model. Icarus **127**, 290–306 (1997)

M.K. Weisberg, T.M. McCoy, A.N. Krot, Systematics and evaluation of meteorite classification, in *Meteorites and the Early Solar System II*, ed. by D. Lauretta, H.Y. McSween (University of Arizona Press, Tucson, 2006), pp. 19–52

P.R. Weismann, W.F. Bottke, H.F. Levison, Evolution of comets into asteroids, in *Asteroids III*, ed. by W.F. Bottke, A. Cellino, P. Paolicchi, R.P. Binzel (University of Arizona Press, Tucson, 2002), pp. 669–686

B.P. Weiss, L.T. Elkins-Tanton, Differentiated planetesimals and the parent bodies of chondrites. Annu. Rev. Earth Planet. Sci. **41**, 529–560 (2013)

B.P. Weiss, E.-T. Linda, M.A. Barucci, H. Sierks, C. Snodgrass, J.-B. Vincent, S. Marchi, P.R. Weissman, M. Pätzold, I. Richter, M. Fulchignoni, R.P. Binzel, R. Schulz, Possible evidence for partial differentiation of asteroid Lutetia from Rosetta. Planet. Space Sci. **66**, 137–146 (2012)

B.B. Wilcox, M.S. Robinson, P.C. Thomas, Regolith thickness, distribution, and processes examined at sub-meter resolution, in *The Moon Beyond 2002: Next Steps in Lunar Science and Exploration* (2002), p. 66

L. Wilkening, Foreign inclusions in stony meteorites I. Carbonaceous chondritic zenoliths in the Kapoeta howardite. Geochim. Cosmochim. Acta **37**, 1955–1989 (1973)

W.Z. Wisniewski, M.A. Barucci, M. Fulchignoni, C. De Sanctis, E. Dotto, A. Rotundi, R.P. Binzel, C.D. Madras, S.F. Green, M.L. Kelly, P.J. Newman, A.W. Harris, J.W. Young, C. Blanco, M. di Martino, W. Ferreri, M. Gonano-Beurer, S. Mottola, D.J. Tholen, J.D. Goldader, M. Coradini, P. Magnusson, Ground-based photometry of asteroid 951 Gaspra. Icarus **101**, 213–222 (1993)

H. Yano, T. Kubota, H. Miyamoto, T. Okada, D. Scheeres, Y. Takagi, K. Yoshida, M. Abe, S. Abe, O. Barnouin-Jha, A. Fujiwara, S. Hasegawa, T. Hashimoto, M. Ishiguro, M. Kato, J. Kawaguchi, T. Mukai, J. Saito, S. Sasaki, M. Yoshikawa, Touchdown of the Hayabusa spacecraft at the Muses Sea on Itokawa. Science **312**, 1350–1353 (2006)

D.K. Yeomans, Asteroid 433 Eros: The target body of the NEAR mission (undated). As of April 2014 available at http://trs-new.jpl.nasa.gov/dspace/bitstream/2014/31429/1/95-1108.pdf?origin=publication_detail

J. Yeomans, D.K.P. Barriot, D.W. Dunham, R.W. Farquhar, J.D. Giorgini, C.E. Helfrich, A.S. Konopliv, J.V. McAdams, J.K. Miller, W.M. Owen Jr., D.J. Scheeres, S.P. Synnott, B.G. Williams, Estimating the mass of Asteroid 253 Mathilde from tracking data during the NEAR flyby. Science **278**, 2106–2109 (1997)

D.K. Yeomans, P.G. Antreasian, J.-P. Barriot, S.R. Chesley, D.W. Dunham, R.W. Farquhar, J.D. Giorgini, C.E. Helfrich, A.S. Konopliv, J.V. McAdams, J.K. Miller, W.M. Owen, D.J. Scheeres, P.C. Thomas, J. Veverka, B.G. Williams, Radio science results during the NEAR-Shoemaker a spacecraft rendezvous with Eros. Science **289**, 2085–2088 (2000)

M. Yoshikawa, The next asteroid sample return mission of Japan—Hayabusa-2, in *The Importance of Solar System Sample Return Missions to the Future of Planetary Science*, The Woodlands, March 5–6 (2011). LPI Contribution No. 1611, 2011, id. 5046.

M.Yu. Zolotov, On the composition and differentiation of Ceres. Icarus **204**, 183–193 (2009)

F. Zambon, M.C. De Sanctis, F. Tosi, A. Longobardo, E. Palomba, F. Capaccioni, E. Ammannito, A. Frigeri, M.T. Capria, M. Ciarniello, A. Raponi, C.T. Russell, C.A. Raymond (The Dawn/VIR Team), Identification of homogeneous units on Ceres. First results by Dawn. Presented at the 46th Lunar and Planetary Science Conference, The Woodlands, TX, March 16–20 (2015). Abstract #1365

V. Zappala, M. di Martino, Z. Knezevic, G. Djurasevic, New evidence for the effect of phase angle on asteroid lightcurve shape—21 Lutetia. Astron. Astrophys. **130**, 208–210 (1984)

A.F. Zausaev, A.N. Pushkarev, Evolution of the orbit of asteroid 4179 Toutatis over 11,550 years. Sol. Syst. Res. **27**, 585–587 (1994)

B. Zellner, D.J. Tholen, E.F. Tedesco, The eight-color asteroid survey: Results for 589 minor planets. Icarus **61**, 355–416 (1985)

M.E. Zolensky, T.J. Zega, H. Yano, S. Wirick, A.J. Westphal, M.K. Weisberg, I. Weber, J.L. Warren, M.A. Velbel, A. Tsuchiyama, P. Tsou, A. Toppani, N. Tomioka, K. Tomeoka, N. Teslich, M. Taheri, J. Susini, R. Stroud, T. Stephan, F.J. Stadermann, C.J. Snead, S.B. Simon, A. Simionovici, T.H. See, F. Robert, F.J.M. Rietmeijer, W. Rao, M.C. Perronnet, D.A. Papanastassiou, K. Okudaira, K. Ohsumi, I. Ohnishi, K. Nakamura-Messenger, T. Nakamura, S. Mostefaoui, T. Mikouchi, A. Meibom, G. Matrajt, M.A. Marcus, H. Leroux, L. Lemelle, L. Le, A. Lanzirotti, F. Langenhorst, A.N. Krot, L.P. Keller, A.T. Kearsley, D. Joswiak, D. Jacob, H. Ishii, R. Harvey, K. Hagiya, J.N. Grossman, G.A. Graham, M. Gounelle, P. Gillet, M.J. Genge, G. Flynn, T. Ferroir, S. Fallon, S. Fakra, D.S. Ebel, Z.R. Dai, P. Cordier, B. Clark, M. Chi, A.L. Butterworth, D.E. Brownlee, J.C. Bridges, S. Brennan, A. Brearley, J.P. Bradley, P. Bleuet, P.A. Bland, R. Bastien, Mineralogy and petrology of Comet 81P/Wild 2 nucleus samples. Science **314**, 1735–1739 (2006)

X. Zou, C. Li, J. Liu, W. Wang, H. Li, J. Ping, The preliminary analysis of the 4179 Toutatis snapshots of the Chang'E-2 flyby. Icarus **229**, 348–354 (2014)

M.T. Zuber, D.E. Smith, A.F. Cheng, J.B. Garvin, O. Aharonson, T.D. Cole, P.J. Dunn, Y. Guo, G. Lemoine, G.A. Neumann, D.D. Rowlands, M.H. Torrence, The shape of 433 Eros from the NEAR-Shoemaker Laser Rangefinder. Science **289**, 2097–2101 (2000)